IOP Publishing Reports on Progress in Physics
Rep. Prog. Phys. **83** (2020) 066501 (46pp) https://doi.org/10.1088/1361-6633/ab7a42

Review

Binding and electronic level alignment of π-conjugated systems on metals

Antoni Franco-Cañellas[1], Steffen Duhm[2], Alexander Gerlach[1] and Frank Schreiber[1,3]

[1] Institut für Angewandte Physik, Universität Tübingen, Auf der Morgenstelle 10, 72076 Tübingen, Germany
[2] Institute of Functional Nano & Soft Materials (FUNSOM), Jiangsu Key Laboratory for Carbon-Based Functional Materials & Devices and Joint International Research Laboratory of Carbon-Based Functional Materials and Devices, Soochow University, Suzhou 215123, People's Republic of China

E-mail: frank.schreiber@uni-tuebingen.de

Received 19 July 2019, revised 22 January 2020
Accepted for publication 26 February 2020
Published 1 June 2020

Abstract

We review the binding and energy level alignment of π-conjugated systems on metals, a field which during the last two decades has seen tremendous progress both in terms of experimental characterization as well as in the depth of theoretical understanding. Precise measurements of vertical adsorption distances and the electronic structure together with *ab initio* calculations have shown that most of the molecular systems have to be considered as intermediate cases between weak physisorption and strong chemisorption. In this regime, the subtle interplay of different effects such as covalent bonding, charge transfer, electrostatic and van der Waals interactions yields a complex situation with different adsorption mechanisms. In order to establish a better understanding of the binding and the electronic level alignment of π-conjugated molecules on metals, we provide an up-to-date overview of the literature, explain the fundamental concepts as well as the experimental techniques and discuss typical case studies. Thereby, we relate the geometric with the electronic structure in a consistent picture and cover the entire range from weak to strong coupling.

Keywords: π-conjugated molecules on metals, vertical adsorption distances, energy-level alignment, x-ray standing waves, photoelectron spectroscopy

(Some figures may appear in colour only in the online journal)

1. Introduction

The interface between π-conjugated organic semiconductor molecules and metals is at the heart of a number of important scientific questions, both from a fundamental as well as from an applied perspective. It is a key issue for the different energy-level alignment (ELA) schemes as well as for charge carrier injection/extraction efficiencies and related issues in organic (opto)electronics devices [1–5]. At the same time, already the question of the interaction and binding is non-trivial, in particular, for systems which are between the limiting cases of (clearly weak) physisorption and (clearly strong) chemisorption. Importantly, there is a subtle interplay between geometric and electronic structure, with a frequently substantial (but not necessarily dominating) contribution of dispersion interactions, which makes predictions of the metal–organic interface rather challenging, if only 'simple rules' are employed. Rather advanced theoretical methods, developed in the last decade, have enabled substantial progress [6–11]. In parallel with that, a satisfactory understanding of these systems requires the experimental determination of both the exact adsorption (i.e.,

[3] Author to whom any correspondence should be addressed.
Corresponding editor: Professor Horst-Guenter Rubahn.

binding) geometry as well as the resulting electronic structure including possible charge transfer, interface dipoles, and shifts of the electronic levels. Fortunately, the last years have also seen tremendous progress in experimental results, so that we are now looking at a reasonably large and representative set of experimental data on a number of systems, which allow a more comprehensive discussion. This is the main goal of the present review.

We shall first emphasize the importance of the structural properties. In line with the motivation above, it has become clear that the precise knowledge of the molecular arrangement on the surface is necessary to assess and interpret the electronic properties and eventually the ELA. The nature of the interaction of (aromatic) π-systems with metals is less obvious than, say, CO on Ni(111) or other chemisorbing systems [12], which can be safely assumed to exhibit a well-established chemical bond on the one hand, and, say, noble gases, which are obviously physisorption, i.e. dispersion-interaction dominated on the other hand [13]. The interaction and interface for the intermediate case has been subject to intense research with two largely complementary approaches:

(a) Experimental high-precision determination of adsorption distances, mostly using the x-ray standing wave (XSW) technique. Remarkably, while XSW had been developed in the 1960s for the localization of interstitial dopants in the bulk [14] and thereafter used also for simple adsorbates on surfaces [15, 16], the first investigations of larger aromatic compounds were published only in 2005 [17, 18]. Since then, numerous studies using the XSW technique have revealed that π-conjugated molecules on metals show a surprisingly rich phenomenology, e.g., with significant distortions of the molecules on noble metal surfaces. Of course, also other techniques such as photoelectron diffraction (PhD) [19], rod-scans in x-ray diffraction [20] or LEED I–V [21–23], which are used for structural investigations on surfaces, have their merits but do not exhibit the same precision and/or element specificity as the XSW technique.

(b) Quantum theoretical calculations that managed to include long-range dispersion forces in density functional theory (DFT) codes [24–28], which became more popular than previous attempts involving, e.g., Hartree–Fock self-consistent field wave functions [29] or Møller–Plesset perturbation theory (MP2) [30]. Different schemes going beyond standard DFT were developed to tackle the fundamental problem, how to treat exchange–correlation effects. While those approximations with dispersion corrections involve increased computational costs, they have become more and more accurate for calculating the adsorption geometry of organic molecules on metals. In this context, the reader seeking more information is referred to reviews of vdW-corrected DFT [7, 10, 31] and to reference [9] for its application in the context of metal–organic interfaces.

Regarding the electronic properties of such systems, it has already been recognized in the 1970s that the electronic structure of molecular solids is considerably different to that in the gas phase [32, 33]. However, it took 20 more years until 'energy-level alignment' and 'interface dipoles' for π-systems at interfaces came into the focus of research [34–36] and the seminal review by Ishii *et al* has been published [1]. In the last decade a systematic understanding and phenomenology has been established [2, 37–44]. In particular, ELA is now relatively well studied for multilayers on *inert* substrates, i.e., if substrate–adsorbate interactions can be neglected [45–47]. However, this is frequently not the case on metal substrates, and it is clear that the complete binding scenario including possible distortions of the adsorbate is required for a thorough understanding of ELA [3, 48–51].

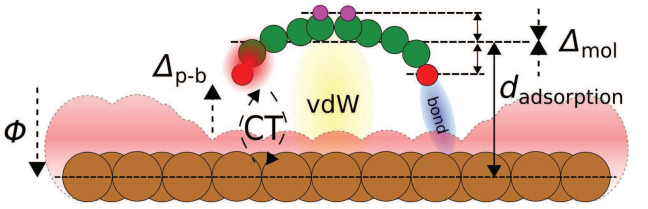

Figure 1. Sketch of the fundamental quantities and phenomena central to this review: ϕ is the substrate work function, Δ_{p-b} the change of surface dipole due to the push-back effect, CT the charge transfer effects between adsorbate and substrate, vdW are van der Waals forces, Δ_{mol} the intramolecular dipoles intrinsic as well as adsorption induced, $d_{adsorption}$ the average adsorption distance of the molecule and 'bond' refers to the possible formation of chemical bonds between the molecule and the substrate. The magnitude of the energy shifts (dashed arrows) is intimately related to the adsorption geometry (solid arrows) as will be discussed in the main text.

As mentioned above, it is by now accepted that ELA at organic–metal interfaces is of utmost importance for the performance of organic (opto)electronic devices [41, 43, 52–57]. Moreover, energy-levels and thus charge injection barriers can be tuned by engineering the substrate work function [4, 58–61]. This can be done by pre-covering a metal electrode with a monolayer of an electron acceptor (donor) for increasing (decreasing) the effective substrate work function and thus lowering the hole (electron) injection barrier into subsequently deposited organic layers [58, 62–65]. The contact formation at such strongly coupled interfaces goes usually along with a complex electronic scenario involving donation and back-donation of charges (see figure 1) [66–73]. Furthermore, the adsorption distances including a possible intramolecular distortion impacting the molecular dipole are essential. This is why in-depth discussion of the electronic structure usually requires a precise determination of the geometric structure (figure 1), and why XSW results have a key role in this context. Several original research articles (e.g. references [66, 71, 73–81]) and, more recently, some review articles and book contributions (references [9, 51, 82–86]) have demonstrated that correlating electronic structure and vertical adsorption heights gives new insights.

This review is organized as follows: initially, we explain the basic concepts of organic–metal contact formation (section 2), followed by some experimental considerations related to XSW, photoelectron spectroscopy and complementary techniques (section 3). After providing a comprehensive list of XSW data obtained for conjugated organic molecules (COMs,

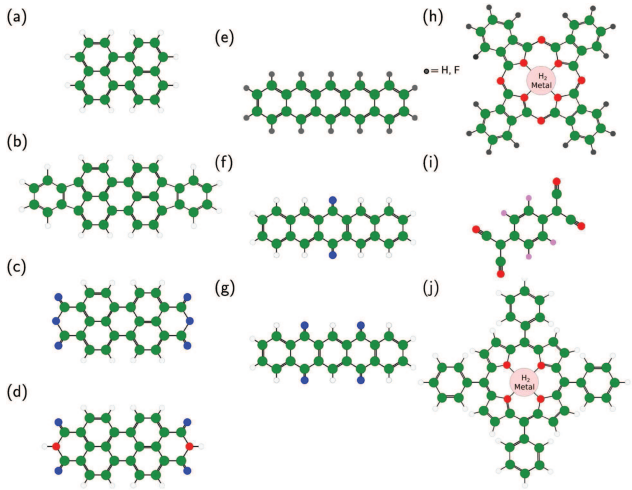

Figure 2. Chemical structure of the main molecules reviewed here (green for carbon, blue for oxygen, red for nitrogen, pink for fluorine and white for hydrogen). (a) Perylene. (b) Diindenoperylene (DIP). (c) Perylene-3,4,9,10-tetracarboxylic dianhydride (PTCDA). (d) Perylene-3,4,9,10-tetracarboxylic-3,4,9,10-diimide (PTCDI). (e) Pentacene (PEN) if the peripheral atoms are hydrogen or perfluoropentacene (PFP) if they are fluorine. (f) 6,13-Pentacenequinone (P2O). (g) 5,7,12,14-Pentacenetetrone (P4O). (h) (Metal) phthalocyanines (MePc) with or without perfluorination. (i) 2,3,5,6-Tetrafluoro-7,7,8,8 tetracyanoquinodimethane (F_4TCNQ). (j) (Metal) tetraphenylporphyrin (MeTPP).

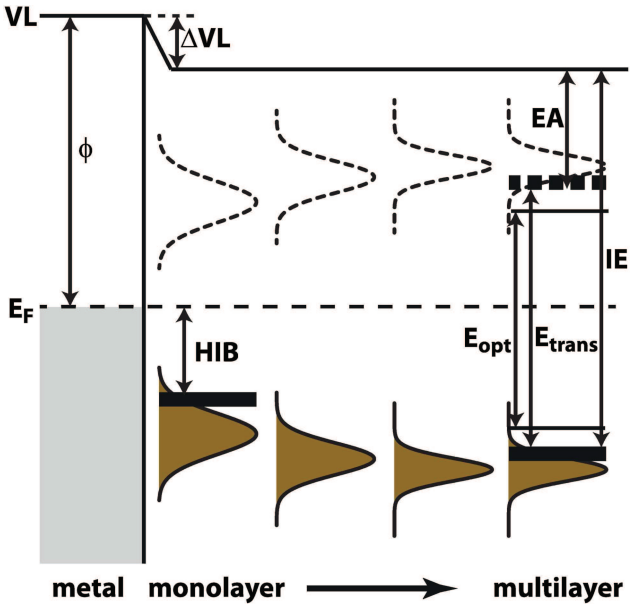

Figure 3. Schematic energy-level diagram of a weakly interacting organic–metal interface. The metal is characterized by its work function ϕ, which is the energetic difference between the vacuum level (VL) and the Fermi level E_F. In the shown limiting case of physisorption, the vacuum level shift ΔVL is due to the push-back effect. For the organic adsorbate the density of states of the frontier molecular orbitals (HOMO and LUMO) are approximated as Gaussian peaks and are shown from monolayer to multilayer coverage. The energetic difference between E_F and the onset of the HOMO level defines the hole injection barrier (HIB). The ionization energy (IE), the electron affinity (EA), the transport gap E_{trans} and the optical gap E_{opt} are usually taken from multilayer measurements.

representative chemical structures are shown in figure 2) on metals, which may serve as reference and general overview, we discuss several typical adsorbate systems (section 4). In each case, we explore the geometric and electronic structure of these systems as well as how these properties are related for different adsorption scenarios. Finally, we shall summarize the important findings (section 5).

2. General considerations and fundamentals

First, we shall introduce the basic quantities, concepts and phenomena that describe and govern the metal–organic interface, in particular with respect to the different effects influencing the ELA in the monolayer regime.

2.1. Interface energetics

The most relevant energy-levels at an organic–metal interface in the limiting case of physisorption are shown in figure 3. A metal has electrons occupying energy-levels up to the Fermi level E_F. The energy to bring them to the vacuum level (VL) corresponds to the metal work function ϕ. In the COM the most important energy-levels are those of the highest occupied molecular orbital (HOMO) and the lowest unoccupied molecular orbital (LUMO), which are also referred to as the frontier molecular orbitals. The energy difference between the HOMO and the LUMO defines the transport gap E_{trans}. Because typical exciton binding energies of COM thin films are in the range of several 100 meV [87–89], i.e. much higher than for most inorganic semiconductors, the optical gap E_{opt} is considerably smaller than E_{trans} [90–92], with the latter being the relevant parameter for ELA and the charge-transport characteristics of the thin film. We note that the ionization energy (IE), which is defined as the energy necessary to move an electron from the HOMO to the vacuum, and the electron affinity (EA), which is the energy necessary to bring an electron from the vacuum to the LUMO, cannot be considered as materials parameters: the collective impact of intramolecular dipole moments, which depend on the molecular orientation within the thin film, influences the IE as well as the EA [93–96]. Therefore, one has to determine these values for each specific thin film structure.

For the IE and EA often the *onsets* of experimentally determined HOMO and LUMO levels are used [2, 97], (cf figure 3) because the onsets govern the transport properties [98]. However, the onset of a peak measured by (inverse) photoemission depends, naturally, on the experimental resolution. Furthermore, the signal-to-noise-ratio can also play a significant role for the onset, especially if the peak shape is not simply Gaussian and/or gap states are involved [47, 99]. Whether the use of onsets or peak maxima is more beneficial depends on the specific adsorbate/substrate system and the scientific question. Unfortunately, no general convention has been established yet and, consequently, great care has to be taken when comparing values from different publications or when comparing experiment and theory.

For COM thin films polarization leads to a rearrangement of energy-levels in the solid state compared to the gas phase

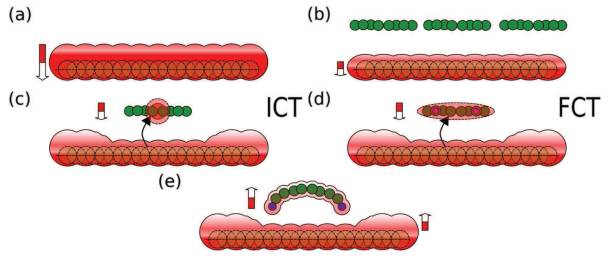

Figure 4. Dipoles at organic–metal interfaces. (a) The electron density spilling out of a clean metal surface gives rise to a surface dipole. (b) This surface dipole is weakened by the adsorption of COMs (push-back effect due to Pauli repulsion). (c) and (d) Charge transfer yields an additional interface dipole. The charge transfer can be integer (ICT) or fractional (FCT). (e) Adsorption induced distortions or the adsorption of polar COMs can lead to additional dipoles.

[11, 96, 100–102]. The polarizability of metals is, in general, much higher than that of organic thin films. The image-charge effect (often called screening) leads thus to a further narrowing of the transport gap in monolayers on a metal substrate compared to multilayers [37, 103] as shown in figure 3. Moreover, even for physisorption the vicinity of a metal leads to broadening of the energy-levels through electronic, quantum-mechanical interaction of the localized molecular states with the continuum of metal states [85, 104, 105].

Upon contact formation of a COM and a metal, vacuum level alignment is rather the exception than the rule [1–3, 38, 43, 106, 107]. There are various reasons for vacuum level shifts ΔVL upon contact formation, which are not restricted to metal substrates, but may also take place when the molecules are adsorbed on inorganic semiconductors and insulators [40, 108–111]. The magnitude of interface dipoles is often related to vertical adsorption distances and the most relevant possible contributions as they are illustrated in figure 4 are:

(a) *Push-back effect* Δ_{p-b} caused by the Pauli repulsion between the electrons of the adsorbate and the metal
(b) *Charge transfer* between adsorbate and substrate
(c) *Chemical bond formation* between adsorbate and substrate
(d) *Molecular dipole moment* Δ_{mol}, which can be intrinsic (polar COMs) or due to adsorption induced distortions

For the physisorbed system shown in figure 3 only the push-back effect is considered. For systems with stronger interactions the impact of the interfacial coupling on ΔVL has to be taken into account. In general, whether an adsorbate is physisorbed or chemisorbed on a substrate is clearly defined by adsorption energies [112] and can be accessed theoretically [9, 113–117]. However, the adsorption type is not directly accessible by standard experimental techniques. To overcome this issue we use a simple definition based on peak shifts between mono- and multilayer in photoemission data [118]: for rigid shifts of valence electron features (typically the HOMO-derived peak) and core-levels we assume physisorption and chemisorption in all other cases. Within this definition it becomes apparent that the pentacene oxo-derivative P2O is physisorbed on Ag(111) and P4O is chemisorbed on the same

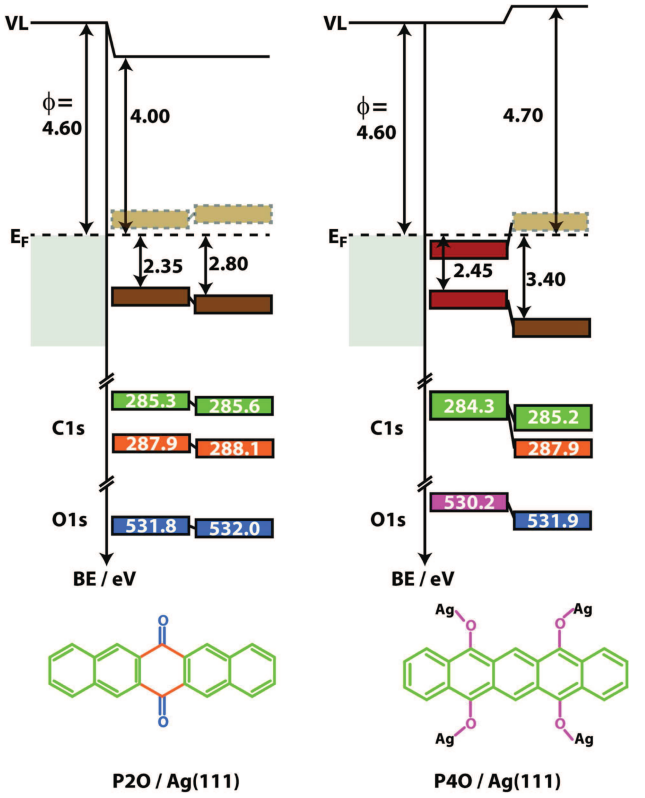

Figure 5. Schematic energy-level diagrams for P2O and P4O on Ag(111). On the left the Ag substrate with its work function ϕ and Fermi level E_F is displayed. The middle panels correspond to a P2O monolayer, with the position of the vacuum level (VL), the position of the (former) LUMO, the HOMO position and the energetic position of C1s and O1s core-levels. In the right panels the corresponding values for multilayer coverage are displayed. All binding energy values are given in eV, energy axes are not to scale. The molecular structures on the bottom show possible resonance structures in the monolayer. The energy-level diagrams are drawn using UPS and XPS data published in references [78, 118].

substrate. Thus, we use schematic energy-level diagrams based on photoemission data [78, 118] of P2O and P4O on Ag(111) (figure 5) to illustrate the impact of organic–metal coupling strength on interface dipoles and ELA.

The push-back effect, which leads to Δ_{p-b}, is related to the electron density spilling out into vacuum at clean metal surfaces [119–121]. Push-back takes place at virtually all organic–metal interfaces as the surface dipole part of the metal work function will be decreased by the mere presence of the molecular monolayer [29, 37, 122]. There is a clear correlation between Δ_{p-b} and adsorption distances [107, 123–125]. For physisorbed systems the push-back effect is often the main contribution to ΔVL and can be held responsible for most of the 0.60 eV shift at the P2O/Ag(111) interface.

For the discussion of interfacial charge transfer it is helpful to distinguish between *integer* and *fractional* charge transfer (figures 4(c) and (d)) [115, 126, 127]. While the latter is usually related to chemical bond formation, the former can also occur for weakly interacting systems and is then a result of *Fermi level pinning* [38, 128]. This happens for high (or low) substrate work functions for which a vacuum level controlled ELA would lead to a situation with the HOMO (LUMO) being

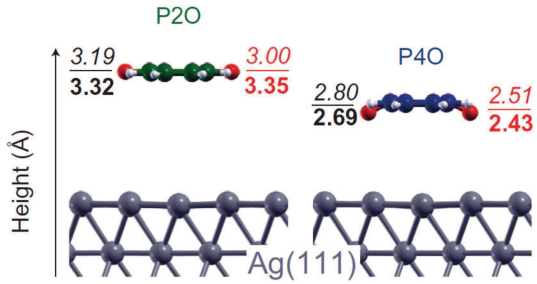

Figure 6. Vertical adsorption heights of P2O and P4O on Ag(111). Bold numbers refer to experimental and italic numbers to theoretical results, black numbers to carbon and red numbers to oxygen. For better visibility, the molecular distortions are not drawn to scale. Reprinted by permission from Macmillan Publishers Ltd: Nature Chemistry [78], Copyright (2013).

above (below) the Fermi level. In such cases thermodynamic equilibrium is maintained by an interfacial charge transfer. Thus, notably, also in the absence of any specific interfacial interaction charge transfer across an organic–inorganic interface can take place. Interestingly, the HOMO- (LUMO-) levels are typically pinned several 100 meV below (above) E_F [38, 45, 46, 98, 129, 130]. This is due to a certain degree of disorder in molecular thin films leading to a broadening of HOMO and LUMO density-of-states (DOS) [46, 47]. The relationship between DOS shape and ELA has been addressed in several publications [46, 47, 98, 131, 132] and is beyond the scope of this review. Likewise, for ELA at organic–organic interfaces, the reader is referred to references [38, 41, 106, 133–136].

The above mentioned screening effect leads to rigid energy-level shifts (typically several 100 meV) of valence and core-levels to higher binding energies between monolayer and multilayer coverage of organic thin films [37, 103]. This is the case for physisorbed P2O on Ag(111) (figure 5). For chemisorbed systems, the expected shifts due to screening can be overcompensated by the strong chemical coupling at the organic–metal interface. This becomes apparent for P4O on Ag(111); in this particular case, chemisorption goes along with a filling of the former LUMO. The charge transfer counteracts the VL decrease by push back leading to a constant VL upon contact formation. The apparent vacuum level alignment is, however, most likely coincidental. For related systems also a pronounced *increase* in the effective metal work function has been observed [58, 137, 138]. Such systems will be discussed in more detail in section 4.3. The relatively strong chemisorption of P4O on Ag(111) leads to a rehybridization of the molecules in the monolayer (a possible resonance structure is shown in the bottom of figure 5). This is in line with the experimentally determined vertical adsorption distances (figure 6), which show a pronounced distortion of P4O upon adsorption on Ag(111) [78].

Overall, the P*x*O/Ag(111) systems (figure 5) demonstrate some potential pitfalls in interpreting energy-level diagrams: for P2O/Ag(111) an apparent interface dipole mimics strong interaction, whereas the charge transfer at the P4O/Ag(111) interface leads to apparent vacuum level alignment. Thus, additional information is necessary to fully understand and describe organic–metal interface energetics. In particular, a precise knowledge of the vertical adsorption distance is necessary for a proper description of the adsorption behavior.

2.2. Role of the substrate

As discussed above, one can distinguish two limiting cases within the domain of metal–organic interactions, namely, physisorption and chemisorption. The adsorption distances are therefore expected to range between the sum of the van der Waals radii $\sum r_{vdW}$ for pure physisorptive bonding and the sum of the covalent radii $\sum r_{cov}$ for pure chemisorptive bonding. The corresponding values for carbon atoms interacting with the three noble metals are given in table 1. Obviously, the differences between van der Waals and covalent bonding for a given substrate material (being 1.1–1.3 Å) are much larger than the differences related to the choice of the substrate, i.e. Cu, Ag or Au. XSW experiments, however, consistently show that typical adsorption distances on these substrates are not similar and that the different *reactivity* of those materials is a key factor. For that purpose, the electronic properties of the substrates have to be discussed in some detail [139].

In metals, narrow d- and broad sp-bands form the valence-band states, where the latter are more likely to interact with a given adsorbate. At a certain distance, the molecular orbitals will start to overlap with those of the surface atoms. Initially, the adsorbate orbitals will broaden and shift in energy (see figure 3) as a consequence of the interactions with the rather delocalized sp-electrons and only if the d-orbitals are involved will the adsorbate levels split into bonding and antibonding states, generally one being below and the other above the metal band. In this context, one can relate the interaction strength and the degree of chemisorption to the different orbitals involved. For instance, the term *weak chemisorption* is used for the case where only sp-orbitals are involved. When d-orbitals are also at play, the filling of the bonding and antibonding states influences the interaction strength as well. Thus, a strong bond is associated to the filling of only bonding states. Conversely, the partial or total filling of antibonding states induces a repulsive interaction that counteracts the attractive forces exerted by the sp-electrons. The degree of filling is related to the relative position of the d-states with respect to the Fermi level. Also, the broadening of these states is responsible for the degree of repulsion with the adsorbate states. Indeed, a broader state increases the overlap with the adsorbate orbitals and subsequently the cost of orthogonalizing the wave functions to avoid Pauli repulsion. In light of this, moving from left to right in the periodic table, i.e. from transition to coinage metals, the outmost d-states shift down in energy away from the Fermi level [147], thus explaining the decreasing reactivity within this series. The broadening of the band, on the other hand, increases when moving down the column or from right to left in the periodic table, which explains why Cu is said to be more reactive than Au. This trend is also reflected in the averaged vertical adsorption distances d_H of the carbon atoms in the molecular backbone of adsorbates on such surfaces. Figure 7 shows that d_H decreases for each perylene derivative on the (111)-surfaces of noble metals in the order Au–Ag–Cu. This finding can be considered as a qualitative trend for most COMs

Table 1. Selected substrate parameters: atomic number Z; sum of van der Waals radii $\sum r_{vdW}$ for carbon and noble metal atoms [140]; sum of covalent radii $\sum r_{cov}$ for carbon and noble metal atoms [141]; lattice plane spacing d_0 for the (111) Bragg reflection; corresponding photon energy $E_{Bragg} = hc/2d_0$ in back-reflection ($\theta_{Bragg} \approx 90°$); work function ϕ_{subs} of the bare substrates [142]. Note that the small surface relaxations of Cu(111) [143] and Ag(111) [144] are often neglected for the determination of the adsorption distances, whereas the reconstruction of Au(111) [145, 146] should be taken into account.

	Z	$\sum r_{vdW}$ (Å)	$\sum r_{cov}$ (Å)	d_0 (Å)	E_{Bragg} (keV)	ϕ_{subs} (eV)	(111) surface
Cu	29	3.17	2.08	2.086	2.972	~4.9	Small relaxation [143]
Ag	47	3.49	2.21	2.357	2.630	~4.6	Small relaxation [144]
Au	79	3.43	2.12	2.353	2.634	~5.3	$(22 \times \sqrt{3})$ herringbone reconstruction [145, 146]

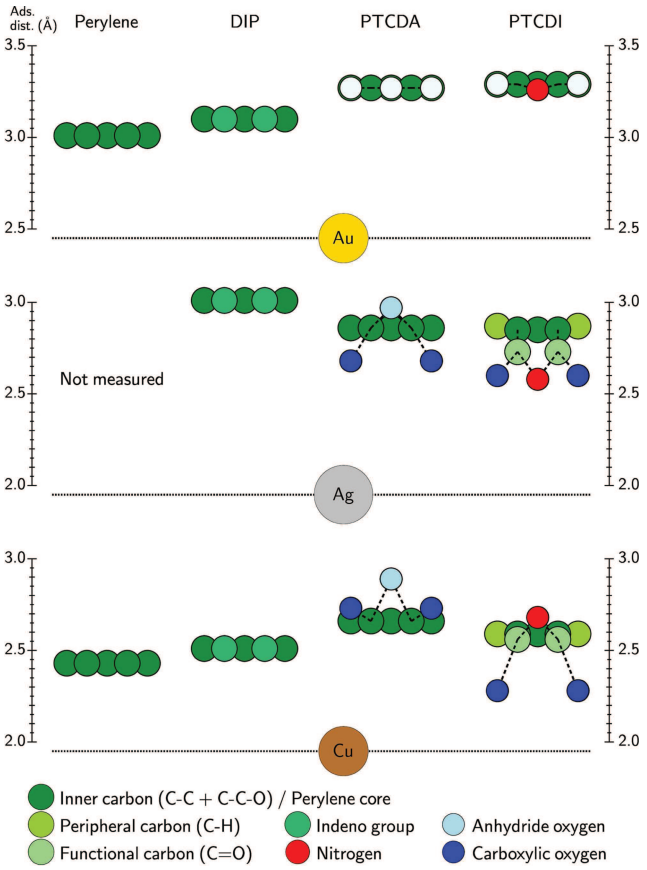

Figure 7. Experimentally determined vertical adsorption distances of perylene (derivatives) on the (111)-surfaces of the noble metals. Reprinted figure with permission from [80], Copyright (2017) by the American Physical Society. The data is taken from these references: perylene and PTCDI from reference [80], PTCDA on Au(111) from reference [148], PTCDA on Ag(111) from reference [149], PTCDA on Cu(111) from reference [150], DIP from reference [151].

on these surfaces, but precise quantitative predictions can only be done if the nature of the adsorbate is taken into account.

For the interaction with a given adsorbate, not only the chemical composition of the bulk crystal is important, but also its surface structure and termination. Both the transfer of charge across the interface and the formation of bonds often need some energy barriers to be overcome. For all metal substrates the work function ϕ decreases with increasing 'openness' of the surface being considered. Thus, closed-packed surface structures, i.e. fcc(111), bcc(110), and hcp(001), show the highest ϕ and the lowest reactivity. Likewise, defects, step edges and kinks act as interaction centers for adsorbates, which in some cases migrate across the flat terraces until they find a suitable location. In all these cases, the electronic and/or chemical interaction, with the extreme case of adsorbate dissociation, is favored by the lower energy barriers caused by elements that disrupt the surface potential landscape due to dangling bonds or excess/defect of charges, which may be recovered by the interaction with the adsorbate.

Of particular importance for CT effects is the presence of surface states, which form as a consequence of the reduced coordination of the topmost atoms compared to those in the bulk [152, 153]. Due to the termination of the crystal and the change of the electronic band structure new states confined to a region very close to the surface may exist. While these states appear even on perfect surfaces, the presence of defects, impurities or even adsorbates may create new *interface states* localized around them. Similar to the doping in semiconductors, surface/interface states may act as a center for charge exchange or reaction when a certain adsorbate is present.

In the context of this review, a large fraction of the studies in the literature have focused on the (111)-surfaces of Au, Ag and Cu. These are relatively inert and less prone to reacting with aromatic adsorbates. Also, for the noble metals they are the ones with the lowest energy, meaning that they are preferred in evaporation processes, giving them a slightly higher practical relevance than, e.g., (110) and (100). Recently, also other orientations of the noble metals [154–156], alloys [157, 158] as well as ZnO [108, 110, 586] have been investigated, see the list in section 4. For more details on the substrate surface without adsorbates, we refer to reference [159].

2.3. Role of the molecule

The description of organic molecules is largely based on the concept of *localized bonds* [160]. On metal surfaces, however, this approach might be questioned and is scrutinized, e.g., by specific chemical modifications of the π-conjugated systems being investigated. It is well known and understood how functional groups impact gas phase properties of COMs [161–164]. The particular nature of those functional groups may stabilize the COM or modify the HOMO–LUMO gap and other energy-levels. For instance, electronegative side-groups like fluorine generally increase the EA and render the COM thus more n-type [165].

For molecules in contact with the metal substrate functionalization can lead to additional effects like fostering or hindering intermolecular interactions and thereby increasing or decreasing the interaction strength. That way, e.g. perfluorination of pentacene reinforces the repulsion with metal substrates and can change the interaction from chemisorption to physisorption [74]. Moreover, in the contact layer the desired functionalization effect can even be nullified as shown in the bottom of figure 5 for P4O: the possible resonance structure of weakly interacting P2O molecules in the contact layer to Ag(111) are identical to the gas phase structure. Importantly, the conjugation does not extend over the pentacene backbone but is broken by the keto-groups. For chemisorbed P4O on Ag(111), however, by re-hybridization on the surface the conjugation can extend over the entire backbone of the molecule and thereby resemble PEN molecules [78]. For perylene derivatives, substitution can lead to significant differences of the adsorption distances and adsorption induced distortions [80], which are especially pronounced on the relatively reactive Ag(111) and Cu(111) surfaces (figure 7).

Notably, all *site-specific interactions* affect also the electronic structure and can therefore be used to tailor interface energetics [66, 166, 167]. In general, a competition of adsorbate–substrate interaction between the π-system of the COM and the functional groups can take place. For example, a submonolayer of the acceptor molecule HATCN (1,4,5,8,9,11-hexaazatriphenylenehexacarbonitrile, $C_{18}N_{12}$) is lying flat on Ag(111) to maximize the interaction of the π-system and the substrate. Increasing the coverage to a full monolayer, however, induces a re-orientation of the HATCN to an edge-on geometry due to the efficient interaction of the cyano-groups with the substrate [168]. Moreover, the flexibility of the COM plays also an important role. While peripheral substitution of the molecules often leads to large adsorption induced molecular distortions [66, 169], functional groups belonging to a central part of the conjugated molecular backbone induce no or only negligible distortions [170]—even at strongly coupled organic–metal interfaces.

2.4. Role of in-plane interactions

While the focus of this review is on the vertical interactions, we may briefly comment on the impact of lateral forces. Obviously, the influence of the surrounding molecules dominates the purely organic environment of the multilayer regime, most prominently through the π–π interactions of adjacent molecules [171, 172]. For a monolayer on a metal, though, the molecule–molecule (i.e. in-plane) interactions are usually much weaker than those between the molecules and the substrate. Thus, lateral interactions are often only a small correction, and the substrate largely controls the interface properties and the ELA. There are two notable exceptions, though. One is for molecules with a large intrinsic molecular dipole. For these, the electrostatic interaction of nearby molecules, which can be experimentally tuned via the molecular coverage, influences the alignment of the molecular dipoles and is directly responsible for the overall interface dipole, which in turn induces work-function changes of the substrate [173]. The other is for heteromolecular monolayers adsorbed on metal substrates [50, 83, 174]. In this case, combining pairs of donor–acceptor molecules has been proven to be an effective method to tune the metal work function [175].

From a more fundamental perspective, it is known that an increased intermolecular interaction can weaken the molecule–substrate coupling and vice versa [176], as evidenced by changes in the adsorption distance and the frontier orbitals of the molecule. In this regard, for homomolecular systems, the balance favoring one or the other may be tuned by changing the temperature [77, 176–178], the coverage [76, 179] as well as the nature of the substrate [80, 180, 181]. A nice example of this is found in reference [176] with STM and XSW measurements of PTCDA taken at RT, which show the well-known herringbone structure, and at LT, where the first layer becomes disordered. The decrease of the intermolecular interactions at LT lowers the average adsorption distance of PTCDA and increases the bending of the oxygen atoms towards the surface and goes along with an increased filling of the former LUMO level [176], all pointing towards an enhanced coupling with the substrate. For a detailed discussion of the in-plane arrangement of molecules and their epitaxy with the substrate, the reader is referred to references [182–184].

3. Experimental methods

Pivotal to this review are studies performed with the XSW technique and photoelectron spectroscopy. In this section we will give a general overview of the fundamentals and the experimental challenges of these, mainly within the context of organic–metal interfaces. Some other complementary techniques in this context will also be mentioned without going into much detail or claiming to be exhaustive.

3.1. The x-ray standing wave technique

The XSW technique is an interferometric method that exploits the standing wave field I_{XSW} created by Bragg diffraction of the incoming x-ray beam. By measuring characteristic photoemission signals, that are related to the local field strength at the position of the excited atomic species, one can derive high-precision and chemically sensitive adsorption distances of molecules on single crystals (see figure 8 for a schematic).

3.1.1. Concept of XSW measurements. In 1964 Boris W Batterman first demonstrated that the fluorescence intensity emitted from a single crystal, illuminated with x-rays, changed characteristically when rocking the crystal around the Bragg condition due to the presence of an x-ray standing wave field [185]. By matching the maxima and minima of the fluorescence signal with the reflected x-ray intensity around the Bragg angle, he correlated them with the relative position of the atomic planes of the crystal. A few years later, he used this concept to locate, within a silicon single crystal, the position of arsenic atoms, used as dopants, relative to the silicon

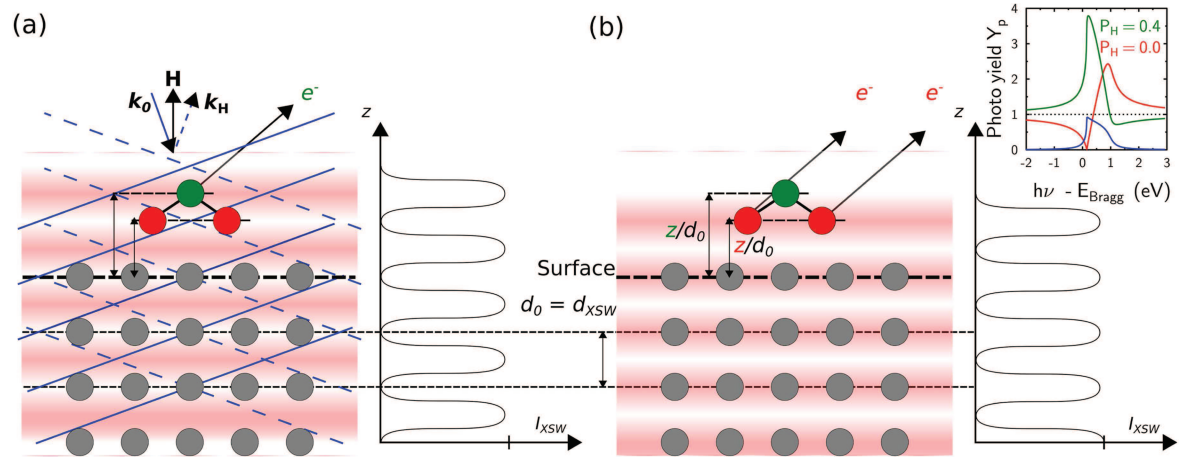

Figure 8. Schematics of the XSW-field formation. (a) An incoming x-ray plane wave with wave vector $\mathbf{k}_0$ interferes with the Bragg-reflected wave with the corresponding wave vector $\mathbf{k}_H$ and creates an interferences field inside as well as above the crystal surface. Here, the periodicity between maxima (or minima) of intensity d_{XSW} equals the lattice plane spacing d_0 along the diffraction direction **H**. (b) For a given scattering geometry the interference field is stationary, but if one scans the incident angle or photon energy around the Bragg condition, the intensity profile I_{XSW} can be shifted by $d_0/2$. Since the absorption of x-rays around the Bragg conditions, which depends on the relative position of the atoms (z/d_0) within the field, determines the number of emitted photoelectrons, the photo yield variation Y_p reveals the corresponding adsorption distance. Importantly, different elements within the adsorbed molecule, as symbolized by the green and red color of the atoms, can be distiguished using their specific core-level signal. In the inset, two simulated XSW scans are shown, with the normalized reflectivity (blue line) and the photoelectron yields as a function of the beam energy relative to the Bragg condition (green and red line). The coherent positions P_H of the two species, as introduced in equation (1), can be easily converted to the adsorption distance. The strong dependence of the photoelectron yield with respect to the position of the emitter within the XSW field, which is the origin of the precision of this technique, can be readily seen by the characteristic modulation of these curves.

atomic planes [186]. Soon thereafter, it was exploited that the XSW field extends outside the crystal surface [187], opening up the door to not only the mapping of dopants within a crystal structure [14, 188] and the study of buried interfaces [189–191], but also the location of adsorbates on the crystal surface [15]. For the latter, initially, adsorbed atoms were studied [15, 16], Langmuir–Blodgett films [192] and atomic layers followed [193]. Some smaller molecules deposited on different surfaces started to be studied in the 1990s [194–197], while, the first measurements of conjugated organic molecules on metal surfaces came a few years later [17, 18, 198, 199].

Without entering into the exact mathematical derivation of the XSW field, which is based on dynamical diffraction theory [200], one can explain the basic principle of the XSW technique using the fundamental equation [14, 82, 188, 201–203]

$$Y_p(h\nu) = 1 + R + 2\sqrt{R}\, f_H \cos(\nu - 2\pi P_H) \qquad (1)$$

which relates the normalized photo yield Y_p from a given chemical species, the intrinsic reflectivity R of the crystal and the relative phase ν between the incoming and the reflected wave with the two structural parameters f_H and P_H. The so-called coherent position P_H, which takes values between 0 and 1 (being both geometrically equivalent), is directly related to the (mean) position of the species being considered via

$$d_H = (n + P_H)d_0 \quad n = 0, 1, 2, \ldots \qquad (2)$$

where n introduces an ambiguity that stems from the periodicity of the XSW field of period d_0 (cf table 1). In most cases, this ambiguity can be removed with common sense and the physical constraints of the system. The index H in equations (1) and (2) refers to the reciprocal lattice vector of the Bragg reflection employed in the experiment. The coherent fraction f_H is related to the vertical ordering of the species contributing to a given d_H. It assumes values between 0 and 1, with 0 as the outcome of randomly distributed emitters around d_H and 1 the case where all are adsorbing at d_H. Different effects contribute to the decrement of f_H, for instance, thermal vibrations and static disorder. We note that, besides the obvious reason that the adsorption distance only makes sense within the first adsorbed layer of molecules, the significance of the experimental P_H values is limited by f_H. In other words, for a highly disordered layer ($f_H \approx 0$), it is pointless to associate any adsorption distance. This has two direct consequences: first, f_H can be used as confidence parameter for the obtained adsorption distance and secondly, coverages below or equal to a full monolayer are desirable to avoid artificially decreasing f_H.

We note that for practical purposes equation (1) has to be refined to account, e.g., for the broadening of the reflectivity curve due to the monochromator and the imperfections of the crystals. Also, non-dipole effects in the photoemission process, which affect the angular distribution of the photoelectrons [204, 205], have to be considered in the data analysis.

3.1.2. Experimental considerations. Generally, datasets for two experimental quantities are required to model the XSW field and subsequently extract the position of a given species

relative to the lattice planes of the crystal, i.e. the reflectivity $R = R(E)$ and photo yield $Y_p(E)$ when scanning around the Bragg condition $E = E_{Bragg}$. The reflectivity can be measured with a camera directed at a fluorescence screen conveniently located in the chamber and the photo yield is extracted from fluorescence, Auger or photoelectron spectroscopy data from the species of interest: here, we restrict our discussion to photoelectrons, which are measured through XPS scans performed with different photon energies around E_{Bragg} (cf table 1).

The use of the XSW technique is constrained by rather demanding experimental requirements. Certainly, the first major challenge is the indispensable crystal quality of the substrate, both at the surface as well as in the bulk, which is responsible for the coherence of the standing wave field. In addition to the high photon flux required for these experiments the need to tune the x-ray energy limits the usage of the technique to synchrotron facilities [206]. Here, beamlines with insertion devices, crystal monochromators and complex x-ray optics can provide a stable and highly brilliant x-ray beam, that can be (de-)focused to avoid beam damage on the samples. The reader is referred to references [207–209] for a more detailed explanation of the beamline requirements.

The experimental geometry, namely, the relative direction of the incoming beam with respect to the sample and the electron analyzer is essential. It can be shown that when creating the interference field in back-reflection (see figure 8), i.e. the incoming and the Bragg-reflected beam being almost perpendicular to the diffracting crystal planes (diffraction angles θ_{Bragg} close to 90°), the intrinsic angular width of the reflectivity curve is largest. Thereby, the need for nearly perfect crystallinity of the substrates is relaxed [210]. XSW experiments performed under these conditions are referred to as normal-incidence (NI)XSW and have become standard for measuring adsorption distances of larger molecules on metals.

Recently, it has been demonstrated that dedicated beamlines such as I09 at Diamond Light Source (UK) [209], which is operational since 2013, can implement significant improvements in performance and usability compared to previous installations. Due to the optimized experimental setup and data-acquisition methods the signal-to-background and signal-to-noise ratio of the photoelectron spectra could be improved without risking extensive beam damage even for molecular systems. If the electron analyzer is positioned at an angle of 90° with respect to the incident x-ray beam (as realized at I09), the substrate background in the spectra is strongly suppressed and also the non-dipole contributions to the photoelectron yield are minimized. Overall, the challenges associated with XSW measurements have to some degree shifted away from the technical side and more towards the sample preparation and data analysis. Indeed, by using a proper core-level model to account for the different contributions to the photoelectron yield one can extract adsorption distances for the chemically inequivalent species within a molecule. Hence, the systematic combination of XSW experiments with high-resolution XPS allows to resolve intramolecular distortions that were not accessible before and thereby extend the significance of XSW results beyond average adsorption distances [80, 154, 211]. For that matter, accurate [212] and preferably theory-backed core-level models [213, 214] are necessary.

Over the years, different software packages have been used for handling (NI)XSW data. For fitting the core-level spectra the commercial CasaXPS [215] has become very popular. For the analysis of the resulting photoelectron yield data, on the other hand, there are various specialized tools available. Recently, Bocquet *et al* discussed the general formalism and contributed a new open source program with graphical user interface (Torricelli) that facilitates the fitting of XSW data [216]. As also pointed out in reference [205], the analysis can be non-trivial, if the large angular aperture of the analyzer and the finite tilt of the sample are considered. As a concluding remark, we also note that via off-normal XSW measurements, i.e. using a Bragg reflection with a finite in-plane component of **H**, it is in principle possible to triangulate the position of adsorption sites [217]. Since for large adsorbate molecules this can be difficult [155], our focus is on the vertical structure along the surface normal.

3.2. Photoelectron spectroscopy

Photoelectron spectroscopy (PES) is a well-known and established technique to determine the electronic structure of solids and is described in detail in various books and review articles [218–227]. In this section we will, thus, deal with issues specific to PES on organic thin films [228–240] including the main pitfalls and obstacles.

3.2.1. Ultraviolet photoelectron spectroscopy. First, we will focus on ultraviolet photoelectron spectroscopy (UPS). Figure 9 displays on the left side two energy-levels (HOMO and HOMO − 1) of an organic thin film on a metal substrate, for which the continuous occupied DOS is shown. The sample is irradiated with monochromatic UV-light with photon energy $h\nu$ and the resulting photoemission intensity is shown on the right side of figure 9. An electron analyzer measures the kinetic energy E_{kin} and intensity of photoelectrons. The resulting spectra are usually plotted as function of binding energy E_B with the Fermi level serving as energy reference ($E_B^F = 0$ eV). The information depth is limited by the inelastic mean free path of photoelectrons. The so-called 'universal curve' gives a value of ∼7 Å for electrons with a kinetic energy of 15 eV (typical for measurements with HeI) in organic materials [241]. Consequently, for (sub)monolayer coverages of a flat lying COM film on a metal, molecular features and substrate features appear concomitantly.

In addition to valence electron features, also secondary electrons (gray in figure 9) contribute to the spectrum. These electrons have been inelastically scattered in the sample and thus lost the information about their initial state. However, they can be used to determine the VL of the sample, since

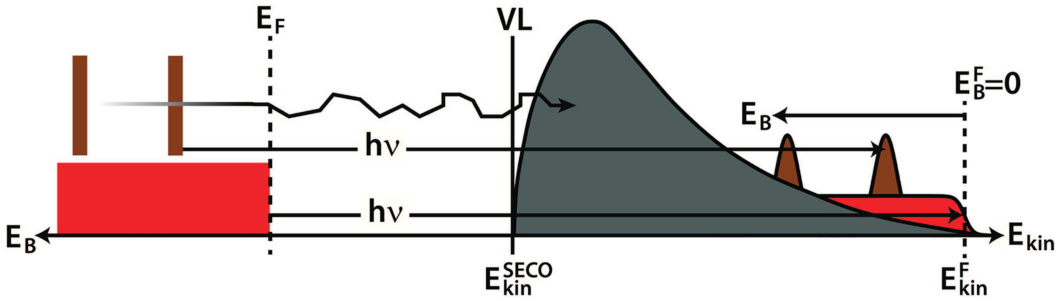

Figure 9. Schematic valence energy-levels and UP spectrum of a COM monolayer on a metal substrate. The sample is illuminated by photons with energy $h\nu$. Photoelectrons from the metal Fermi level E_F have the highest kinetic energy (E_{kin}^{F}). Usually, the Fermi level is used as energy reference to define the binding energy E_B of valence electron features. Inelastically scattered secondary electrons lost the information about their initial state and the position of the secondary electron cutoff E_{kin}^{SECO} allows to determine the vacuum level (VL) of the sample. The sketch is strongly simplified, in particular the measurement process itself, i.e., the impact of the spectrometer on measured kinetic energies, is neglected. More detailed sketches can be found, e.g., in references [1, 228].

at a certain kinetic energy (E_{kin}^{SECO}) the energy of secondary electrons is not sufficient to overcome the surface potential of the sample. At this energy their intensity is dropping to zero, which is often called secondary-electron cutoff (SECO). The VL of the sample (w.r.t. E_F) is given by the difference of the photon energy and the whole width of the spectrum, i.e.:

$$\mathrm{VL} = h\nu - (E_{kin}^{F} - E_{kin}^{SECO}). \quad (3)$$

This rather simplified description is sufficient to determine the VL of samples with a homogenous surface potential. However, as mentioned above, the adsorption of COMs usually modifies the work function of clean metal surfaces. For submonolayer coverages or in the case of island growth, the sample features local surface potentials [119, 238, 242–247]. Depending on the lateral dimensions of these inhomogeneities, either two separate SECOs can be observed (for large island sizes) or the SECO position is determined by the area-weighted mean of the local surface potentials. A detailed description and guidelines on how to analyze SECOs are given in reference [244]. This publication describes, furthermore, how to determine IEs of organic thin films, which are defined by the SECO and the onset of the HOMO-derived peak [1–3, 228, 244, 248].

In general, for discussing interfacial interactions often 'monolayer' and 'multilayer' energy-levels are compared (cf figure 5). The thickness of vacuum-sublimed thin films in organic molecular beam deposition (OMBD) is usually measured by a quartz-crystal micro balance and corresponds, thus, to a nominal mass thickness. In that process, layer-by-layer growth is rather the exception than the rule and island or Stranski–Krastanov (island on wetting layer) growth dominates [249–253]. Thus, the first step in interpreting photoemission data is to identify the spectrum which is most dominated by monolayer contributions. A first hint gives the evolution of the SECO as adsorption induced charge rearrangements often saturate upon monolayer formation. For PEN, which may be regarded as the 'fruit fly' of organic surface science [74, 86, 124, 179, 236, 254–275], thickness-dependent UP spectra on Au(111), Ag(111) and Cu(111) [181] are shown in figure 10 as a typical example of UPS at organic–metal interfaces. Indeed, for PEN on Au(111) the VL (as deduced from the SECO position in figure 10(a)) decreases rapidly up to a nominal PEN thickness of 4 Å. However, this does not mean that a nominal thickness of 4 Å corresponds to a closed monolayer. It simply tells that from this thickness on, subsequently deposited molecules grow predominantly in multilayers.

The suppression of substrate features, e.g., the Au d-bands in a BE range from 2 to 8 eV in figure 10(b) or the Fermi-edge in figure 10(c), with increasing coverage can be used to estimate the growth mode of the adsorbate. However, the applicability of the universal curve to organic thin films has been questioned [276–278] and only qualitative statements are straightforward. For PEN/Au(111) the substrate Fermi-edge is still visible for a nominal coverage of 96 Å, which corresponded to more than 20 layers of flat lying PEN. This clearly shows that the growth mode is not layer-by-layer. For the spectra with a nominal thickness of 96 Å on Ag(111) and Cu(111), on the other hand, the Fermi-edge is (almost) invisible, pointing to less pronounced island growth.

The shape of HOMO-derived UPS peaks is often not simply Gaussian. For well ordered monolayers and sufficient experimental resolution, hole–phonon coupling [262, 279, 280] becomes evident in UP spectra as can be seen by the high-BE shoulder of the HOMO-derived peak in the spectra for a nominal coverage of 2 Å on Au(111) and Ag(111) (figures 10(c) and (d)). Furthermore, factors like the measurement geometry and the photon energy impact photoemission intensities. For example, the emission from the HOMO of flat-lying π-conjugated molecules has typically a maximum for an emission angle of 45° and a minimum for normal emission [115, 236, 281, 282].

The spectra in figure 10 are measured with an hemispherical analyzer and angle-integrated over ±12° along k_x, which is a typical measurement geometry. Also such angle-integrated spectra can reflect energy dispersing features, in particular

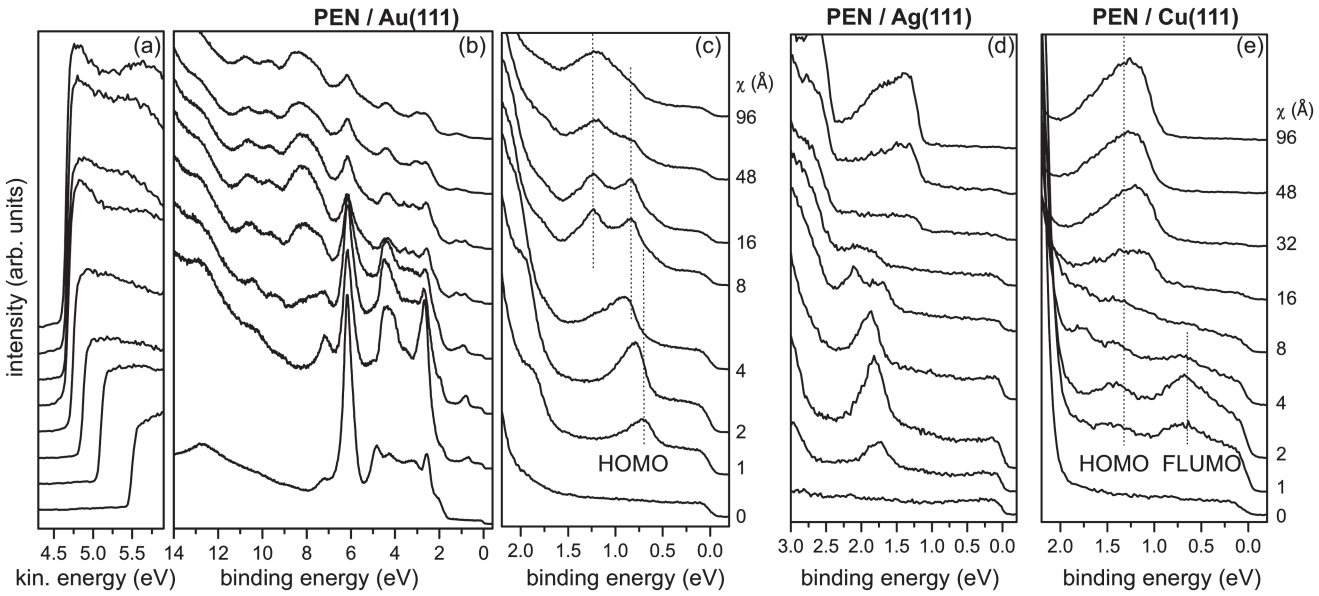

Figure 10. UP spectra of pentacene deposited on the (111)-surfaces of noble metals measured with the HeI excitation line. χ denotes the nominal pentacene thickness. For PEN on Au(111) the SECO region (a), a valence survey spectrum (b), and a zoom into the region close to the Fermi level (c) are shown. For PEN on Ag(111) (d) and on Cu(111) (e) only the zooms are shown. All valence electron spectra are measured with an emission angle of 45°. The lines are guides for the eye and mark the evolution of HOMO and FLUMO (former LUMO) features of PEN on Au(111) and Cu(111), respectively. The energy scale of the plots of the secondary electron spectra is corrected by the analyzer work function and the applied bias voltage. Thus, the SECO position corresponds to the VL position above the Fermi level. Reproduced from [181].

if rotational domains related to the substrate symmetry are involved. This explains the HOMO-shape of PEN in multilayers on Ag(111), in which PEN adopts a herringbone arrangement [283] and exhibits a band dispersion [284]. Notably, also former LUMO derived energy-levels of organic monolayers on metals can show intermolecular energy dispersion [285, 286]. For PEN on Au(111) the multilayer growth mode is still under debate [258, 261] and, hence, the multilayer HOMO features have not been unambiguously assigned [181]. Overall, great care has to be taken when comparing measurements obtained in different experimental setups. For example, in an early publication of PEN on Cu(111) the former LUMO-derived peak just below the Fermi level (figure 10(e)) has been overlooked [74]. Moreover, small differences in, e.g., temperature, substrate cleanness, evaporation rate or impurities, can have a significant impact on organic thin film growth and, consequently, the electronic structure [253, 255, 268, 287–291].

3.2.2. X-ray photoelectron spectroscopy. For XPS the electronic structure of the sample is probed with x-rays, whose higher photon energy make core-levels accessible [220, 223, 292, 293]. Core-levels provide information about the local chemical environment of the atoms, which gives rise to so-called chemical shifts in XP spectra [294, 295]. Figure 11(a) shows the C1s spectrum of a PTCDI multilayer on Au(111) [80] illustrating the strong chemical shift between carbon atoms in the functional groups (C=O) and in the perylene backbone. The chemically inequivalent carbon atoms within the molecule can be precisely resolved if the shift in energy is large enough, which is often the case for carbon bound to electronegative atoms (e.g. O and F). The binding-energy (or core-level) shifts associated with the chemical structure can be further modified by the molecular environment, for instance if there are strong intermolecular interactions, and/or by the proximity of the substrate. Intrinsic or extrinsic peak broadening is another complication when describing core-level signals. Its origin is manifold and a proper description often requires electronic structure calculations.

The fine structure of the core-levels can only be resolved using a sufficiently high energy resolution, which is feasible when measuring at synchrotron radiation facilities or with monochromatized lab-sources. Generally, monolayer spectra may include fingerprints of (chemical) interactions with the substrate [232, 296–298]. For PTCDI on Au(111) the interaction is weak [80] and therefore the multilayer (figure 11(a)) and monolayer (figure 11(c)) spectra are—except for a rigid shift due to screening—almost identical. PTCDI monolayers on Ag(111) and Cu(111), however, are chemisorbed [80], which is reflected in non-rigid shifts of the components attributed to different chemical environments of the multilayer versus the monolayer spectra; in particular, the energetic spacing between the C=O-derived peak and the main peak decreases for the PTCDI monolayer (figure 11(c)). In addition to the insight in the chemistry of adsorbates, chemical shifts in XPS facilitate the experimental determination of individual vertical binding distances for each carbon species using the XSW technique (figure 7).

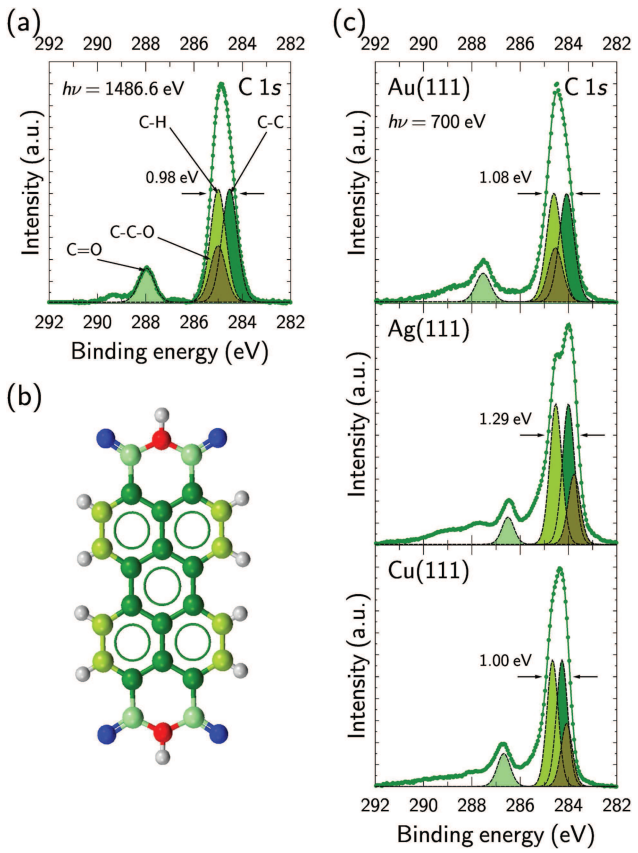

Figure 11. Influence of the environment on the core-level signals. Multilayer spectrum (a) of the C1s signal of PTCDI (b) compared to (sub)-monolayer coverages of the same molecule adsorbed on the noble metals (c). Reprinted figure with permission from [80], Copyright (2017) by the American Physical Society.

3.3. Complementary techniques

The XSW technique is mostly applied to the measurement of adsorption distances and molecular distortions perpendicular to the surface. Alternatively, photoelectron diffraction (PhD) [299] provides a full, local 3D positioning of a given species with respect to the surface atoms [300–302]. However, while rather successful for certain (preferably simple) systems, the data analysis and interpretation are not straightforward since inequivalent positions may be difficult to decouple, thus challenging its application to larger adsorbates [303, 304]. Similarly, LEED I–V may provide a 3D picture of an adsorbate [21–23], but the analysis of the data is computationally expensive and requires some initial guess of the adsorbate position. Both, PhD and LEED I–V require a certain degree of registry/commensurability between the adsorbate and the substrate, which limits their use to systems with in-plane order. Surface x-ray diffraction [20, 305–307], and specifically the so-called rod scans (along q_z) for the vertical structure, are slightly less demanding to model (thanks to the applicability of the kinematic, i.e. single-scattering, approximation), but the sensitivity to light elements is limited because of low x-rays scattering cross-sections. Importantly, it is very difficult to obtain element-specific positions needed to determine possible distortions/bending of the adsorbates. In contrast, relative positions, such as tilt angles, can be inferred with NEXAFS by exploiting the geometry-dependent absorption of x-rays without the need of long-range order [308–310]. We note that other popular techniques in the study of inorganic surfaces and interfaces such as reflection high-energy electron diffraction (RHEED), scanning-electron microscopy (SEM) or ion scattering-based techniques are not very common in our context because of the probable beam damage induced by the high energy of incoming particles. Some notable exceptions can be found though [311].

Although not the focus of this review, a full characterization of the interface geometry involves the in-plane structure of the adsorbed layers and their registry with the surface atoms. Scanning-tunneling microscopy (STM) [49, 174, 312–320] and low-energy electron diffraction (LEED) [182–184] are the most popular techniques in this context in addition to grazing-incidence x-ray diffraction [305], which provides the highest resolution. STM offers real-space images with atomic resolution, which can be combined with local spectroscopy measurements. However, any quantitative determination of vertical adsorption structures with STM is still challenging [321]. Notably, with atomic force microscopy (AFM) under UHV conditions one can estimate vertical bonding distances, although input from DFT-modeling is necessary to extract absolute numbers [322]. LEED offers reciprocal-space information that is averaged over a large sample area. With more elaborate versions such as LEED I–V, mentioned above, and spot-profile analysis LEED (SPA-LEED) a precise description of the adsorbate unit cell can be achieved [323]. Finally, low-energy electron microscopy (LEEM) provides in particular real-time information of the in-plane arrangement and morphology during growth [156, 324, 325].

In section 3.2 photoemission spectroscopy was introduced as a tool to study the energy-level alignment and interfacial coupling by using the energy information of photoelectrons. Beyond that, i.e. by exploiting also the momentum information of the electrons [115, 230, 235, 236, 281, 282, 326–328], new possibilities arise, which—although not within the scope of this article—shall be briefly summarized here. By angle-resolved and photon-energy dependent UPS measurement possible in-plane [235, 329–331] and out-of-plane [235, 285, 332] band dispersions of organic thin films can be accessed. Moreover, even for largely angle-integrated measurements the photoelectron angular distribution (PAD) provides insight into, e.g., the orientation of COMs on the surface [115, 236, 281, 282]. The vibrational fine structure of HOMO-peaks allows to assess charge reorganization energies and thus to estimate hopping mobilities by a 'first-principle' experiment [279, 333–336]. Moreover, the development of instrumentation over the last decades has made it possible to measure photoelectron reciprocal-space maps, often termed 'orbital tomography', which can be used to reconstruct molecular orbitals in real space and/or to precisely assign

photoemission intensities to a particular molecular orbital [115, 236, 286, 337–340].

Two-photon photoemission (2PPE) spectroscopy provides insight into electron dynamics of interface states [341–345]. In conjunction with real-space information, e.g., by LEED or STM, detailed insight in organic–metal coupling is possible [346–348]. Accessing the unoccupied density of states by inverse photoemission (IPES) is demanding, as cross-sections and overall energy resolution are notoriously low and, most importantly, beam damage can be a problem for organic thin films [97, 349, 350]. Some of these issues can be overcome by low-energy inverse photoemission spectroscopy (LEIPS) [266, 351]. Scanning tunneling spectroscopy (STS), as a local probe, accesses unoccupied states as well as occupied states close to E_F and can furthermore identify site-specific interactions at organic–metal interfaces [49, 352–357], also measurable with high-resolution electron energy-loss spectroscopy (HREELS) [358–361]. With *in situ* optical differential reflectance spectroscopy (DRS) optical properties can be measured during deposition [362–366].

Temperature-programmed desorption (TPD), with a proper modelling of the data, is used to measure the adsorption energy of a particular adsorbate on a given substrate [251, 367–373]. This parameter is important for a precise and quantitative distinction between adsorption regimes and has become, together with the adsorption distance, a benchmark parameter for state-of-the-art DFT calculations [8, 9]. Other uses include the study of thermally-activated on-surface reactions [374–377], the assessment of the thin-film growth, desorption kinetics and the thermal stability of a given system [251, 378–383]. Finally, *in situ* IR spectroscopy provides insight into the vibrational modes and changes thereof upon adsorption. It is also useful for identifying unknown sample compositions and may give information on changes in the adsorbate charge [168]. Of course, there are also many other spectroscopic techniques including, e.g., Raman and photoluminescence, that can be applied to study some of the isssues discussed here, but rather indirectly and outside the scope of this review.

4. Case studies

4.1. Overview and compilation of adsorption distances

We organize the case studies according to the strength of the interaction with the substrate. In the following sections, we present some well-studied systems that illustrate the current understanding of the different adsorption regimes, i.e. (vdW-dominated) physisorption, clear chemisorption and different cases in between. Most of the systems have been studied with both XSW and UPS.

For a general overview, we also refer to table 2 which provides a comprehensive list with adsorption distances of COMs on metals obtained by XSW measurements. For reasons of space only the molecule, the substrate and the adsorption distance for the different elements (if applicable) are reported.

4.2. Weakly interacting systems

Weakly interacting systems, which are dominated by dispersion forces and lack stronger covalent interactions, represent the limiting case of physisorptive bonding. Because they may be considered as test ground for DFT calculations with van der Waals (vdW) corrections, precise XSW results have become particularly important for evaluating the accuracy of these methods. A prototypical system falling in this category would be simply benzene on Ag(111), which was also pursued in references [8, 373]. With regard to possible applications in organic electronics, though, larger acenes or similar systems have greater practical relevance due to their more suitable energy-levels and smaller HOMO–LUMO gap, as well as greater thermal stability, since benzene desorbs already at 300 K.

As model system we may consider diindenoperylene (DIP, see figure 2), a π-conjugated organic semiconductor with excellent optoelectronic device performance, which has been studied over the last decade both in thin films [414–420] and in monolayers on noble metal surfaces [151, 421–426]. With respect to its chemical structure, DIP is a relatively simple, planar hydrocarbon without heteroatoms. In contrast to the intensely studied PTCDA [427–435], i.e. a molecule with the same perylene core but with four carbonyl groups, the specific DIP–substrate interaction is not complicated by polar side groups—see figure 7 which illustrates the significant influence of funtional groups on the bonding distances for these molecules. Moreover, the influence of intermolecular (lateral) interactions is expected to be smaller than for PTCDA.

Generally, the reliable prediction of the equilibrium structure and energetics of hybrid inorganic/organic systems from first principles represents a significant challenge for theoretical methods due to the interplay of, generally, covalentinteractions, electron transfer processes, Pauli repulsion, and vdW interactions. Recent years have seen substantial efforts to incorporate vdW interactions into density functional theory (DFT) calculations in order to determine the structure and stability of π-conjugated organic molecules on metal surfaces [7, 9, 10, 436–438]. This is particularly important for systems with significant vdW contributions to the overall bonding (i.e. in the absence of covalent interactions, etc) such as most π-conjugated molecules on weakly interacting substrates.

The effect of dispersion forces is nicely demonstrated in figure 12 by comparing DFT results obtained with the PBE exchange–correlation functional with and without including vdW interactions. It was found that dispersion corrected DFT calculations applied to DIP on three different noble metal surfaces yield vertical bonding distances that agree very well with the experimental data. The XSW results averaged over all carbon species of DIP, i.e. $d_H = 2.51 \pm 0.03$ Å for Cu(111), 3.01 ± 0.04 Å for Ag(111) and, taking the reconstruction of the gold surface into account, 3.10 ± 0.03 Å for Au(111), differ less than 0.12 Å from the minima of the calculated adsorption energies $E_{ads}(z)$ as they are marked by arrows in figure 12. As expected, those energies follow the trend

Table 2. List of experimental and element-resolved adsorption distances d_H determined with the XSW technique for COMs on (111) noble metal surfaces.

Molecule	Comment	Signal	d_H (Å)
Pentacene (PEN) derivatives on Cu(111)			
F_{4PEN} [169]		C 1s—total	2.37(4)
		C 1s—PEN backbone	2.36(2)
		C 1s—C(1,2)	2.24(8)
		C 1s—C(3,4)	2.42(2)
		C 1s—C–F	3.15(5)
		F 1s	3.40
P2O [78]		C 1s	2.34
		O 1s	2.02
P4O [78]		C 1s	2.25
		O 1s	1.98
PEN [74]		C 1s	2.34(2)
PFP [74]		C 1s	2.98(7)
		F 1s	3.08(4)
Perylene derivatives on Cu(111)			
DIP [151]	0.6 ML	C 1s	2.51(3)
DPDI [384]	Mobile phase	C 1s	2.68(6)
		N 1s—NH_2	2.40(11)
		N 1s—NH	2.20(3)
	Porous phase	C 1s	3.00(4)
		N 1s—N–Cu	2.83(3)
Perylene [80]	RT	C 1s	2.43(2)
	200 K	C 1s	2.38(2)
PTCDA [150]		C 1s	2.61
		O 1s—carb.	2.73
		O 1s—anh.	2.89
PTCDI [80]		C 1s—perylene core	2.61(2)
		C 1s—C==O	2.56(4)
		C 1s—C–H	2.59(4)
		C 1s—C–C + C–C–O	2.59(5)
		N 1s	2.68(2)
		O 1s	2.28(2)
TAT [170]		C 1s	2.48(4)
		N 1s	2.44(6)
Phthalocyanine (Pc) derivatives on Cu(111)			
CuPc	[178] 0.4 ML, 300 K	C 1s	2.64(7)
		N 1s	2.54(7)
	[178] 0.6 ML, 300 K	C 1s	2.57(7)
		N 1s	2.48(7)
	[178] 0.9 ML, 300 K	C 1s	2.79(7)
		N 1s	2.69(7)
	[178] 0.4 ML, 183 K	C 1s	2.62(7)
		N 1s	2.56(7)
	[178] 0.6 ML, 183 K	C 1s	2.53(7)
		N 1s	2.55(7)
	[178] 0.9 ML, 183 K	C 1s	2.82(7)
		N 1s	2.73(7)

Table 2. Continued

Molecule	Comment	Signal	d_H (Å)
F_{16}CuPc	[17]	C 1s	2.61
		N 1s	2.70
		F 1s	2.88
	[385]	C 1s	2.68
		F 1s	3.21
H_2Pc	0.7 ML	C 1s	2.45(7)
		N 1s	2.39(6)
GaClPc [386]	0.8 ML, Cl down	C 1s	4.44(7)
		N 1s	4.71(3)
		Ga 1s	4.21(5)
		Cl KLL	1.88(3)
VOPc [387]	0.5 ML, RT O up/ down coex.	C 1s	
		N 1s	
		V 2p	
		O 1s	
ZnPc [167]	0.7 ML	C 1s	2.49(3)
		N 1s	2.55(2)
		Zn $2p_{3/2}$	2.25(5)
F_{16}ZnPc [167]		C1s	2.66(10)
		N 1s	2.85(2)
		F 1s	3.15(9)
		Zn $2p_{3/2}$	2.58(5)
Porphyrin derivatives on Cu(111)			
2HTPP [388]	0.8 ML, 294 K	C 1s	2.40(3)
		N 1s—aminic	2.23(5)
		N 1s—iminic	2.02(8)
	0.8 ML, 146 K	C 1s	2.34(2)
		N 1s—aminic	2.28(5)
		N 1s—iminic	1.97(8)
CuTPP [388]	0.8 ML, 294 K	C 1s	2.38(2)
		N 1s	2.25(2)
	0.8 ML, 146 K	C 1s	2.33(2)
		N 1s	2.25(2)
CoP [389]		C 1s—C–C	2.44(9)
		C 1s—C–N	2.37(5)
		N 1s	2.33(6)
		Co 2p	2.25(4)
Other compounds on Cu(111)			
Azobenzene [390]	subML, 60 K	C 1s—C–C	2.36(2)
		C 1s—C–N	2.23(6)
	ML, 60 K	N 1s	2.02(2)
		N 1s	—
COHON [73]	0.4 ML	C 1s	2.46(4)
		O 1s	2.15(3)
F_4TCNQ [66]		C 1s	—
		N 1s	2.7(1)
		F 1s	3.3(1)
		C 1s	4.25(4)
Phenyl nitrene [390]	60 K	N 1s	1.17(4)
PYT [73]	0.9ML	C1s	2.31(3)
		O1s	2.04(6)
Naphtalene [391]	ML, 150 K	C 1s	3.04(3)
Azulene [391]	ML, 150 K	C 1s	2.30(3)

Table 2. Continued

Molecule	Comment	Signal	d_H (Å)
Pentacene (PEN) derivatives on Ag(111)			
P2O [78]		C 1s	3.32
		O 1s	3.35
P4O [78]		C 1s	2.69
		O 1s	2.43
PEN [179]	0.50 ML, 295 K	C 1s	2.99(1)
	0.50 ML, 145 K	C 1s	3.04(1)
	0.75 ML, 295 K	C 1s	3.13(1)
	0.75 ML, 145 K	C 1s	3.13(1)
PFP [392]		C 1s	3.16(6)
		F 1s	3.16(6)
Perylene derivatives on Ag(111)			
DIP [151]	0.5 ML	C 1s	3.01(4)
NTCDA	[199] relaxed ML	O 1s	3.02(2)
		O KLL	3.03
	[199] compressed ML	O 1s	3.12(3)
		O KLL	3.06
	[393]	C 1s	2.997(16)
		O 1s—total/O KLL	2.872(14)
		O 1s—carb.	2.747(25)
		O 1s—anh.	3.004(15)
PTCDA	[18, 148, 150]	C 1s	2.86
		O 1s—carb.	2.68
		O 1s—anh.	2.97
	[176] LT	C 1s	2.80(2)
		O 1s—carb.	2.49(4)
		O 1s—anh.	2.83(4)
	[149] 300 K	C 1s	2.86(1)
		O 1s—total	2.86(2)
		O 1s—carb.	2.66(3)
		O 1s—anh.	2.98(8)
	[149] 100 K	C 1s	2.81(2)
		O 1s—total	2.67(3)
		O 1s—carb.	2.50(4)
		O 1s—anh.	2.83(4)
PTCDA	[394] Surf.	C 1s site A	3.63(4)
	Pb_1Ag_2 alloy	C 1s site B	3.80(4)
		O 1s—carb. site A	3.33(2)
		O 1s—carb. site B	3.61(2)
		O 1s—anh. site A	3.52(9)
		O 1s—anh. site B	3.74(5)
		Pb 4f—bare	0.41(2)
		Pb 4f—PTCDA	0.49(1)
	[79] K-doped ML	C 1s perylene core	3.12(2)
	(K_2PTCDA)	C 1s C==O	3.26(7)
		O 1s—carb.	3.36(7)
	(K_2PTCDA)	O 1s—anh.	3.36(5)
		K 2p—PTCDA	3.23(3)
		K 2p—Ag	3.26(30)

Table 2. Continued

Molecule	Comment	Signal	d_H (Å)
PTCDI [80]		C 1s—perylene core	2.86(2)
		C 1s—C==O	2.73(3)
		C 1s—C–H	2.87(2)
		C 1s—C–C + C–C–O	2.85(2)
		N 1s	2.58(3)
		O 1s	2.60(3)
TAT [170]		C 1s	2.99(5)
		N 1s	2.88(10)
Phthalocyanine (Pc) derivatives on Ag(111)			
CuPc	[77] 0.5 ML, 300 K	C 1s	3.049(5)
		N 1s	3.00(4)
		Cu $2p_{3/2}$	2.98(4)
	[77] 0.85 ML, 300 K	C 1s	2.993(3)
		N 1s	3.03(4)
		Cu $2p_{3/2}$	2.90(4)
	[77] 1.00 ML, 300 K	C 1s	3.089(3)
		N 1s	3.04(4)
		Cu $2p_{3/2}$	2.97(4)
	[77] 0.5 ML, 153 K	C 1s	2.999(4)
		N 1s	2.94(4)
		Cu $2p_{3/2}$	2.89(4)
	[77] 0.85 ML, 140 K	C 1s	3.010(2)
		N 1s	3.01(4)
		Cu $2p_{3/2}$	2.94(4)
	[77] 1.00 ML, 140 K	C 1s	3.077(2)
		N 1s	3.07(4)
		Cu $2p_{3/2}$	3.02(4)
	[395] 1.00 ML, RT	C 1s	3.02(5)
		N 1s	3.00(5)
		Cu $2p_{3/2}$	3.09(5)
	[394] Surface	C 1s	3.77(2)
	Pb_1Ag_2 alloy	N 1s	3.68(2)
		Cu $2p_{3/2}$	3.62(2)
		Pb 4f—bare	0.44(1)
		Pb 4f—CuPc	0.44(1)
F_{16}CuPc	[17]	C 1s	3.25
		F 1s	3.45
FePc [396]	No dosing	C 1s—C–C	2.92(5)
		C 1s—C–N	2.83(5)
		N 1s	2.71(7)
		Fe $2p_{3/2}$	2.61(1)
	NH_3 dosing	C 1s—C–C	2.98(3)
		C 1s—C–N	2.90(3)
		N 1s	2.84(2)
		Fe $2p_{3/2}$	2.80(7)
	H_2O dosing	C 1s—C–C	2.90(1)
		C 1s—C–N	2.84(2)
		N 1s	2.79(6)
		Fe $2p_{3/2}$	2.68(4)
H_2Pc [397]	0.7 ML, 300 K	C 1s	3.04(7)
		N 1s	2.81(7)
	0.8 ML, 300 K	C 1s	3.07(7)
		N 1s	2.82(7)

Table 2. Continued

Molecule	Comment	Signal	d_H (Å)
	0.93 ML, 300 K	C 1s	3.07(7)
		N 1s	2.90(7)
	0.7 ML, 183 K	C 1s	3.06(7)
		N 1s	2.82(7)
	0.8 ML, 183 K	C 1s	3.03(7)
		N 1s	2.93(7)
	0.93 ML, 183 K	C 1s	3.08(7)
		N 1s	3.02(7)
SnPc [398]	1 ML, 300 K	C 1s	3.16(3)
		N 1s	3.24(6)
		Sn 3d	2.46(3)
	0.87 ML, 150 K	C 1s	2.93(6)
	Sn down/up	N 1s	3.12(7)
		Sn 3d	2.59/4.01
TiOPc [399]	0.95 ML, all up	C 1s	3.01(3)
		N 1s	2.88(6)
		O 1s	5.38(10)
		Ti $2p_{3/2}$	3.70(8)
Other compounds on Ag(111)			
Azobenzene	[400]	C 1s	—
		N 1s	3.07(2)
	[401] 210 K	C 1s	—
		N 1s	2.97(5)
	[402] 210 K	C 1s	2.99(5)
		N 1s	2.97(5)
Benzene [8]	80 K	C 1s	3.04(2)
EC4T [198]		S 1s	3.15(5)
NO_{2PYT} [403]	0.6 ML	C 1s	2.82(2)
		O 1s—carb.	2.23(3)
		O 1s—nitr.	2.61(7)
PYT [403]	0.6 ML	C1s	2.46(3)
		O 1s	2.31(4)
TBA [404]		N 1s	3.21(5)
Other compounds on Ag(111) (cont.)			
TCNQ	[211]	C 1s—C–H	2.86(2)
		C 1s—C–C	2.78(2)
		C 1s—C–N	2.76(2)
		N 1s	2.75(3)
	[211] K-doped ML	C 1s—C–H	2.85(1)
	(K-TCNQ)	C 1s—C–C	2.79(1)
		C 1s—C–N	2.79(1)
		N 1s	2.79(5)
		K 2p—bare	2.81(1)
		K 2p—TCNQ	3.56(3)
Pentacene (PEN) derivatives on Au(111)			
P4O [78]	1.0 ML	C 1s	3.27
Perylene derivatives on Au(111)			
DIP [151]	0.8 ML	C 1s	3.10(3)

Table 2. Continued

Molecule	Comment	Signal	d_H (Å)
Perylene [80]		C 1s	3.01(6)
PTCDA [148]		C 1s	3.27(2)
PTCDI [80]		C 1s	3.29(2)
		N 1s	3.26(3)
TAT [170]		C 1s	3.06(7)
		N 1s	3.04(2)
Phthalocyanine (Pc) derivatives on Au(111)			
CuPc [178]	0.7 ML, 300 K	C 1s	3.31(7)
		N 1s	3.26(7)
		Cu $2p_{3/2}$	3.20(7)
	1.0 ML, 300 K	C 1s	3.31(7)
		N 1s	3.26(7)
		Cu $2p_{3/2}$	3.25(7)
	0.7 ML, 133 K	C 1s	3.37(7)
		N 1s	3.25(7)
		Cu $2p_{3/2}$	3.25(7)
	1.0 ML, 133 K	C 1s	3.28(7)
		N 1s	3.27(7)
		Cu $2p_{3/2}$	3.29(7)
F_{16CuPc} [385]		C 1s	3.25
		F 1s	3.26
Various COMs on other surfaces			
MnPc	(002) reflection	C 1s total	2.403(28)
on Cu(001) [405]		C 1s—C–C	2.412(28)
		C 1s—C–N	2.376(26)
		N 1s	2.312(19)
		Mn $2p_{3/2}$	2.24(45)
PTCDA	(200) reflection	C 1s—perylene core	2.44(2)
on Cu(100)		C 1s—C==O	2.53(2)
[155]		O 1s—carb.	2.47(5)
		O 1s—anh.	2.76(2)
	(111) reflection	C 1s—perylene core	—
		C 1s—C==O	—
		O 1s—carb.	—
		O 1s—anh.	—
CoTPP	(200) reflection	C 1s—core	3.10
on Ag(100)		C 1s—phenyl rings	2.45
[406]		N 1s	3.10
		Co $2p_{3/2}$	3.00
PTCDA	0.8 ML,	C 1s—total	2.81(2)
on Ag(100)	(200) reflection	C 1s—perylene core	2.84(2)
[407]		C 1s—C==O	2.73(1)
		O 1s—total	2.64(2)
		O 1s—carb.	2.53(2)
		O 1s—anh.	2.78(2)
	0.8 ML,	C 1s—total	—
	(111) reflection	C 1s—perylene core	—
		C 1s—C==O	—
		O 1s—total	—

Table 2. Continued

Molecule	Comment	Signal	d_H (Å)
NTCDA on Ag(100) [156]	0.x ML, (200) reflection	C 1s—total	2.384(9)
		O 1s—carb.	2.25(2)
		O 1s—anh.	2.42(4)
PTCDA on Ag(110)	[407] 0.9 ML, (220) reflection	C 1s—total	2.56(1)
		C 1s—perylene core	2.58(1)
		C 1s—C==O	2.45(11)
		O 1s—total	2.33(3)
		O 1s—carb.	2.30(4)
		O 1s—anh.	2.38(3)
	[154] 0.89 ML, (220) reflection	C 1s total	2.56(2)
		C 1s—perylene core	2.59(1)
		C 1s—C==O	2.45(11)
		O 1s—total	2.36(5)
		O 1s—carb.	2.32(5)
		O 1s—anh.	2.41(6)
	[408] K-doped (K-PTCDA), (220) reflection	C 1s—total	2.66(3)
		C 1s—perylene core	2.64(3)
		C 1s—C==O	2.73(6)
		O 1s—total	2.70(10)
		O 1s—carb.	2.63(10)
		O 1s—anh.	2.76(11)
		K 1s	1.44(6)
Graphene (Gr)on Ir(111) [409]	0.22 ML	C 1s	—
	0.39 ML	C 1s	—
	0.63 ML	C 1s	—
	1.00 ML	C 1s	—
Graphene on SiC (0001) [410]	UHV-grown 0.5 ML	C 1s—second layer	—
	UHV-grown 1.3 ML	C 1s—first layer (1)	2.3(2)
		C 1s—first layer (2)	2.0(1)
		C 1s—second layer	—
		C 1s—first layer (1)	2.4(1)
		C 1s—first layer (2)	2.1(1)
	Ar-grown 1.7 ML	C 1s—second layer	—
		C 1s—first layer (1)	2.52(13)
		C 1s—first layer (2)	2.12(7)
Graphene on 6H-SiC (0001) [411]	Gr buffer layer (BL) bare	C 1s—graphene	4.272(60)
		C 1s—BL bare	2.30(1)
	Epitaxial	C 1s—BL bare doped	2.28(2)
		C 1s—BL	2.37(2)
	Epitaxial ML on a BL	C 1s—BL doped	2.37(2)
		C 1s—graphene	5.67(1)
		C 1s—graphene doped	5.65(1)
		N 1s—graphene doped	5.72(5)
	ML on 6H-termin.	C 1s—graphene	4.28(1)
		C 1s—graphene doped	4.56(1)
		N 1s—graphene doped	4.49(5)
		N 1s—interstitial	2.71(4)
h-BN on Ir(111) [413]		N 1s—total	—
		N 1s—strongly bound	2.22(2)
		N 1s—weakly bound	3.72(2)
		B 1s—total	—
		B 1s—strongly bound	2.17(2)
		B 1s—weakly bound	3.70(2)

$|E_{ads}(Cu)| > |E_{ads}(Ag)| > |E_{ads}(Au)|$ (i.e., with the strongest interaction for the most reactive substrate, which matches the discussion in section 2.2). Importantly, the rather shallow and broad minima of $E_{ads}(d)$, which correspond to the equilibrium

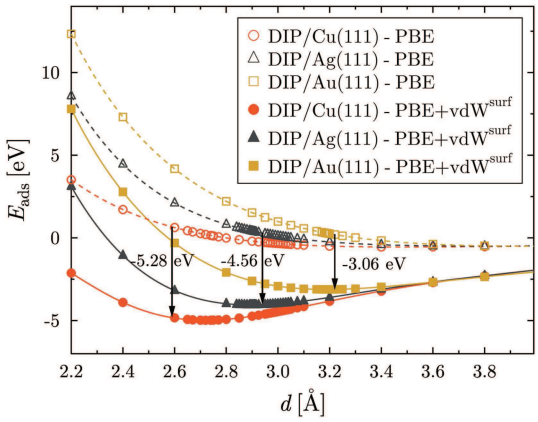

Figure 12. Comparison of DFT calculations performed for DIP adsorbed on the three (111)-surfaces of Cu, Ag and Au using the Perdew, Burke und Ernzerhof (PBE) exchange–correlation functional with and without vdW corrections. Note that in some cases, i.e. if no vdW interactions are included, the outcome would be no binding at all. Reprinted figure with permission from [151], Copyright (2013) by the American Physical Society.

distances, form only if the vdW corrections are included, otherwise there is no stable adsorption at all. Moreover, figure 12 shows that on Cu(111) the Pauli repulsion sets in rather weakly (a less steep $E_{ads}(d)$ for small distances) compared to Ag(111) and Au(111), which is due to significant interaction between DIP and Cu(111), i.e. contributions beyond the vdW attraction.

In order to understand the contribution of the vdW interactions in more detail, first one has to consider the impact of the specific symmetry on the vdW interaction (which for individual atoms goes as (distance)$^{-6}$): integrating the vdW energy of a single atom over the semi-infinite substrate yields the atom–surface vdW energy as $C_3(z-z_0)^{-3}$, where C_3 determines the interaction strength between atom and surface [24, 27], z corresponds to the distance of the atom to the uppermost surface layer, and z_0 indicates the position of the surface image plane. Naively, one might attempt to determine the C_3 coefficients for the different surfaces from all the two-body atom–atom vdW energies and thereby neglect any interactions of the substrate atoms with each other. However, it can be shown that the dielectric function, i.e. the collective electronic response of the underlying solid, has a strong influence on the interaction strength [24, 27].

Using the Lifshitz–Zaremba–Kohn (LZK) expression for calculating the C_3 coefficients, one obtains (in units of Hartree Bohr^3) 0.35 for Cu, 0.35 for Ag and 0.33 for Au, which leads to essentially the same interaction energy at large distances for DIP on Cu(111), Ag(111), and Au(111) (figure 12). However, at shorter molecule–surface distances, which include the equilibrium distance, the adsorption energy is determined by an interplay between the vdW attraction and the Pauli repulsion with a possible covalent component. The Pauli repulsion follows roughly the trend of decreasing vdW radii, with a faster onset in terms of the molecule–surface distance for Au (the largest vdW radius), and then decreases for Ag and Cu. Therefore, for Au the balance between vdW attraction and the Pauli repulsion is obtained further away from the substrate (i.e. at larger adsorption distances) than for Cu, which in turn makes

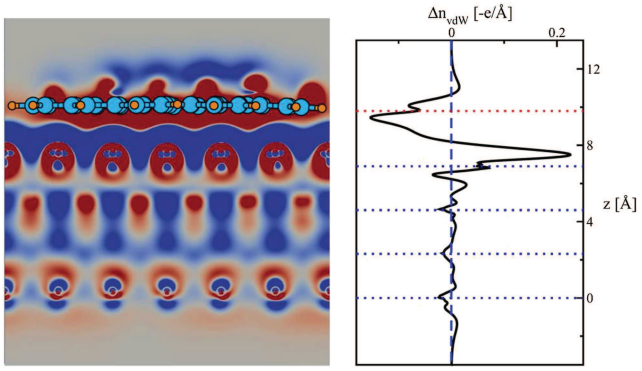

Figure 13. Left panel: vdW effect on the electron density distribution $\Delta n(\mathbf{r})_{\mathrm{vdW}}$ upon adsorption of DIP on Ag(111), accumulation is in blue, depletion is in red. Right panel: the integral of $\Delta n(\mathbf{r})_{\mathrm{vdW}}$ plotted as a function of z, the axis perpendicular to the surface. A dipole-like density redistribution emerges at the interface. Reprinted figure with permission from [125], Copyright (2017) by the American Physical Society.

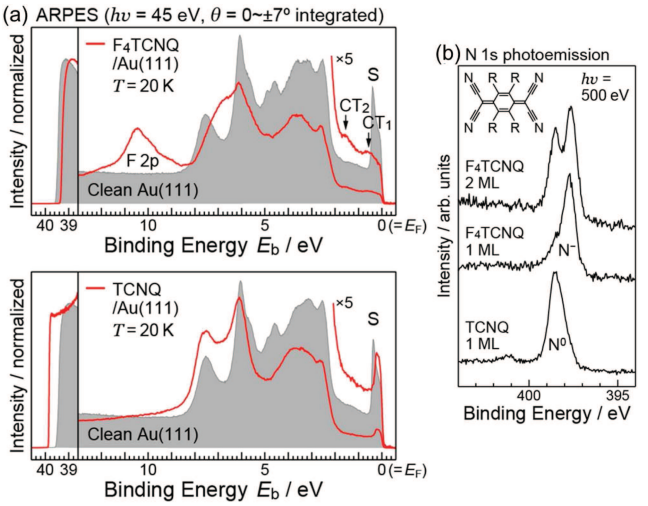

Figure 14. (a) UP spectra of the clean Au(111) surface (gray shadows) and monolayer (F_4)TCNQ films on Au(111) (red curves). For F_4TCNQ two charge transfer states (CT_1 and CT_2) close to the substrate Fermi level E_F are apparent. The shift of the secondary-electron cutoff (left panel) to lower binding energy upon F_4TCNQ deposition evidences a work function increase. (b) N1s core-level: no charge transfer takes place into the TCNQ monolayer and all molecules are neutral (N^0). In contrast, in the F_4TCNQ monolayer almost all molecules are charged (N^-). Reprinted with permission from [329]. Copyright (2017) American Chemical Society.

the adsorption energies lower for Au than for Cu, in contrast to the possible naive expectation of Au with its higher electron density and polarizability leading to stronger interactions than Cu.

Generally, we note that semi-local DFT calculations, i.e. the different versions of the generalized gradient approximation (GGA), might not provide very accurate energy-levels [9]. More advanced methods, however, are computationally prohibitively expensive because of the large number of atoms within the unit cell of larger molecules on surfaces [31]. For weakly interacting systems, one may not expect major changes of the electronic structure. Nevertheless, even for purely vdW-driven systems there will be at least variations of the molecular energy-levels and the vacuum level. As discussed in section 2.1, the push-back effect [107, 119–121, 123, 124] decreases the interface dipole of the clean metal surface. However, recently it was shown [125] that vdW interactions can also cause significant charge rearrangements in the vicinity of the adsorbed COM, as shown for DIP on Ag(111) in figure 13. Using DIP on noble metals as a model system, we believe that the limiting case of weakly interacting systems—although indeed not as simple as at first assumed—is essentially understood. The key for this are state-of-the-art vdW-corrected DFT calculations in combination with very precise experimental data from XSW and other techniques, which agree within less than ∼0.1 Å for the adsorption distance.

This also applies to other examples in this category of weakly interacting systems. Benzene is probably a prototypical case, which, however, due to its smallness and thus high vapor pressure at room temperature, can only be studied at lower temperatures. In a DFT benchmark study Liu *et al* combined XSW and TPD using benzene on Ag(111) as model system to test the accuracy of the performed calculations [8, 373]. They found that the adsorption distance of $d_{\mathrm{ads}} = 3.04 \pm 0.02$ Å and the adsorption energy of 0.68 ± 0.05 eV, which were measured for this clearly physisorptive system, are in excellent agreement with their DFT calculations.

Again, we note that there is a gradual transition from truly weakly interacting systems such as DIP or benzene on Au(111) to those on Ag(111) or Cu(111), which are more reactive due to the increased orbital overlap of molecular states at smaller adsorption distances (see also section 2.2).

4.3. Strongly interacting systems

In the other limiting case, the coupling and the interaction between molecule and substrate is so strong that there is, *inter alia*, significant charge donation and/or back donation, significant shifts of energy-levels and presumably an associated significant distortion of the molecule (but, notably, not yet a chemical reaction). In section 2 we used P4O on Ag(111) as example for a strongly coupled system. The schematic energy-level diagram (figure 5) shows the charge transfer from the substrate into the former LUMO of P4O in the monolayer. This CT goes along with strong chemical shifts of the core-levels and a bending of the P4O oxygen atoms below the plane of the carbon backbone (figure 6) [78]. Overall, P4O rehybridizes in the contact layer to Ag(111) (possible resonance structures shown in the bottom of figure 5). P4O exhibits a similar chemisorptive behavior on Cu(111), but physisorbs on Au(111) [73, 78]. In contrast, F_4TCNQ chemisorbs on virtually *all* clean metal surfaces [58, 66, 329, 439–445] showing a qualitatively similar behavior. These systems shall hence be discussed as model systems for strongly coupled organic–metal interfaces.

The EA of F_4TCNQ in multilayer thin films on Au is 5.08 eV [349] to 5.25 eV [90] and thus larger than the work functions of most clean noble metals [142]. Therefore, one can expect a charge transfer into the LUMO of F_4TCNQ

in monolayers on such substrates to increase the effective work function and maintain thermodynamic equilibrium. In fact, monolayers of F_4TCNQ increase the work functions of Au(111) [329], Ag(111) [440, 443] and Cu(111) [66]. As an example figure 14(a) shows UP spectra of F_4TCNQ on Au(111) and compares them with spectra of the unfluorinated parent molecule, TCNQ, which interacts only weakly with Au(111) [329]. The increase in the work function (evidenced by the SECO shift) is accompanied by two charge transfer peaks (CT_1 and CT_2) close to E_F. Likewise, the N1s core-level shows strong chemical shifts from mono- to multilayer F_4TCNQ coverage (figure 14(b)), which are caused by the charge transfer into F_4TCNQ.

The work function increase on Au(111) and all other metal surfaces is smaller than 1 eV [66, 329, 440, 443]. However, a complete filling of the LUMO of the molecules in the monolayer would lead approximately to a work function increase of around 5 eV [66]. The calculated occupation of the lowest 60 molecular orbitals (MOs) for a F_{4TCNQ} monolayer on Cu(111) as displayed in figure 15 indicates that the charge donation to the LUMO is, in fact, accompanied by a back-donation to deeper lying MOs. Especially, the HOMO − 9 to HOMO − 12 levels are involved and each is only 80%–90% occupied after adsorption. They correspond to σ-orbitals localized on the four nitrile groups of the molecule, which participate most prominently in the chemical bonding with the substrate. Summing over all MOs gives a net negative charge of $\sim$0.6e per F_4TCNQ molecule, which is significantly less than 2e corresponding to a complete filling of the F_4TCNQ LUMO. In addition, as discussed below in more detail, adsorption induced conformation changes—shown in figure 16 for F_4TCNQ on Ag(111)—lead to additional interface dipole moments.

The significant molecular charging causes aromatization of the central quinone ring and makes the molecule structurally flexible. This allows the molecule to bend and hybridize with the substrate through the lone electron pairs of nitrogen [442]. On Cu(111), the fluorine atoms are found $\sim$0.6 Å above the nitrogen atoms as determined by XSW [66]. This is a consequence of the carbon atoms carrying the nitrile groups rehybridizing from sp^2 toward sp^3 upon contact formation [66]. Additionally, the strong molecule–metal interaction leads to marked changes in bond lengths within F_4TCNQ. In the gas phase the molecule adopts a fully planar, quinoid-like geometry [446]. Adsorption on the Cu(111) surface results in a nearly aromatic ring [66]. In the context of strong chemisorption and hybridization with metal surfaces also surface adatoms have been discussed, this applies especially to F_4TCNQ on Au(111) [329, 444] and for TCNQ on Ag(111) [447].

For strongly coupled systems, fractional charge transfer including donation and back-donation is usually observed. The impact of such charge rearrangements on the VL shall be discussed with the example of F_4TCNQ on Ag(111) [440]. For a better understanding of vacuum level shifts caused by organic/inorganic contact formation, the calculated total change of the VL, i.e., the interface dipole ΔVL, is often decomposed into two contributions [66, 403, 431, 440, 448]: (i) the molecular contribution ΔVL_{mol} related to the surface-normal component of the molecular dipole (permanent or adsorption induced) and (ii) the contribution due to the interfacial charge rearrangement (including charge transfer from or to the metal), the so-called bond dipole ΔVL_{bond}, i.e.:

$$\Delta VL = \Delta VL_{mol} + \Delta VL_{bond}. \quad (4)$$

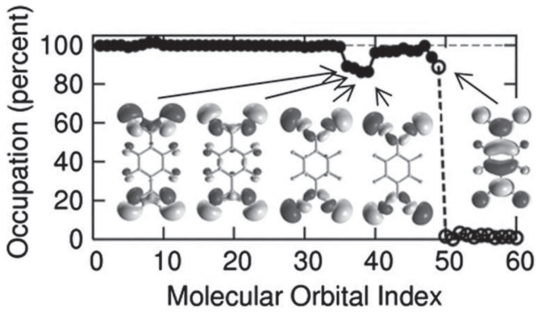

Figure 15. Calculated occupation (in percent) of the lowest 60 molecular orbitals of F_4TCNQ in a monolayer on Cu(111). The full (open) circles and solid (dashed) lines correspond to the orbitals which are occupied (unoccupied) in the isolated molecule. Reprinted figure with permission from [66], Copyright (2007) by the American Physical Society.

An (infinitely) extended dipole layer results in a shift of the vacuum level by

$$\Delta VL = \frac{1}{\varepsilon_0 A}\mu_\perp, \quad (5)$$

where $\mu_\perp$ refers to the surface-normal component of the dipole moment per molecule in the monolayer (including depolarization effects [449, 450]), ε_0 to the vacuum permittivity and A to the area per molecule. In the gas phase F_4TCNQ is planar, thus, all contributions to ΔVL_{mol} are due to adsorption-induced conformation changes. In the distorted conformation of the monolayer (figure 16), each individual F_4TCNQ molecule possesses a dipole moment of −2.69 D. In effect, it points away from the metal surface and would result in a work function decrease by −0.85 eV. In addition to the distortion, however, also ΔVL_{bond} due to adsorption-induced charge rearrangements, $\Delta\rho_{bond}$, has to be taken into account. $\Delta\rho_{bond}$ is calculated as the difference of the total electron density of the combined metal–organic interface ρ^{sys} and the non-interacting densities of metal ρ^{metal} and monolayer $\rho^{monolayer}$:

$$\Delta\rho_{bond} = \rho^{sys} - (\rho^{metal} + \rho^{monolayer}). \quad (6)$$

From $\Delta\rho_{bond}$, ΔVL_{bond} is then obtained by solving the Poisson equation. For F_4TCNQ, ΔVL_{bond} amounts to +1.70 eV. The net effect, i.e., the sum of ΔVL_{bond} and ΔVL_{mol}, is a work function increase by +0.85 eV, which fits very well with the experimental value of 0.65 eV [440]. For molecules that undergo charge-transfer reactions with the surface, ΔVL_{mol} and ΔVL_{bond} are *not* independent. Rather, any error in the description of the bending is made up for by a change in charge transfer, making ΔVL, which is the experimental observable, a very robust quantity [403, 451].

Figure 16 shows the x–y-plane integrated charge density rearrangements $\Delta\rho_{bond}(z)$ of a monolayer F_4TCNQ on Ag(111). The pronounced electron depletion directly above the top metal layer is attributed to push-back. The largest

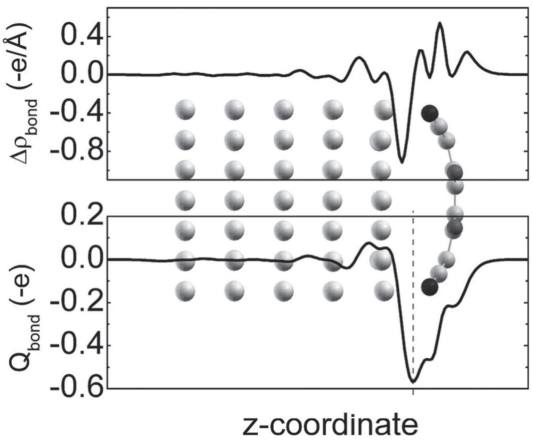

Figure 16. Top: charge-density rearrangement, $\Delta\rho_{bond}$, upon adsorption of a densely packed F_4TCNQ monolayer on a Ag(111) surface integrated over the x–y plane within the unit cell; bottom: resulting total charge transferred, Q_{bond}. The vertical line denotes the maximum value of Q_{bond}. The structure of the combined system is shown in the background as a guide to the eye. e corresponds to the (positive) elementary charge and positive $\Delta\rho_{bond}$ values correspond thus to electron accumulation and negative values to electron depletion. Reprinted figure with permission from [440], Copyright (2009) by the American Physical Society.

electron accumulation can be found in the π-electron region of F_4TCNQ. The dip in $\Delta\rho_{bond}(z)$ in the region of the CN groups is consistent with the decreased σ-electron density in that part of the molecule (cf figure 15) [440].

In general, such strongly coupled systems can be used for work function engineering and consequently for energy-level tuning of subsequently deposited organic layers. This has been first demonstrated for the molecular acceptor TCAQ, which lowers the hole injection barrier into 6T layers on Au and Ag [452]. Other examples of strongly coupled electron accepting molecules on metal surfaces include PEN [74, 181], DIP [422, 423], PTCDA [18, 70, 75, 79, 85, 128, 138, 150, 427–433], PTCDI [80], TAT [170], FAQ [137], HATCN [168, 453], Pcs [77, 166, 454–457], and TCNQ [67, 458–460]. Most of the above mentioned COMs can serve different purposes in addition to being a suitable ELA modifier [52, 53, 461–464]. For example, F_4TCNQ is also a popular molecular dopant [53, 464–469]. Furthermore, work function modification is not restricted to metal surfaces [271, 470–477] and electron donating COMs can also *lower* effective work functions [62, 65, 448, 478, 479] by the reversed process as electron accepting molecules, i.e., by an electron transfer from the adsorbate to the substrate. Strongly interacting organic–metal systems have thus a significant relevance for applications.

4.4. Intermediate cases

Between the two extreme scenarios discussed above, there exist plenty of systems whose phenomenology can neither be described by only considering 'chemical' interactions nor vdW attraction alone. Most interestingly, these cases may tend towards one or the other side depending on the particular characteristics of the system. The following consists mostly of prototypical systems of the kind 'molecule A on substrate B', which are taken as a reference to discuss the interfacial changes that occur when A or B are (slightly) modified. In addition, particular cases that exemplify the possibilities of surface/interface tuning are also outlined. We note that some systems may fit in two or more subsections.

4.4.1. Fluorination. Among the many options to functionalize a COM through specific chemical modifications [481], fluorination, i.e. the substitution of peripheral hydrogen atoms by fluorine, is one of the most widely employed. In the gas phase and thin films, it increases the resistance to oxidation, changes the electron affinity, modifies the intrinsic molecular dipole as well as the optical properties [482]. At the interface, fluorination modifies the ELA and the nature of the substrate–molecule and molecule–molecule interactions. One of the most illustrative examples when discussing the effects of fluorination is the case of PEN and its perfluorinated derivative PFP [165] adsorbed on copper surfaces [74, 265, 322, 483–488]. Even on the moderately reactive (111) noble metal surfaces, PEN molecules can experience strong interactions.

The hybridization of the molecular states with the surface atoms [74, 181, 487] renders a completely filled LUMO on Cu(111) well below the Fermi level [181] and a remarkably short adsorption distance (figure 17) [74]. In contrast, PFP shows no LUMO filling, no sign of hybridization is seen in XPS [487] and the average adsorption distance of carbon is ∼0.6 Å higher than PEN, with the fluorine atoms further up (see figure 17), on average, by ∼0.1 Å [74]. DFT calculations with vdW-corrections [480] yielded adsorption geometries with average adsorption distances in perfect agreement with experiments and gave a more precise description of the actual arrangement: PEN would adsorb forming a small canoe-like shape with the short molecular edges slightly above the average carbon distance, whereas PFP would adsorb in a strong V-shape with the central carbon atoms, being the most reactive in acenes, very close to the surface and the short edges ∼1 Å above. These dramatic changes in the interface properties upon fluorination are due to the strong Pauli and steric repulsion (fluorine is larger than hydrogen) between the fluorine atoms and the substrate that weakens the electronic coupling. In this direction, a recent PES-XSW combined study on the partially fluorinated PEN derivative F_4PEN [169], with fluorine atoms only at the short molecular edges, adsorbed on Cu(111) revealed that the selective fluorination of PEN only yields a local conformational change. Despite the increased adsorption distance of the fluorine and carbon atoms nearby (see figure 17), the structural, electronic and chemical properties of the PEN backbone remain unaffected because the strong interaction of the core with the copper atoms prevails [169].

On the less interacting silver surface, PEN has been shown to have different growth phases that depend on the temperature as well as on the coverage [179, 264]. Such behavior has been defined as 'soft chemisorption' [179] since from TPD a remarkable thermal stability is found and NEXAFS shows a significant modification of the PEN orbitals in the monolayer [283], but there is no trace of LUMO filling [181] and the molecules form a disordered liquid-like phase at RT. Indeed, different studies have reported the disorder present in the first

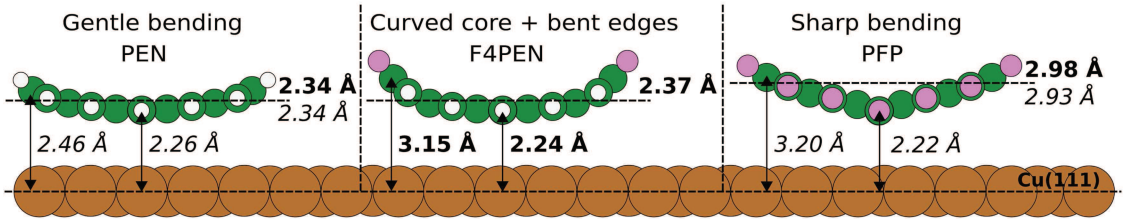

Figure 17. Adsorption geometry of PEN, F_4PEN and PFP on Cu(111) that combines experimental data obtained with XSW (in bold) and state-of-the-art DFT calculations with vdW corrections (in italics). The calculations are obtained from reference [480], the measured adsorption distances for PEN and PFP from reference [74] and F_4PEN from reference [169]. Note that only values for different carbon positions are included. In addition, the average adsorption distance of the fluorine atoms in F_4PEN is 3.40 Å [169] and in PFP 3.08 Å [74]. Reprinted figure with permission from [169]. Copyright (2018) by the American Physical Society.

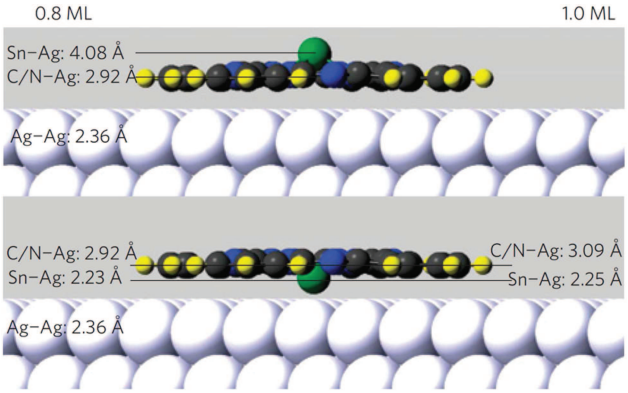

Figure 18. Side views of a molecule in the Sn-up (upper part of the figure) and Sn-down position (lower part) on Ag(111). For a coverage of 0.8 monolayers (left side) Sn-up and Sn-down oriented molecules are present on the surface and the vertical bonding distances (as measured by XSW) are given. For a monolayer coverage (right side) only Sn-down oriented molecules are present on the surface. Reprinted from [76] by permission from Springer Nature Customer Service Centre GmbH: Nature Physics © 2009.

PEN layer in contact with Ag(111) [181, 259, 264, 283] with the interesting and controversial [283] fact that an *ordered second layer* may grow on top [259, 264]. Upon cooling, ordered areas are found in STM [264] but no clear diffraction pattern is observable in LEED [181]. Notably, cooling as well as increasing the coverage modify the adsorption distances, with the remarkable displacement of +0.14 Å in adsorption distance upon coverage increase from 0.5 to 0.75 ML at RT [179] as a consequence of the shifting balance between intermolecular and substrate–molecule interactions (see section 2.4). In this situation, fluorination of PEN has a similar effect as on copper, namely, the molecule–substrate interaction decreases. As reported by Götzen *et al* [283] the TPD spectrum of PFP, compared to that of PEN, does not show a monolayer feature, which indicates that the bonding strength for the latter is higher. This appears in line with the increased adsorption distance of PFP compared to PEN for a similar coverage (2.98 Å [179] vs 3.16 Å [392]) and the absence of CT to the LUMO [86, 392]. Similar to PEN on Ag(111), temperature, coverage and even the preparation method seem to impact the supramolecular arrangement of PFP: monolayers prepared via desorption of a multilayer appear as ordered patches that leave substrate regions uncovered [489] at $T < 130$ K, then become disordered and homogeneously distributed all over the surface at $T > 160$ K. On the contrary, (sub)monolayers prepared via direct evaporation of the desired coverage adopt ordered arrangements at LT (dislocation network) and RT (Moiré pattern) [490].

On gold, both PEN and PFP, show a clear physisorptive behavior with no evidence of LUMO filling, nor hybridization of the molecular orbitals [181, 262, 491]. Quite interestingly, despite the *a priori* higher ionization energy of PFP, an almost identical HIB was measured for both molecules on gold, which comes along with a larger (by 0.45 eV) VL shift for PEN [262]. The authors argued that the weaker pushback effect and the unexpected ELA should be explained by a much larger adsorption distance of PFP compared to PEN [262]. Recently, direct XSW measurements have confirmed this [492]. Another interesting finding, which indicates a considerable interaction even within the physisorptive regime, was reported by Lo *et al* [491]: using STM it was found that PEN may change the surface reconstruction of Au(111) and thereby suggesting a stronger interaction with the substrate than PFP. Yet, the PEN molecules appear to be mobile while PFP forms assemblies that are stabilized by intermolecular interactions [491].

For the sake of completeness, we shall mention that the influence of fluorination on the metal–organic interface has been studied also for phthalocyanines [385, 493–496], rubrene [497] and thiophenes [498]. Of course not only (111) surfaces, but also several others have been studied, e.g., PFP on Ag(110) [499] or F_4PEN on Au(100) [500, 501].

As concluding remark, it is worth noting that within the monolayer regime the combination of fluorinated and non-fluorinated compounds has been shown to be an effective way to tune the work function of a metal substrate [175] and, in the thin-film regime, the ionization energy as well [496, 502, 503]. In both cases, this method provides a suitable pathway to systematically modify the interface properties and adapt them to the particular device requirements.

4.4.2. Core substitutions of phthalocyanines All COMs discussed so far are intrinsically non-polar and therefore do not offer the possibility to tune the ELA by a permanent molecular dipole moment, whose magnitude and orientation may influence the vacuum level and thus the ELA [348, 386, 449, 450,

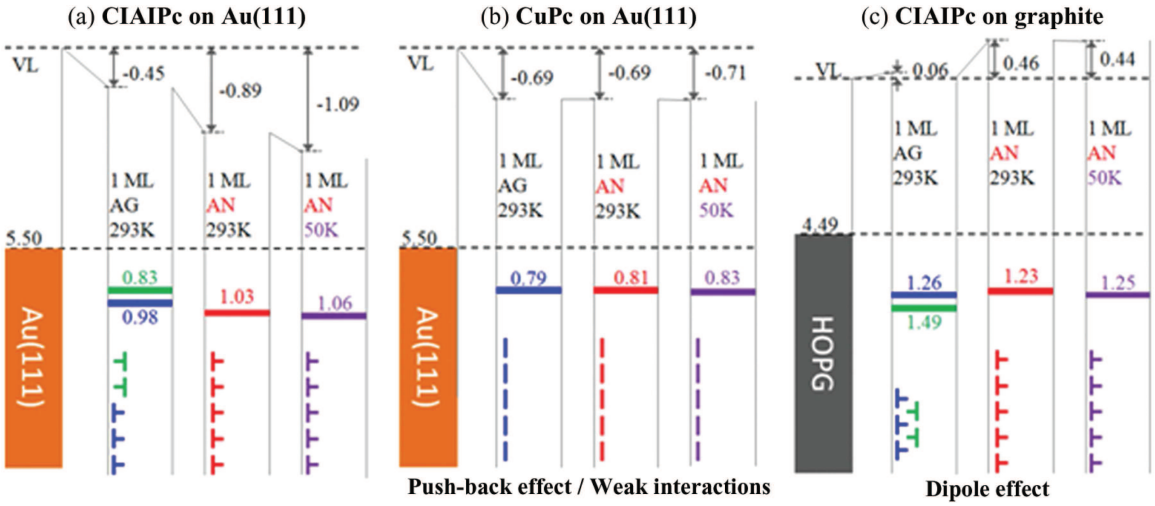

Figure 19. Energy-level diagrams for monolayers (ML) of (a) ClAlPc/Au(111), (b) CuPc/Au(111), and (c) ClAlPc/HOPG. For each system, UPS measurements of the as-grown (AG) film at room temperature (RT) and of the annealed (AN) film at RT and low temperature (LT) are shown. Upon annealing and cooling, vacuum level (VL) shifts and changes of HOMO states are observed. Here, $\perp$ corresponds to the Cl-up and the reversed symbol to the Cl-down orientation. Reprinted figure with permission from [505], Copyright (2013) by the American Physical Society.

454, 504–506]. An important class of polar COMs are particular porphyrins and phthalocyanines, as they offer numerous possibilities of functionalization through substitution of the central metal atom and insertion of further heteroatoms [76, 166, 167, 316, 348, 386, 398, 449, 454, 505–515]. Since only a few adsorption distances have been measured for porphyrins by XSW [388, 389], we focus on Pcs. We shall discuss SnPc [76, 398, 510, 516–520] as example for a Pc for which the central atom is simply too big to fit into the aromatic macrocycle and which is thus polar in the gas phase. Thus, it can adsorb in two different flat-lying geometries (figure 18), i.e. with the Sn atom either below (Sn-down) or above the molecular plane (Sn-up). For a submonolayer coverage on Ag(111) both orientations were found and the adsorption distances have been measured by XSW [76, 398, 510]. For a full monolayer coverage substrate mediated intermolecular interactions lead to a reorientation of the Sn-up molecules and only Sn-down can be found on the surface [76]. In this case the tin atom plays a crucial role in the coupling with the substrate leading to pronounced charge rearrangements, which are negligible for the Sn-up orientation [517, 518]. Overall, for such systems the orientation has a significant impact on the intermolecular interaction. However, the molecular dipole moments are rather weak and hence the impact on the vacuum level marginal.

For 'umbrella-shaped' Pc molecules with an additional heteroatom attached to the central metal ion the situation is different. For example, the dipole moment of ClAlPc in the gas phase is 1.87 D [521] and, according to equation (5), the collective impact of these dipoles on the vacuum level (ΔVL_{mol}) for an aligned monolayer should yield a ΔVL value of several 100 meV. For as-deposited ClAlPc on Au(111) a mixed Cl-up/down orientation has been observed and the resulting $\Delta VL = -0.45$ eV (figure 19(a)) has been mainly ascribed to the push-back effect [505]. Strikingly, aligning the molecules to a Cl-up orientation by annealing leads to a further VL decrease ($\Delta VL = -0.89$ eV) and the total ΔVL is larger than that of planar CuPc on the same substrate (figure 19(b)). Apparently, the permanent dipole moment of ClAlPc is decreasing the vacuum level—whereas in fact a Cl-up orientation should lead to an VL increase (by $+0.47$ eV), which was indeed observed for ClAlPc on HOPG (figure 19(c)). On inert HOPG the dipole moment of the adsorbate is thus not changed in the contact layer to the substrate. On metal substrates, however, adsorption induced bond-length changes, which can lead to a partial depolarization of the COM on the surface, are frequently observed [522–525]. In addition, interfacial charge rearrangements due to strong interactions can further impact the vacuum level, which has been suggested to be the reason for the unexpected ELA of ClAlPc on Au(111) [505]. A similar behavior has been observed on Ag(111): also on this substrate annealing changes a mixed orientation of a ClAlPc monolayer to a predominant Cl-up arrangement and concomitantly decreases VL [506]. Interestingly, for very low deposition rates of ClAlPc on Ag(111) ($\sim$0.1 Å min^{-1}) a Cl-down orientation is favorable.

Unfortunately, the modulo-d ambiguity of the XSW technique (equation (2)) can hinder a straightforward assignment of adsorption distances and even the orientation (X-down or X-up). For example, the DFT-modeled adsorption distances of GaClPc on Cu(111) in the Cl-up and Cl-down orientation [524] do not match the experimental values [386]. It turns out that in the most likely adsorption geometry the Cl atom is dissociated [524]. Moreover, as mentioned above, the 'up' and 'down' orientation can also coexist, as also observed for VOPc on Cu(111) [387]. In these cases, having a very well characterized system may help to address this issue [399].

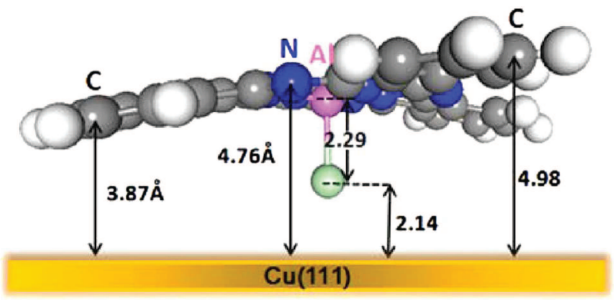

Figure 20. DFT-based adsorption geometry of ClAlPc on Cu(111). Reprinted with permission from [523]. Copyright (2013) American Chemical Society.

Another challenge for XSW measurements are the above mentioned pronounced distortions of the π-system leading to significantly different adsorption distance of the carbon atoms. For example, for ClAlPc on Cu(111) [523] in the Cl-down orientation the DFT-modeled adsorption distances of individual carbon atoms differ by up to 1.11 Å (figure 20). The strong distortion is a consequence of a charge transfer from the Cu(111) into ClAlPc, which is mainly localized on two of the four ClAlPc lobes as shown by STM [523]. This involves a symmetry reduction of ClAlPc from four-fold in the gas phase [and the Cl-up orientation on Cu(111)] to two-fold in the Cl-down orientation on Cu(111). Similar symmetry reductions have been observed also for other Pcs on different substrates, e.g., for CuPc on Cu(111) [526] and on Ag(100) [527], for FePc on Cu(111) [528] and for PtPc as well as PdPc on Ag(111) [529]. In general, both orientations (Cl-up or Cl-down) have been observed for vacuum-sublimed ClAlPc on the (111)-surfaces of noble metals [505, 506, 523, 530]. Moreover, the orientation can be changed by, e.g., the deposition rate [506], post-deposition annealing [505] or by pulsing using an STM tip [531] and can thus act as molecular switches [531, 532].

4.4.3. Functional groups. Obviously, also COMs other than phthalocyanines can be functionalized. We already discussed the impact of oxygen substitution on the coupling of pentacene with metal substrates (figures 5 and 6). In that case, the oxygen atoms break the conjugation of the pentacene backbone and the impact on the gas phase properties (namely, it increases IE and EA) as well as on the coupling with metal substrates is severe [78]. Also nitrogen substitution is frequently used to increase the EAs of COMs [163]. One example is the nitrogen-substituted terrylene analogue TAT [170, 533, 534]. However, in this case, the nitrogen atoms are a central part of the TAT π-system and, although a nitrogen-specific interaction in TAT monolayers on Ag(111) takes place, the vertical adsorption distances are not substantially affected [170]. We also briefly discussed the impact of functionalization of perylene (figure 7). Intriguingly, already the substitution with indeno-groups, i.e., the change from perylene to DIP, changes the adsorption behavior significantly [80, 151]. In contrast, the functionalization of perylene with oxygen (PTCDA) or with oxygen and nitrogen (PTCDI) does *not* change the averaged adsorption distances of the carbon atoms on the (111)-surfaces of noble metals (figure 7) [18, 80, 148, 150]. However, the adsorption distances of the atoms in the functional groups differ notably and the ELA is considerably different: the energy-levels of PTCDA are Fermi level pinned on the (111)-surfaces of noble metals [75] and virtually all substrates [128], whereas for PTCDI the ELA is vacuum-level controlled [80]. The coupling of PTCDA (and to minor extent also of PTCDI) to metals has been subject to extensive research (see references [18, 75, 80, 148, 150, 407, 430, 433, 535–543] as well as the review papers [83, 85, 432]).

In the following, we will focus on molecular functionalizations that change the orientation of the COM on metal surfaces. It is well known that the organic–inorganic ELA depends on the orientation of the COMs in the molecular thin film [43, 95, 135, 544]. For all cases discussed so far, the molecules have a lying-down orientation in the contact layer to the metal, as such a face-on orientation maximizes the wave function overlap between adsorbate and substrate. Monolayers of tilted or standing COMs on metal surfaces are rather exceptional and in most cases the result of a transition from flat-lying in a loosely packed monolayer to a standing or tilted orientation in a closely packed monolayer [168, 403, 545]. In some other rare cases the molecular surface unit cell includes two molecules with one of them lying flat and the other one being tilted [546–548]. On other surfaces, e.g., on metal oxides, standing orientations of (polar) COMs in monolayers are successfully used for ELA engineering [475, 549, 550]. The question arises how this can be achieved for organic–metal interfaces, i.e., what are the driving forces for a molecular semiconductor to adopt a tilted or standing orientation on a clean metal surface?

One of the first experimental demonstration of a COM with a standing orientation on a clean metal surface has been made for the electron accepting COM HATCN on Ag(111) [168]. In a combined UPS, TPD, RAIRS, DFT and Kelvin probe study Bröker *et al* showed that, up to a threshold coverage, HATCN adopts a lying-down orientation on Ag(111). Increasing the coverage leads to an orientational transition to standing molecules, i.e., HATCN forms a transient monolayer on Ag(111). In the standing monolayer ΔVL is almost 1 eV [168] and thus considerably larger than for monolayers of lying-down electron accepting molecules on the same surface such as F_4TCNQ [440, 443], PTCDA [138] or FAQ [137]. For HATCN specific interactions of the peripheral molecular cyano groups with the metal are believed to be one of the driving forces for an orientational transition, since for the edge-on conformation the CT becomes more localized on the C≡N docking groups. In contrast, for the face-on conformation the whole molecule is involved in the interaction with the substrate, including the σ-electrons of the C≡N groups as well as the entire π-system [168].

While HATCN has been an early example showing a large ΔVL for a monolayer of edge-on COMs, a more recent example is dinitropyrene-tetraone (NO_2-PyT) on Ag(111), which also exhibits a transient monolayer structure and where ΔVL for the edge-on orientation even amounts to ∼1.6 eV (figure 21(a)) [403]. The unsubstituted parent molecule pyrene-tetraone (PyT), which is flat-lying for all coverages, only increases the work function of Ag(111) by

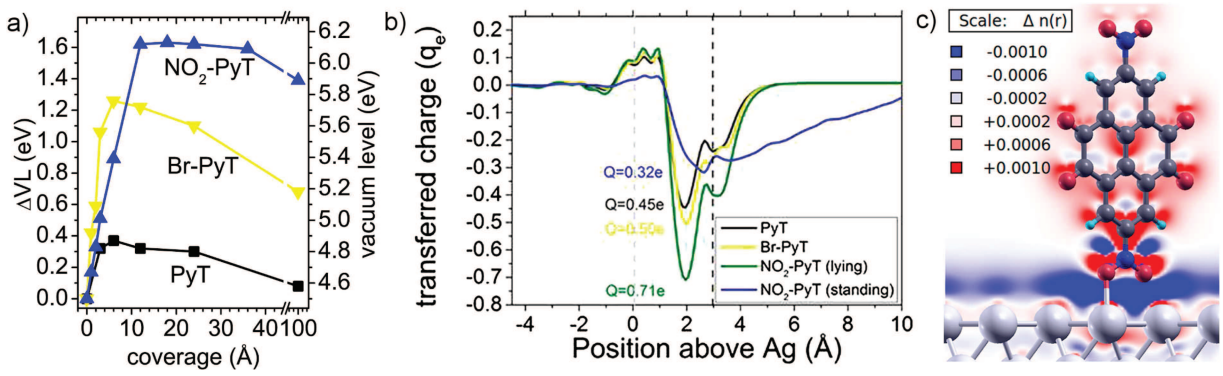

Figure 21. (a) Experimentally determined vacuum level changes (ΔVL) upon stepwise deposition of pyrene-tetraone (PyT) and its derivatives on Ag(111). (b) Calculated cumulative charge transfer. The averaged position of the carbon atoms (for lying molecules) and the topmost Ag plane are indicated by vertical dashed lines. (c) adsorption induced charge rearrangements derived by DFT calculations for the adsorption of an upright standing NO_2-PyT monolayer, averaged in the direction perpendicular to the paper plane. Br-PyT, which also shows a rather large increase of the substrate work function, is included for the sake of completeness. It could not be unambiguously shown whether the molecules adsorb intact or whether Br atoms detach during the adsorption process. Adapted from [403]. CC BY 4.0.

∼0.3 eV. For submonolayer coverages the valence electronic structure of NO_2-PyT and PyT on Ag(111) as measured by UPS is nearly identical: the former LUMO is partially filled due to a CT from the substrate and the work function increases by ∼0.3 eV. Also, the adsorption distances of the oxygen atoms in the carbonyl groups (around 2.30 Å) as measured by XSW are rather similar. However, the averaged adsorption distances of the carbon atoms are strikingly different: 2.46 Å for PyT and 2.83 Å for NO_2-PyT [403]. This was attributed to the bulky NO_2 groups 'pushing away' the carbon skeleton from the substrate. In fact, the oxygen atoms in these groups have adsorption distances of 2.75 Å. The valence electron structure and the measured adsorption distances could be reproduced quite well by DFT modelling with vdW corrections [403].

While these calculations were confirming the ΔVL data for PyT, the results for NO_2-PyT were at variance. This can be attributed to an orientational transition of NO_2-PyT to a standing monolayer. As XSW is intrinsically limited to lying (sub)monolayers, one has to rely on DFT for the adsorption geometry. Indeed, DFT modelling of a standing monolayer of NO_2-PyT on Ag(111) yields almost the same ΔVL as the measurements [403]. Figure 21(b) compares the charge rearrangements upon adsorption. For PyT and lying NO_2-PyT they are qualitatively similar and, moreover, they also fit with the charge rearrangements of F_4TCNQ upon adsorption on the same substrate (figure 16). In all cases, the minimum of charge density rearrangements (i.e., the maximum in electron density accumulation) can be found between the metal surface and the molecular π-system. For standing NO_2-PyT the minimum is located at the NO_2 docking groups (figure 21(c)). Moreover, the electron accumulation extends more than 10 Å above the surface and thus much further than for lying NO_2-PyT. Notably, the averaged charge transfer per molecule is smaller for standing (0.32e) than for lying (0.71e) NO_2-PyT. The dipole moment, however, is increased due the larger charge separation, which causes in turn a pronounced work function increase. Finally, one finds that the electron affinity measured for standing NO_2-PyT molecules is significantly increased because of electrostatic effects.

4.4.4. Surface modification and decoupling. Another area, in which the connection between electronic and geometric structure becomes evident, are efforts towards decoupling adsorbates from the metal substrate, which are often related to effects of charge transfer or exciton lifetimes. In the spirit of pioneering studies, such as the decoupling of Xe from Pd(001) by the adsorption of Kr monolayers [551], salt layers may be used to decouple COMs from metal surfaces [115, 127, 552–554]. Oxidation of Cu(100) via O_2-dosing decouples deposited PTCDA molecules from the surface and hinders organic–metal charge transfer: the averaged adsorption distance of the PTCDA carbon atoms on the oxygen-reconstructed $(\sqrt{2} \times \sqrt{2})R45°$ Cu(100) surface is 3.27 Å [543] and thus much larger than that on pristine Cu(100) (2.46 Å) [155]. The PTCDA/Ag(111) model system has also been studied with respect to doping by K [79, 555]. The experimental and theoretical results point towards a reduced electronic coupling between the adsorbate and the substrate, which goes hand in hand with an increasing adsorption distance of the PTCDA molecules caused by a bending of their carboxylic oxygen away from the substrate and towards the potassium atoms [79]. In principle, the organic–metal interaction strength can also be decreased by molecular functionalization with bulky side-groups [556]. However, only for one system adsorption distances have been measured by XSW and functionalizing azobenzene by alkyl groups only increases the averaged adsorption distance of the carbon atoms on Ag(111) by 0.14 Å [404] compared to the unsubstituted parent molecule [400].

4.5. Chemical reactions at interfaces

Chemical reactions at surfaces [557] involving COM molecules, a very important topic in the context of catalysis and surface functionalization, have been addressed in recent publications (see for instance references [49, 51, 436, 558–563]). Therefore, we shall only highlight some cases that involved a precise determination of the geometric structure by XSW: (i) on-surface formation of porous systems [384], (ii) self-metalation reactions of porphyrins

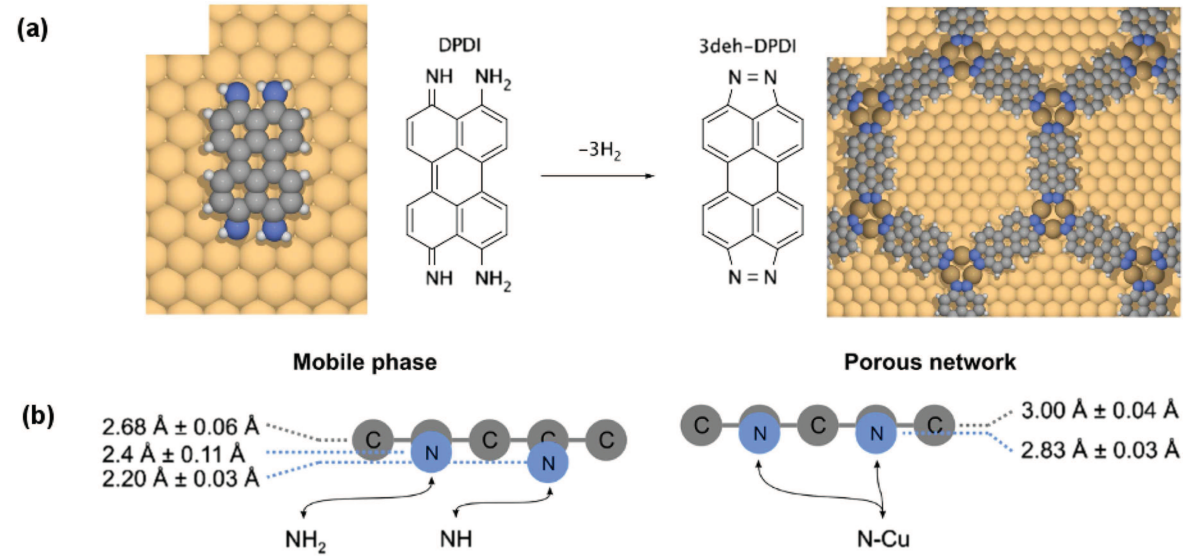

Figure 22. On-surface formation of a 2D porous network and the related chemical and structural molecular changes. (a) Schematics of the reaction leading to the network formation. The annealing at 200°C of a submonolayer coverage of DPDI induces the complete de-hydrogenation of the amine and imine groups, which are stabilized by the mediation of the Cu adatoms thus acting as the coordination centers for the network formation. Reprinted figure with permission from [384], Copyright (2014) by the American Physical Society.

[388], (iii) the dissociation reaction of azobenzene (AB) [390] and (iv) surface-mediated trans-effects [396] involving phthalocyanines.

4.5.1. On-surface formation of porous systems. The perylene derivative 4,9-diaminoperylene-quinone-3,10-diimine (DPDI) has been shown to dehydrogenate and become 3deh-DPDI after annealing of a submonolayer adsorbed on Cu(111) [564]. After loosing the hydrogen atoms, the two nitrogen atoms coordinate to copper adatoms and form a highly ordered nanoporous network (figure 22(a)). Matena and coworkers studied the chemical and structural changes induced by the formation of the network [384]. Initially, the core-level signature of nitrogen is composed of two peaks separated by 1.8 eV that belong to the amine (NH_3) and imide (NH) groups, the latter being ∼0.2 Å closer to the surface, as obtained with XSW (figure 22(b)). Thus, the measurements show two different environments for the nitrogen atoms, which, however, become chemically and structurally indistinguishable upon network formation through the equal binding of the nitrogen ligands to the Cu adatoms. In addition, the XSW measurements show an upward lifting of the molecule, i.e. ∼0.3 Å for the perylene core and ∼0.4 Å for the nitrogen atoms compared to the less interacting NH and NH_2 groups (figure 22(b)). This was interpreted in terms of the interplay between molecule–substrate vs intermolecular interactions, which is clearly balanced towards the latter upon network formation [384]. More precisely, the obtained adsorption distances with respect to the surface correspond to a physisorptive scenario, implying that the molecule is decoupled from the surface and the bonding occurs only through the copper adatoms. Interestingly, DFT calculations of the network with and without the surface indicate that a planar geometry, with the copper adatoms at the same plane as the molecules, is disrupted by the presence of the surface that pulls the copper adatoms closer and thus bend the molecule. Consequently, the adatoms mediate the intermolecular interactions acting as coordination centers but also influence the bonding between the molecules and the substrate [384].

4.5.2. Self-metalation reactions of porphyrins. As introduced in section 4.4.2, porphyrins as well as phthalocyanines can host a metal ion within the molecular core (figure 2). For metal-free molecules, these can also be incorporated through various metalation reactions [316, 565, 566], whereby a H_2-molecule is released and the ion becomes coordinated to the central nitrogen atoms. Similar to what has been discussed in the previous paragraph, the metalation reaction can be followed by monitoring the change in the N1s core-level signal (see figure 23(a)), i.e. from two clearly distinguishable aminic (or pyrrolic, –NH–) and iminic (–N==) nitrogen species for the free-base molecule towards one single species for the equally-coordinated nitrogen atoms [309, 388, 567, 568].

A particular case of metalation is realized through the direct incorporation of surface atoms, the so-called *self-metalation* reaction [309, 567]. In this context, the thermally induced self-metalation of 2*H*-tetraphenylporphyrin (2HTPP, figure 2(j)) adsorbed on Cu(111) and the subsequent formation of copper(II)-tetraphenylporphyrin (CuTPP) is one of the most thoroughly studied reaction [309, 375, 388, 568, 569]. For instance, in a temperature-dependent STM and XPS study of this reaction [568] it was found that along with the self-metalation (starting at 400 K) the molecule undergoes a gradual hydrogen loss until a total de-hydrogenation occurs at 500 K. As imaged with STM (figure 23(a)), 2HTPP molecules appear rather planar, with the phenyl groups parallel to the surface [568] but the increasing loss of hydrogen reduces the

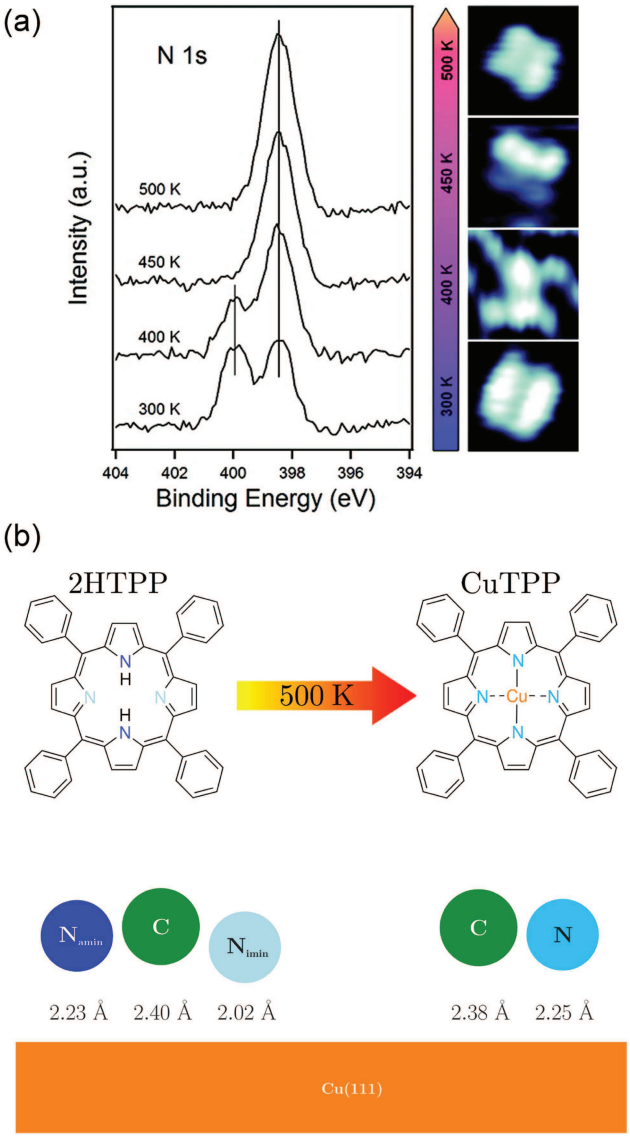

Figure 23. (a) Evolution of the nitrogen N1s core-level signal of 2HTPP as a function of the temperature and the corresponding STM images. Reprinted with permission from [568]. Copyright (2012) American Chemical Society. (b) Adsorption distances of the average carbon atoms and the nitrogen species (aminic in dark and iminic in light blue) before and after annealing at 500 K. Reprinted with permission from [388]. Copyright (2014) American Chemical Society.

steric repulsion between phenyl rings and enables their rotation [568]. Interestingly, the full de-hydrogenation again renders a flat molecule. Consequently, the adsorption geometry has possible contributions from the metalation, which relaxes the strong interaction of the nitrogen atoms with the substrate, and also from the rotation of the functional groups. In order to study the influence of the metalation on the vertical adsorption distance, Bürker *et al* [388] followed the changes in the adsorption upon self-metalation at 500 K to avoid strong contributions of the rotating phenyl groups to the conformational properties. Thus, for the free-base porphyrin the two inequivalent nitrogen atoms have two distinct adsorption distances (see figure 23(b)), i.e. the iminic ones closer to the surface as a

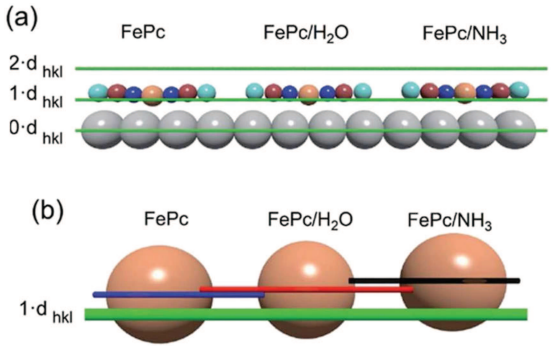

Figure 24. XSW measurements performed for FePc adsorbed on Ag(111) in the case of no-, H_2O- and NH_3-dosing. The *trans*-effect increases in the order $H_2O < NH_3 <$ Ag(111). (a) To-scale schematics of the XSW data (note that the graphic representation of the n ambiguity of the $d_{hkl} = d_0(n + P_{hkl})$. (b) Detail of the change of the Fe adsorption distance for the different cases, which clearly describes the structural implications of the surface *trans*-effect. Reproduced from [396]. CC BY 3.0.

result of the stronger interaction with the copper atoms [309]. Because both nitrogen species are located below the average carbon adsorption distance, the macrocycle takes a saddle-like shape on the surface. Upon metalation at 500 K, the incorporation of the copper atoms lifts this distortion, since the preferential interaction of the iminic nitrogens with the substrate is switched off (figure 23(b)). Interestingly, the average carbon adsorption distance remains virtually unchanged, although the vertical order is increased (as deduced from the higher coherent fractions). The authors therefore conclude that the metalation of 2HTPP relaxes the molecular core without impacting the overall adsorption distance of the molecule and rather possible rotations and/or bending of the phenyl groups determine the overall adsorption geometry [388]. Notably, recent DFT calculations of 2HTPP adsorbed on Cu(111) have shown that an inverted macrocycle reproduces the experimental data better than a saddle-shape geometry [570].

4.5.3. The dissociation reaction of azobenzene. As prototypical molecular switches azobenzene (AB) and its derivative tetrabutyl-AB (TBA) have been studied with XSW on Cu(111) [390] and on Ag(111) [400–402, 404]. Willenbockel *et al* [390] reported a coverage-dependent dissociation of AB on Cu(111), which itself is not observed on the Ag(111) surface [400–402]. The authors attribute the difference to the balance between molecule–molecule and substrate–molecule interactions. More precisely, the stronger bond between the nitrogen atoms of the (–N==N–) azo-bridge and the copper substrate forces AB to decompose into two phenyl nitrene molecules to accommodate the increasing molecular packing. In contrast, the N–Ag bond is weaker and allows the molecule to deform upon coverage increase. Through a sophisticated vector analysis of the XSW data [402] the authors obtained tilt and rotational angles for the phenyl rings on both substrates. The derived rotation of those groups on silver is larger than on copper, which is considered as indication for the increased flexibility of the N–Ag bond.

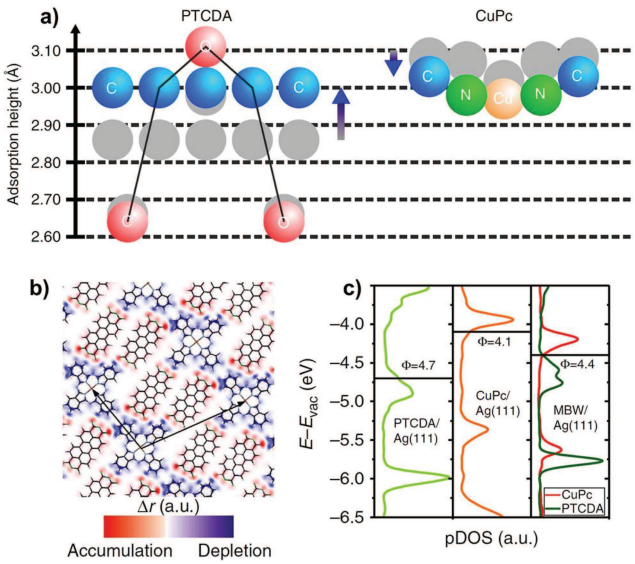

Figure 25. Bimolecular mixed layer of PTCDA and CuPc on Ag(111). (a) Vertical adsorption geometry as revealed by XSW. The adsorption heights of all involved atomic species are illustrated for the bimolecular monolayer (colored spheres) and the homomolecular monolayer (gray spheres). (b) Charge density difference plot showing depletion (blue) and accumulation (red) of electronic charge in a plane parallel to the surface (in a height of maximum DOS of the LUMO orbitals). (c) Projected DOS of the π-orbitals of PTCDA and CuPc in the homomolecular PTCDA/Ag(111) (left), the homomolecular CuPc/Ag(111) (middle) and the bimolecular layer (right). Energies are aligned with the vacuum level, the Fermi energies are indicated by black lines revealing the work functions. Reprinted from [71] by permission from Springer Nature Customer Service Centre GmbH: Nature Communication © 2014.

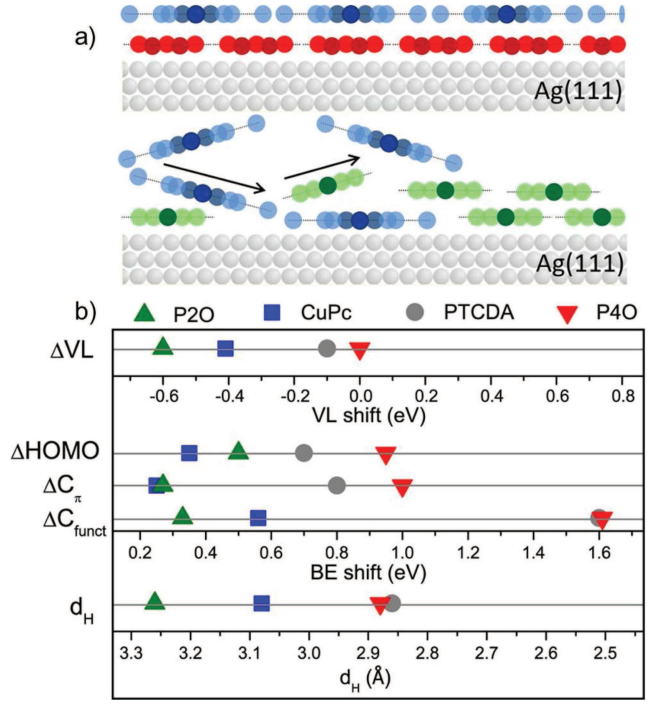

Figure 26. (a) Bilayer formation (top) vs molecular exchange (bottom). In both cases, CuPc (blue) has been vacuum-sublimed on a closed monolayer of P4O (red) or P2O (green) on Ag(111). (b) Vacuum level shift (ΔVL) between clean Ag(111) and a monolayer of the respective COM. Binding-energy shift between monolayer and multilayer of the HOMO-maximum (ΔHOMO) and the C1s peak of the molecular backbone (ΔC_π) and the functional group (ΔC_{funct}) of the respective COM on Ag(111). Averaged bonding distance (d_H) of the carbon atoms in the molecular core in sub-monolayers on Ag(111). Reprinted with permission from [118]. Copyright (2018) American Chemical Society.

Interestingly, in another study it was found that the isomerization reaction of AB, which is essential for the switching mechanism, can be quickly reversed by CT from the substrate to the molecule, thus preventing the switching effect to be measured [571]. This would explain why the switching is observed on Au(111) [572] but not on Ag(111) [573].

4.5.4. Surface-mediated trans-effects of MePc. In inorganic chemistry, it is known that adding a new ligand to a metal ion influences the bond between the ion and the other previously present ligands. One can distinguish two cases: the ligands are opposed (trans) to each other or the ligands are at the same side (cis). The new coordination affects the ground-state properties, the length as well as the thermodynamic and vibrational properties of the other bonds. In an analogous situation, it was seen that one can reproduce the *trans*-effect with metal-ion-containing molecules adsorbed on a metal surface, where the substrate acts as one of the ligands. This is known as surface *trans*-effect. For the particular case of metal phthalocyanines (MePc) adsorbed on Ag(111), a study with complementary PES, STM and DFT determined that Co and Fe ions are forming bonds with the substrate, but not Zn [574]. Interestingly, upon dosing of nitric oxide (NO), the changes in the electronic characteristics indicate that the ion-to-substrate bond is weakened or entirely suppressed and DFT calculations show that the Ag–Me bond length is increased [574].

In this context, it was recently found that the coordination of ligands with different reactive character to the Fe ion of FePc adsorbed on Ag(111) indeed changes the Ag-to-Fe adsorption distance [396]. More precisely, H_2O and ammonia (NH_3) were dosed, which renders an increasing trans-effect in the order $H_2O < NH_3 <$ Ag(111), thus one expects that the Fe atom should show a larger adsorption distance when the Ag(111) surface is *trans* to the ammonia than to water. As shown in figure 24, the XSW results confirmed this scheme as the Fe atom is rather shifted away from the surface when NH_3 is dosed compared to H_2O. This behavior was also reproduced with vdW-corrected DFT.

4.6. Heterostructures

Organic heterostructures in the monolayer or bilayer regime on clean metals [50, 83, 174, 318, 575] may be considered as model systems for organic–organic interfaces, i.e. the essential component for most electronic devices applications. Most studies in the area are dealing with bimolecular mixed layers [71, 175, 325, 576], whereas only a few studies focus on bilayers [118, 383, 577–579, 587]. For both types of heterostructures CuPc and PTCDA on Ag(111) have become

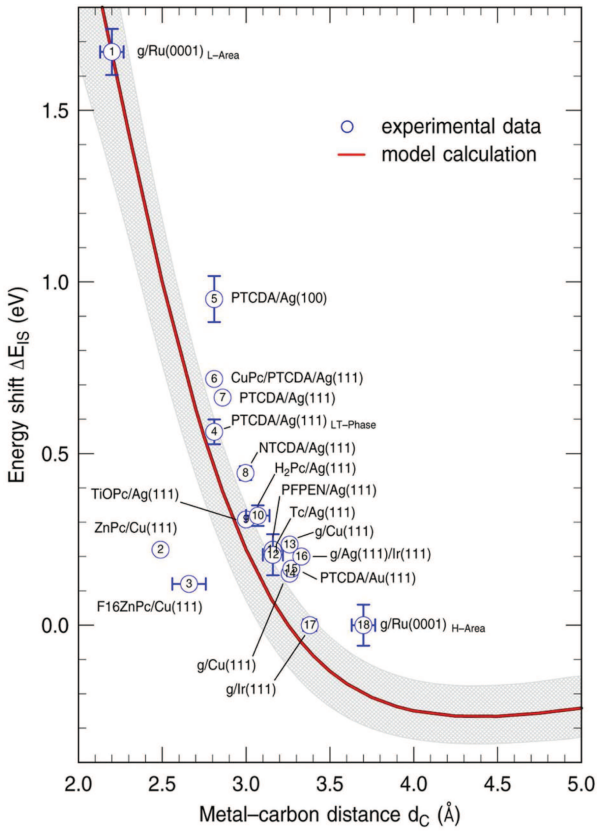

Figure 27. Energy shift ΔE_{IS} of the interface state with respect to the Shockley surface state on the pristine metal as a function of the carbon–metal distance d_C. The solid red line shows the calculated results for a carbon layer on Ag(111). Reprinted from [585] by permission from Springer Nature Customer Service Centre GmbH: Springer. Sci. Rep. © 2017.

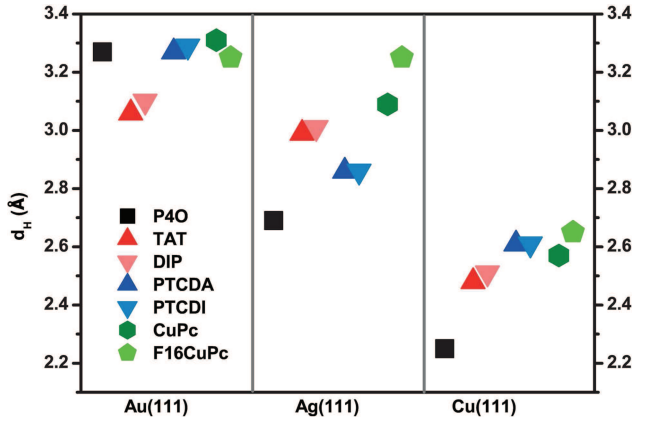

Figure 28. Compilation of vertical adsorption distances d_H for carbon atoms within the molecular backbone of selected COMs. The plot includes those systems for which XSW results on all (111)-surfaces of the noble metals Au, Ag, and Cu are available. The data shown here are taken from references [17, 18, 77, 78, 80, 148, 150, 151, 170, 178, 385, 395].

popular [71, 325, 345, 383, 578–582]. Figure 25(a) shows the experimentally determined adsorption geometries of PTCDA and CuPc in their respective monolayers on Ag(111) and in the bimolecular mixed layer [71]. Strikingly, PTCDA is lifted up in the bimolecular system, whereas CuPc is pushed down. Naively, this could lead to the notion that the coupling of PTCDA with Ag(111) decreases and that of CuPc with Ag(111) increases. However, the situation is more complex and Stadtmüller *et al* [71] showed by means of STM, STS, orbital tomography and DFT modelling that the adsorption height changes are driven by intermolecular interactions, which are increased by the equalization of adsorption heights. As illustrated in figure 25(b), which highlights the charge rearrangement between PTCDA and CuPc, the acceptor character of PTCDA and the donor character of CuPc are increased in the bimolecular system. Consequently, the LUMOs of PTCDA and CuPc move away from the common Fermi level in opposite directions (figure 25(c)). Overall, this example shows how observables such as vertical adsorption distances, frontier orbital binding energies and charge transfer are linked and influence each other.

For bilayer systems, the most fundamental question is whether the deposition sequence reflects the actual arrangement in the heterostructure. At room temperature, this is the case for CuPc deposited on a closed monolayer of PTCDA on Ag(111) [383]. However, for the reverse deposition sequence, i.e., PTCDA on CuPc, molecular exchange occurs and PTCDA replaces CuPc in the contact layer to Ag(111) [383, 578]. One could expect that this is related to the different interaction strength of the adsorbates with the substrate, which is weaker for CuPc than for PTCDA. This assumption has been tested by using P2O and P4O monolayers on Ag(111), which have been introduced as reference systems for physisorption and chemisorption (figures 5 and 6). Indeed, subsequently deposited CuPc molecules can replace P2O in the contact layer to Ag(111), while they remain on top of P4O on Ag(111) (figure 26(a)) [118]. The different behavior of the CuPc/P*x*O/Ag(111) bilayer systems allows, thus, to conclude that the interaction of CuPc with Ag(111) is beyond physisorption (although still relatively 'weak' [77]).

As mentioned in section 2.1, rigid shifts of valence and core-levels observed for monolayer and multilayer coverage can serve as indicator for organic–metal interaction strength. These shifts are shown in figure 26(b) for P2O, P4O, CuPc and PTCDA on Ag(111). With the exception of the shift between HOMO position in the monolayer and the multilayer (ΔHOMO) all indicators show that the interaction strength with Ag(111) increases in the order P2O–CuPc–PTCDA–P4O. The largest shifts have been found for the core-levels of carbon atoms in functional groups (ΔC_{funct}), which might be the best indicator for the interaction strength. Notably, all the data are taken from measurements of monomolecular systems [75, 77, 118, 150, 433, 583], but still allow to predict the sequential arrangement in heterostructures. However, we are aware that also other factors such as the particular molecular weight or shape also impact possible molecular exchange processes [466, 584].

Figure 26(b) also includes vacuum level shifts between the clean Ag(111) surface and the respective monolayer and the vertical adsorption heights. As discussed throughout this review, several often competing factors impact dipoles at

organic–metal interfaces. The 'correct' order of the ΔVLs might thus be merely coincidental. Vertical adsorption distances are a better indicator (for a detailed discussion see section 5). However, they have the disadvantage of requiring measurements at highly specialized beamlines at synchrotron radiation facilities, whereas the photoelectron spectroscopy based indicators can be accessed with standard lab equipment.

5. Summary and conclusions

As discussed in this review, the contact formation of specific adsorbate–substrate systems is by now reasonably well understood. At the same time, numerous studies addressing the relation of structural and electronic properties at organic–metal interfaces [50, 51, 82, 83, 85, 86, 391] have demonstrated that there are actually no 'simple rules' and that a prediction of the energy-level alignment requires significant computational efforts.

Nevertheless, we can identify a few general trends that connect the adsorption geometry and the energy-level alignment. For example, a clear correlation was found for the shift of the Shockley surface state ΔE_{IS} on clean metals due to adsorption of a molecular monolayer (cf figure 27). Apparently, this shift is related to the organic–metal coupling strength and can be explained using a relatively simple one-dimensional model potential [585]. A closer inspection of figure 27, however, reveals that most of the data points refer to Ag(111) surfaces and that the two outliers on the left of the calculated model curve correspond to energy shifts on Cu(111) surfaces. This indicates that the situation is more complicated and that in some cases effects beyond LUMO filling [585] play a role for the surface state shift.

Elaborating on this issue, figure 28 shows adsorption distances d_H of carbon atoms in an aromatic environment of seven COMs, for which they have been determined on all three (111)-surfaces of the noble metals. While the plot is certainly simplistic (possible coverage and/or temperature effects are neglected) and the selection of molecules is to some degree arbitrary, it highlights some important findings for organic–metal interfaces. Obviously, for all COMs the adsorption distances decrease in the order Au–Ag–Cu (see also section 2.2). Moreover, on Au(111) and Cu(111) the bonding distances exhibit a rather narrow distribution of only ∼0.25 Å (if the outlier P4O on Cu(111) is excluded), whereas on Ag(111) the bonding distances span ∼0.60 Å. This difference can be explained by noting that generally—and in particular for the selected COMs in figure 28—the interaction with Au(111) is mostly physisorptive and that with Cu(111) mostly chemisorptive, whereas COMs on Ag(111) may tend to either weak or strong coupling.

To illustrate this variability we may first consider two pairs of COMs, i.e. TAT/DIP (red symbols in figure 28) and PTCDA/PTCDI (blue symbols in figure 28), which each have nearly the same vertical adsorption distances on the different surfaces. For TAT/DIP, the adsorption distances on Au(111) and Ag(111) are very similar, but decrease significantly on Cu(111). For PTCDA/PTCDI, on the other hand, a pronounced decrease occurs already when going from Au(111) to Ag(111). This behavior shows that for molecules with more reactive functional groups (see also section 2.3) chemisorption already sets in on Ag(111), as confirmed by the pronounced molecular distortion (figure 7) and strong chemical core-level shifts (figures 11 and 26) on this surface. We note that having virtually the same vertical adsorption distances, does not imply that the energy-level alignment is identical: PTCDA is Fermi-level pinned on all the three surfaces [75] (and virtually all other substrates [128]), whereas the ELA of PTCDI is vacuum level controlled on the (111)-surfaces of the noble metals [80]. The influence of site-specific interactions is even more pronounced for P4O on these surfaces (black symbol in figure 28), showing adsorption distances which differ by more than 1 Å due to the re-hybridization of P4O on Ag(111) (figure 5) and Cu(111). In fact, the vertical adsorption distances of PEN and P4O on Cu(111) are rather similar (2.34 Å and 2.25 Å, respectively) [74, 78]. While P4O is Fermi-level pinned, the ELA of P2O and PEN are vacuum level controlled on these three surfaces [73].

A common approach to reduce the organic–metal interaction strength is (per)fluorination of the adsorbate [17, 77, 385]. Comparing CuPc and F_{16}CuPc (green symbols in figure 26) shows that on Ag(111) this method is indeed working and the repulsive interaction of the fluorine atoms prevent coupling beyond physisorption—as observed for CuPc/Ag(111). On Cu(111), however, where the adsorption distances of both phthalocyanine molecules are rather similar, the attractive interaction between the substrate and the Pc core is already too strong and the fluorine atoms cannot 'repel' the entire molecule. Consequently, for F_{16}CuPc/Cu(111) [17] (and other perfluorinated Pcs such as F_{16}ZnPc/Cu(111) [167]) a significant molecular distortion with the fluorine atoms above the carbon backbone is found.

Overall, these results demonstrate that the interplay between adsorption geometry and electronic structure is complex and measuring the element-specific adsorption distances of π-conjugated molecules on metals is essential for understanding the interface dipoles and thus the energy-level alignment. Because of the different driving forces for charge rearrangements upon contact formation, such as push-back effect or chemical-bond formation, the bonding behavior cannot be characterized using few parameters like the metal work function, the ionization energy and electron affinity of the organic thin film. While XSW has become a well-established high-precision technique in the field of metal–organic interfaces, it has not yet been used extensively to study all relevant systems. However, we are confident that the results reviewed here and, most importantly, new state-of-the-art facilities, such as beamline I09 at the Diamond Light Source will encourage further systematic studies of such a vivid and interesting area of surface science.

Acknowledgments

The authors thank the European Synchrotron Radiation Facility (ESRF) and the Diamond Light Source (DLS) for making their facilities available to us. We thank the different local

contacts and beamline scientist that helped us during the numerous XSW experiments at ID32 (ESRF, until 2011) and I09 (DLS, since 2013), in particular Jörg Zegenhagen and Tien-Lin Lee.

It is a pleasure to acknowledge interactions with a large number of colleagues in the field, including in alphabetical order J Banerjee, C Bürker, B Detlefs, D A Duncan, G Heimel, O T Hofmann, T Hosokai, S Kera, N Koch, C Kumpf, J Niederhausen, I Salzmann, A Schöll, M Sokolowski, P K Thakur, F S Tautz, A Tkatchenko, N Ueno, A Vollmer, Q Wang, E Zojer and others, too many to name them all.

Financial support from the Deutsche Forschungsgemeinschaft (DFG), the Soochow University–Western University Center for Synchrotron Radiation Research, the 111 Project of the Chinese State Administration of Foreign Experts Affairs and the Collaborative Innovation Center of Suzhou Nano Science & Technology (NANO-CIC) is gratefully acknowledged.

ORCID iDs

Antoni Franco-Cañellas https://orcid.org/0000-0001-7767-9611
Steffen Duhm https://orcid.org/0000-0002-5099-5929
Alexander Gerlach https://orcid.org/0000-0003-1787-1868
Frank Schreiber https://orcid.org/0000-0003-3659-6718

References

[1] Ishii H, Sugiyama K, Ito E and Seki K 1999 Energy level alignment and interfacial electronic structures at organic/metal and organic/organic interfaces *Adv. Mater.* **11** 605–25
[2] Kahn A, Koch N and Gao W 2003 Electronic structure and electrical properties of interfaces between metals and π-conjugated molecular films *J. Polym. Sci.* B **41** 2529–48
[3] Koch N 2008 Energy levels at interfaces between metals and conjugated organic molecules *J. Phys.: Condens. Matter.* **20** 184008
[4] Widdascheck F, Hauke A A and Witte G 2019 A solvent-free solution: vacuum-deposited organic monolayers modify work functions of noble metal electrodes *Adv. Funct. Mater.* **29** 1808310–85
[5] Fahlman M, Fabiano S, Gueskine V, Simon D, Berggren M and Crispin X 2019 Interfaces in organic electronics *Nat. Rev. Mater.* **4** 627–50
[6] Tkatchenko A, Romaner L, Hofmann O T, Zojer E, Ambrosch-Draxl C and Scheffler M 2010 van der Waals interactions between organic adsorbates and at organic/inorganic interfaces *MRS Bull.* **35** 435–42
[7] Berland K, Cooper V R, Lee K, Schröder E, Thonhauser T, Hyldgaard P and Lundqvist B I 2015 van der Waals forces in density functional theory: a review of the vdW-DF method *Rep. Prog. Phys.* **78** 066501
[8] Liu W, Maaß F, Willenbockel M, Bronner C, Schulze M, Soubatch S, Tautz F S, Tegeder P and Tkatchenko A 2015 Quantitative prediction of molecular adsorption: structure and binding of benzene on coinage metals *Phys. Rev. Lett.* **115** 036104
[9] Maurer R J, Ruiz V G, Camarillo-Cisneros J, Liu W, Ferri N, Reuter K and Tkatchenko A 2016 Adsorption structures and energetics of molecules on metal surfaces: bridging experiment and theory *Prog. Surf. Sci.* **91** 72–100
[10] Hermann J, DiStasio R A and Tkatchenko A 2017 First-principles models for van der Waals interactions in molecules and materials: concepts, theory, and applications *Chem. Rev.* **117** 4714–58
[11] Liu Z F, Egger D A, Refaely-Abramson S, Kronik L and Neaton J B 2017 Energy level alignment at molecule-metal interfaces from an optimally tuned range-separated hybrid functional *J. Chem. Phys.* **146** 092326–13
[12] Norsko J K 1990 Chemisorption on metal surfaces *Rep. Prog. Phys.* **53** 1253–95
[13] Diehl R D, Seyller T, Caragiu M, Leatherman G S, Ferralis N, Pussi K, Kaukasoina P and Lindroos M 2004 The adsorption sites of rare gases on metallic surfaces: a review *J. Phys.: Condens. Matter.* **16** S2839–62
[14] Zegenhagen J 1993 Surface structure determination with x-ray standing waves *Surf. Sci. Rep.* **18** 202–71
[15] Cowan P L, Golovchenko J A and Robbins M F 1980 X-ray standing waves at crystal surfaces *Phys. Rev. Lett.* **44** 1680
[16] Bedzyk M J and Materlik G 1985 Determination of the position and vibrational amplitude of an adsorbate by means of multiple-of x-ray standing-wave measurements *Phys. Rev.* B **31** 4110–2
[17] Gerlach A, Schreiber F, Sellner S, Dosch H, Vartanyants I A, Cowie B C C, Lee T L and Zegenhagen J 2005 Adsorption-induced distortion of F16CuPc on Cu(111) and Ag(111): an x-ray standing wave study *Phys. Rev.* B **71** 205425
[18] Hauschild A, Karki K, Cowie B C C, Rohlfing M, Tautz F S and Sokolowski M 2005 Molecular distortions and chemical bonding of a large π-conjugated molecule on a metal surface *Phys. Rev. Lett.* **94** 036106
[19] Hofmann P, Schindler K M, Bao S, Fritzsche V, Ricken D, Bradshaw A and Woodruff D 1994 The geometric structure of the surface methoxy species on Cu(111) *Surf. Sci.* **304** 74–84
[20] Krause B, Dürr A C, Schreiber F, Dosch H and Seeck O H 2003 Thermal stability and partial dewetting of crystalline organic thin films: PTCDA on Ag(111) *J. Chem. Phys.* **119** 3429–35
[21] Stellwag C, Held G and Menzel D 1995 The geometry of ordered benzene layers on Ru(001) *Surf. Sci.* **325** L379–84
[22] Zheleva Z V, Eralp T and Held G 2012 Complete experimental structure determination of the p(3 $\times$ 2)pg phase of glycine on Cu(110) *J. Phys. Chem.* C **116** 618–25
[23] Sirtl T, Jelic J, Meyer J, Das K, Heckl W M, Moritz W, Rundgren J, Schmittel M, Reuter K and Lackinger M 2013 Adsorption structure determination of a large polyaromatic trithiolate on Cu(111): combination of LEED-I(V) and DFT-vdW *Phys. Chem. Chem. Phys.* **15** 11054–60
[24] Grimme S 2006 Semiempirical GGA-type density functional constructed with a long-range dispersion correction *J. Comput. Chem.* **27** 1787–99
[25] Rydberg H, Dion M, Jacobson N, Schröder E, Hyldgaard P, Simak S I, Langreth D C and Lundqvist B I 2003 van der Waals density functional for layered structures *Phys. Rev. Lett.* **91** 126402
[26] Dion M, Rydberg H, Schröder E, Langreth D C and Lundqvist B I 2004 van der Waals density functional for general geometries *Phys. Rev. Lett.* **92** 246401
[27] Tkatchenko A and Scheffler M 2009 Accurate molecular van der Waals interactions from ground-state electron density and free-atom reference data *Phys. Rev. Lett.* **102** 073005

[28] Berland K, Chakraborty D and Thonhauser T 2019 van der Waals density functional with corrected C6 coefficients *Phys. Rev.* B **99** 195418

[29] Bagus P S, Staemmler V and Wöll C 2002 Exchangelike effects for closed-shell adsorbates: interface dipole and work function *Phys. Rev. Lett.* **89** 096104

[30] Abbasi A and Scholz R 2009 Ab initio calculation of the dispersion interaction between a polyaromatic molecule and a noble metal substrate: PTCDA on Ag(110) *J. Phys. Chem.* C **113** 19897–904

[31] Klimeš J and Michaelides A 2012 Perspective: advances and challenges in treating van der Waals dispersion forces in density functional theory *J. Chem. Phys.* **137** 120901

[32] Seki K, Harada Y, Ohno K and Inokuchi H 1974 High-resolution photoelectron spectroscopy of naphthacene polycrystal by means of helium 21.22 eV resonance line *Bull. Chem. Soc. Jpn.* **47** 1608–10

[33] Salaneck W R 1978 Intermolecular relaxation energies in anthracene *Phys. Rev. Lett.* **40** 60–3

[34] Ohno T R, Chen Y, Harvey S E, Kroll G H, Weaver J H, Haufler R E and Smalley R E 1991 C60 bonding and energy-level alignment on metal and semiconductor surfaces *Phys. Rev.* B **44** 13747–55

[35] Narioka S, Ishii H, Yoshimura D, Sei M, Ouchi Y, Seki K, Hasegawa S, Miyazaki T, Harima Y and Yamashita K 1995 The electronic structure and energy level alignment of porphyrin/metal interfaces studied by ultraviolet photoelectron spectroscopy *Appl. Phys. Lett.* **67** 1899–901

[36] Lee S T, Hou X Y, Mason M G and Tang C W 1998 Energy level alignment at Alq/metal interfaces *Appl. Phys. Lett.* **72** 1593–5

[37] Koch N 2007 Organic electronic devices and their functional interfaces *ChemPhysChem* **8** 1438–55

[38] Braun S, Salaneck W R and Fahlman M 2009 Energy-level alignment at organic/metal and organic/organic interfaces *Adv. Mater.* **21** 1450–72

[39] Hwang J, Wan A and Kahn A 2009 Energetics of metal-organic interfaces: new experiments and assessment of the field *Mater. Sci. Eng.* R **64** 1–31

[40] Greiner M T, Helander M G, Tang W M, Wang Z B, Qiu J and Lu Z H 2012 Universal energy-level alignment of molecules on metal oxides *Nat. Mater.* **11** 76–81

[41] Opitz A 2017 Energy level alignment at planar organic heterojunctions: influence of contact doping and molecular orientation *J. Phys.: Condens. Matter.* **29** 133001–16

[42] Cinchetti M, Dediu V A and Hueso L E 2017 Activating the molecular spinterface *Nat. Mater.* **16** 507

[43] Akaike K 2018 Advanced understanding on electronic structure of molecular semiconductors and their interfaces *Japan. J. Appl. Phys.* **57** 03EA03–17

[44] Zojer E, Taucher T C and Hofmann O T 2019 The impact of dipolar layers on the electronic properties of organic/inorganic hybrid interfaces *Adv. Mater. Interfaces* **6** 1900581–32

[45] Ley L, Smets Y, Pakes C I and Ristein J 2013 Calculating the universal energy-level alignment of organic molecules on metal oxides *Adv. Funct. Mater.* **23** 794–805

[46] Oehzelt M, Koch N and Heimel G 2014 Organic semiconductor density of states controls the energy level alignment at electrode interfaces *Nat. Commun.* **5** 4174

[47] Yang J P, Bussolotti F, Kera S and Ueno N 2017 Origin and role of gap states in organic semiconductor studied by ups: as the nature of organic molecular crystals *J. Phys. D: Appl. Phys.* **50** 423002

[48] Monti O L A 2012 Understanding interfacial electronic structure and charge transfer: an electrostatic perspective *J. Phys. Chem. Lett.* **3** 2342–51

[49] Klappenberger F 2014 Two-dimensional functional molecular nanoarchitectures—complementary investigations with scanning tunneling microscopy and x-ray spectroscopy *Prog. Surf. Sci.* **89** 1–55

[50] Goiri E, Borghetti P, El-Sayed A, Ortega J E and de Oteyza D G 2016 Multi-component organic layers on metal substrates *Adv. Mater.* **28** 1340–68

[51] Otero R, Vázquez de Parga A and Gallego J 2017 Electronic, structural and chemical effects of charge-transfer at organic/inorganic interfaces *Surf. Sci. Rep.* **72** 105–45

[52] Fung M K, Li Y Q and Liao L S 2016 Tandem organic light-emitting diodes *Adv. Mater.* **28** 10381–408

[53] Lüssem B, Keum C M, Kasemann D, Naab B, Bao Z and Leo K 2016 Doped organic transistors *Chem. Rev.* **116** 13714–51

[54] Nakano K and Tajima K 2017 Organic planar heterojunctions: from models for interfaces in bulk heterojunctions to high-performance solar cells *Adv. Mater.* **29** 1603269–33

[55] Bao Q, Braun S, Wang C, Liu X and Fahlman M 2019 Interfaces of (ultra)thin polymer films in organic electronics *Adv. Mater. Interfaces* **6** 1800897–15

[56] Rockson T, Baek S, Jang H, Choi G, Oh S, Kim J, Cho H, Kim S H and Lee H S 2019 Engineering asymmetric charge injection/extraction to optimize organic transistor performances *ACS Appl. Mater. Interfaces* **11** 10108–17

[57] Gurney R S, Lidzey D G and Wang T 2019 A review of non-fullerene polymer solar cells: from device physics to morphology control *Rep. Prog. Phys.* **82** 036601

[58] Koch N, Duhm S, Rabe J P, Vollmer A and Johnson R L 2005 Optimized hole injection with strong electron acceptors at organic-metal interfaces *Phys. Rev. Lett.* **95** 237601–4

[59] Li F, Zhou Y, Zhang F, Liu X, Zhan Y and Fahlman M 2009 Tuning work function of noble metals as promising cathodes in organic electronic devices *Chem. Mater.* **21** 2798–802

[60] Zhou Y *et al* 2012 A universal method to produce low-work function electrodes for organic electronics *Science* **336** 327–32

[61] Vilan A and Cahen D 2017 Chemical modification of semiconductor surfaces for molecular electronics *Chem. Rev.* **117** 4624–66

[62] Bröker B, Blum R P, Frisch J, Vollmer A, Hofmann O T, Rieger R, Müllen K, Rabe J P, Zojer E and Koch N 2008 Gold work function reduction by 2.2 eV with an air-stable molecular donor layer *Appl. Phys. Lett.* **93** 243303–3

[63] Rana O, Srivastava R, Chauhan G, Zulfequar M, Husain M, Srivastava P C and Kamalasanan M N 2012 Modification of metal-organic interface using F4-TCNQ for enhanced hole injection properties in optoelectronic devices *Phys. Status Solidi* A **209** 2539–45

[64] Gao C H, Zhu X Z, Zhang L, Zhou D Y, Wang Z K and Liao L S 2013 Comparative studies on the inorganic and organic p-type dopants in organic light-emitting diodes with enhanced hole injection *Appl. Phys. Lett.* **102** 153301–5

[65] Timpel M, Li H, Nardi M V, Wegner B, Frisch J, Hotchkiss P J, Marder S R, Barlow S, Bredas J L and Koch N 2018 Electrode work function engineering with phosphonic acid monolayers and molecular acceptors: charge redistribution mechanisms *Adv. Funct. Mater.* **28** 11704438

[66] Romaner L, Heimel G, Brédas J L, Gerlach A, Schreiber F, Johnson R L, Zegenhagen J, Duhm S, Koch N and Zojer E 2007 Impact of bidirectional charge transfer and molecular distortions on the electronic structure of a metal-organic interface *Phys. Rev. Lett.* **99** 256801

[67] Tseng T C *et al* 2010 Charge-transfer-induced structural rearrangements at both sides of organic/metal interfaces *Nat. Chem.* **2** 374–9

[68] Vitali L, Levita G, Ohmann R, Comisso A, De Vita A and Kern K 2010 Portrait of the potential barrier at metal-organic nanocontacts *Nat. Mater.* **9** 320–3

[69] Häming M, Schöll A, Umbach E and Reinert F 2012 Adsorbate-substrate charge transfer and electron-hole correlation at adsorbate/metal interfaces *Phys. Rev.* B **85** 235132

[70] Hofmann O T, Atalla V, Moll N, Rinke P and Scheffler M 2013 Interface dipoles of organic molecules on Ag(111) in hybrid density-functional theory *New J. Phys.* **15** 123028–25

[71] Stadtmüller B *et al* 2014 Unexpected interplay of bonding height and energy level alignment at heteromolecular hybrid interfaces *Nat. Commun.* **5** 3685

[72] Zamborlini G *et al* 2017 Multi-orbital charge transfer at highly oriented organic/metal interfaces *Nat. Commun.* **8** 335

[73] Chen M T *et al* 2019 Energy-level alignment at strongly coupled organic-metal interfaces *J. Phys.: Condens. Matter.* **31** 194002–11

[74] Koch N *et al* 2008 Adsorption induced intramolecular dipole: correlating molecular conformation and interface electronic structure *J. Am. Chem. Soc.* **130** 7300–4

[75] Duhm S, Gerlach A, Salzmann I, Bröker B, Johnson R, Schreiber F and Koch N 2008 PTCDA on Au(111), Ag(111) and Cu(111): correlating bonding distance and interfacial charge transfer *Org. Electron.* **9** 111–8

[76] Stadler C, Hansen S, Kröger I, Kumpf C and Umbach E 2009 Tuning intermolecular interaction in long-range-ordered submonolayer organic films *Nat. Phys.* **5** 153–8

[77] Kröger I *et al* 2010 Submonolayer growth of copper-phthalocyanine on Ag(111) *New J. Phys.* **12** 083038

[78] Heimel G *et al* 2013 Charged and metallic molecular monolayers through surface-induced aromatic stabilization *Nat. Chem.* **5** 187–94

[79] Baby A *et al* 2017 Fully atomistic understanding of the electronic and optical properties of a prototypical doped charge-transfer interface *ACS Nano* **11** 10495–508

[80] Franco-Cañellas A, Wang Q, Broch K, Duncan D A, Thakur P K, Liu L, Kera S, Gerlach A, Duhm S and Schreiber F 2017 Metal-organic interface functionalization via acceptor end groups: PTCDI on coinage metals *Phys. Rev. Mater.* **1** 013001(R)

[81] Klein B P *et al* 2019 Molecule-metal bond of alternant versus nonalternant aromatic systems on coinage metal surfaces: naphthalene versus azulene on Ag(111) and Cu(111) *J. Phys. Chem.* C **123** 29219–30

[82] Gerlach A, Bürker C, Hosokai T and Schreiber F 2013 X-ray standing waves and surfaces x-ray scattering studies of molecule-metal interfaces *The Molecule-Metal Interface* ed N Koch, N Ueno and A Wee (Weinheim: Wiley)

[83] Stadtmüller B, Schröder S and Kumpf C 2015 Heteromolecular metal-organic interfaces: electronic and structural fingerprints of chemical bonding *J. Electron Spectrosc. Relat. Phenom.* **204** 80–91

[84] Duhm S, Bürker C, Hosokai T and Gerlach A 2015 *Vertical Bonding Distances Impact Organic-Metal Interface Energetics* (Springer Series in Materials Science vol 209) ed H Ishii, K Kudo, T Nakayama and N Ueno (Japan: Springer) pp 89–107

[85] Willenbockel M, Lüftner D, Stadtmüller B, Koller G, Kumpf C, Soubatch S, Puschnig P, Ramsey M G and Tautz F S 2014 The interplay between interface structure, energy level alignment and chemical bonding strength at organic-metal interfaces *Phys. Chem. Chem. Phys.* **17** 1530–48

[86] Kera S, Hosokai T and Duhm S 2018 Characteristics of organic-metal interaction: a perspective from bonding distance to orbital delocalization *J. Phys. Soc. Japan* **87** 061008–8

[87] Friend R H, Phillips M, Rao A, Wilson M W B, Li Z and McNeill C R 2012 Excitons and charges at organic semiconductor heterojunctions *Faraday Discuss.* **155** 339–48

[88] Forrest S R 2015 Excitons and the lifetime of organic semiconductor devices *Phil. Trans. R. Soc.* A **373** 2044–7

[89] Djurovich P I, Mayo E I, Forrest S R and Thompson M E 2009 Measurement of the lowest unoccupied molecular orbital energies of molecular organic semiconductors *Org. Electron.* **10** 515–20

[90] Gao W and Kahn A 2001 Controlled p-doping of zinc phthalocyanine by coevaporation with tetrafluorotetracyanoquinodimethane: a direct and inverse photoemission study *Appl. Phys. Lett.* **79** 4040–2

[91] Zahn D R T, Gavrila G N and Salvan G 2007 Electronic and vibrational spectroscopies applied to organic/inorganic interfaces *Chem. Rev.* **107** 1161–232

[92] Bredas J L 2014 Mind the gap! *Mater. Horiz.* **1** 17–19

[93] Han W N *et al* 2013 Quantitatively identical orientation-dependent ionization energy and electron affinity of diindenoperylene *Appl. Phys. Lett.* **103** 253301–4

[94] Heimel G, Salzmann I, Duhm S and Koch N 2011 Design of organic semiconductors from molecular electrostatics *Chem. Mater.* **23** 359–77

[95] Duhm S, Heimel G, Salzmann I, Glowatzki H, Johnson R L, Vollmer A, Rabe J P and Koch N 2008 Orientation-dependent ionization energies and interface dipoles in ordered molecular assemblies *Nat. Mater.* **7** 326–32

[96] D'Avino G, Muccioli L, Castet F, Poelking C, Andrienko D, Soos Z G, Cornil J and Beljonne D 2016 Electrostatic phenomena in organic semiconductors: fundamentals and implications for photovoltaics *J. Phys.: Condens. Matter.* **28** 433002

[97] Zahn D R, Gavrila G N and Gorgoi M 2006 The transport gap of organic semiconductors studied using the combination of direct and inverse photoemission *Chem. Phys.* **325** 99–112

[98] Horowitz G 2015 Validity of the concept of band edge in organic semiconductors *J. Appl. Phys.* **118** 115502–5

[99] Zu F *et al* 2019 Constructing the electronic structure of CH3NH3PbI3 and CH3NH3PbBr3 perovskite thin films from single-crystal band structure measurements *J. Phys. Chem. Lett.* **10** 601–9

[100] Hill I G, Kahn A, Soos Z G and Pascal R A Jr 2000 Charge-separation energy in films of π-conjugated organic molecules *Chem. Phys. Lett.* **327** 181–8

[101] Schwoerer M and Wolf H C 2007 *Organic Molecular Solids* (Weinheim: Wiley)

[102] Li J, D'Avino G, Duchemin I, Beljonne D and Blase X 2018 Accurate description of charged excitations in molecular solids from embedded many-body perturbation theory *Phys. Rev.* B **97** 035108–13

[103] Hill I G, Mäkinen A J and Kafafi Z H 2000 Initial stages of metal/organic semiconductor interface formation *J. Appl. Phys.* **88** 889–95

[104] Anderson P W 1961 Localized magnetic states in metals *Phys. Rev.* **124** 41–53

[105] Heimel G 2016 Introduction to the theory of metal/organic interfaces *The WSPC Reference on Organic Electronics: Organic Semiconductors* ed J L Bredas and S R Marder (Singapore: World Scientific) pp 131–58

[106] Li Y, Li P and Lu Z H 2017 Mapping energy levels for organic heterojunctions *Adv. Mater.* **29** 1700414–7

[107] Egger D A, Liu Z F, Neaton J B and Kronik L 2015 Reliable energy level alignment at physisorbed molecule-metal

interfaces from density functional theory *Nano Lett.* **15** 2448–55
[108] Hewlett R M and McLachlan M A 2016 Surface structure modification of ZnO and the impact on electronic properties *Adv. Mater.* **28** 3893–921
[109] Fu K K, Wang R B, Katase T, Ohta H, Koch N and Duhm S 2018 Stoichiometric and oxygen-deficient VO2 as versatile hole injection electrode for organic semiconductors *ACS Appl. Mater. Interfaces* **10** 10552–9
[110] Erker S and Hofmann O T 2019 Fractional and integer charge transfer at semiconductor/organic interfaces: the role of hybridization and metallicity *J. Phys. Chem. Lett.* **10** 848–54
[111] Futscher M H, Schultz T, Frisch J, Ralaiarisoa M, Metwalli E, Nardi M V, Müller-Buschbaum P and Koch N 2019 Electronic properties of hybrid organic/inorganic semiconductor pn-junctions *J. Phys.: Condens. Matter.* **31** 064002–8
[112] Atkins P and de Paula J 2006 *Atkins' Physical Chemistry* 8th edn (Oxford: Oxford University Press)
[113] Liu W, Filimonov S N, Carrasco J and Tkatchenko A 2013 Molecular switches from benzene derivatives adsorbed on metal surfaces *Nat. Commun.* **4** 2569–6
[114] Jakobs S *et al* 2015 Controlling the spin texture of topological insulators by rational design of organic molecules *Nano Lett.* **15** 6022–9
[115] Hollerer M, Lüftner D, Hurdax P, Ules T, Soubatch S, Tautz F S, Koller G, Puschnig P, Sterrer M and Ramsey M G 2017 Charge transfer and orbital level alignment at inorganic/organic interfaces: the role of dielectric interlayers *ACS Nano* **11** 6252–60
[116] Sarkar S, Yang J, Tan L Z, Rappe A M and Kronik L 2018 Molecule-adsorbed topological insulator and metal surfaces: a comparative first-principles study *Chem. Mater.* **30** 1849–55
[117] Yang S, Li S, Filimonov S N, Fuentes-Cabrera M and Liu W 2018 Principles of design for substrate-supported molecular switches based on physisorbed and chemisorbed states *ACS Appl. Mater. Interfaces* **10** 26772–80
[118] Wang Q *et al* 2018 Bilayer formation vs molecular exchange in organic heterostructures: strong impact of subtle changes in molecular structure *J. Phys. Chem.* C **122** 9480–90
[119] Wandelt K 1997 The local work function: concept and implications *Appl. Surf. Sci.* **111** 1–10
[120] Smoluchowski R 1941 Anisotropy of the electronic work function of metals *Phys. Rev.* **60** 661–74
[121] Witte G, Lukas S, Bagus P S and Wöll C 2005 Vacuum level alignment at organic/metal junctions: 'Cushion' effect and the interface dipole *Appl. Phys. Lett.* **87** 263502
[122] De Renzi V, Rousseau R, Marchetto D, Biagi R, Scandolo S and del Pennino U 2005 Metal work-function changes induced by organic adsorbates: a combined experimental and theoretical study *Phys. Rev. Lett.* **95** 046804
[123] Rusu P C, Giovannetti G, Weijtens C, Coehoorn R and Brocks G 2010 First-principles study of the dipole layer formation at metal-organic interfaces *Phys. Rev.* B **81** 125403–17
[124] Toyoda K, Hamada I, Lee K, Yanagisawa S and Morikawa Y 2010 Density functional theoretical study of pentacene/noble metal interfaces with van der Waals corrections: vacuum level shifts and electronic structures *J. Chem. Phys.* **132** 134703–10
[125] Ferri N, Ambrosetti A and Tkatchenko A 2017 Electronic charge rearrangement at metal/organic interfaces induced by weak van der Waals interactions *Phys. Rev. Mater.* **1** 026003–8
[126] Winkler S, Amsalem P, Frisch J, Oehzelt M, Heimel G and Koch N 2015 Probing the energy levels in hole-doped molecular semiconductors *Mater. Horiz.* **2** 427–33
[127] Hofmann O T, Rinke P, Scheffler M and Heimel G 2015 Integer versus fractional charge transfer at metal(/insulator)/organic interfaces: Cu(/NaCl)/TCNE *ACS Nano* **9** 5391–404
[128] Samadi Khoshkhoo M, Peisert H, Chassé T and Scheele M 2017 The role of the density of interface states in interfacial energy level alignment of PTCDA *Org. Electron.* **49** 249–54
[129] Yang J P, Shang L T, Bussolotti F, Cheng L W, Wang W Q, Zeng X H, Kera S, Li Y Q, Tang J X and Ueno N 2017 Fermi-level pinning appears upon weak electrode-organic contact without gap states: a universal phenomenon *Org. Electron.* **48** 172–8
[130] Fukagawa H, Kera S, Kataoka T, Hosoumi S, Watanabe Y, Kudo K and Ueno N 2007 Role of ionization potential in vacuum-level alignment at organic semiconductors interfaces *Adv. Mater.* **19** 665–8
[131] Zuo G, Abdalla H and Kemerink M 2016 Impact of doping on the density of states and the mobility in organic semiconductors *Phys. Rev.* B **93** 235203–8
[132] Kalb W L, Haas S, Krellner C, Mathis T and Batlogg B 2010 Trap density of states in small-molecule organic semiconductors: a quantitative comparison of thin-film transistors with single crystals *Phys. Rev.* B **81** 155315–13
[133] Tang J X, Lee C S and Lee S T 2007 Electronic structures of organic/organic heterojunctions: from vacuum level alignment to Fermi level pinning *J. Appl. Phys.* **101** 064504–4
[134] Poelking C, Tietze M, Elschner C, Olthof S, Hertel D, Baumeier B, Würthner F, Meerholz K, Leo K and Andrienko D 2014 Impact of mesoscale order on open-circuit voltage in organic solar cells *Nat. Mater.* **14** 434–6
[135] Chen W, Qi D C, Huang H, Gao X and Wee A T S 2011 Organic-organic heterojunction interfaces: effect of molecular orientation *Adv. Funct. Mater.* **21** 410–24
[136] Oehzelt M, Akaike K, Koch N and Heimel G 2015 Energy-level alignment at organic heterointerfaces *Sci. Adv.* **1** e1501127
[137] Duhm S, Glowatzki H, Cimpeanu V, Klankermayer J, Rabe J P, Johnson R L and Koch N 2006 Weak charge transfer between an acceptor molecule and metal surfaces enabling organic/metal energy level tuning *J. Phys. Chem.* B **110** 21069–72
[138] Kawabe E, Yamane H, Sumii R, Koizumi K, Ouchi Y, Seki K and Kanai K 2008 A role of metal d-band in the interfacial electronic structure at organic/metal interface: PTCDA on Au, Ag and Cu *Org. Electron.* **9** 783–9
[139] Brivio G P and Trioni M I 1999 The adiabatic molecule-metal surface interaction: theoretical approaches *Rev. Mod. Phys.* **71** 231–65
[140] Bondi A 1964 van der Waals volumes and radii *J. Phys. Chem.* **68** 441–51
[141] Cordero B, Gómez V, Platero-Prats A E, Revés M, Echeverría J, Cremades E, Barragán F and Alvarez S 2008 Covalent radii revisited *Dalton Trans.* 2832–8
[142] Derry G N, Kern M E and Worth E H 2015 Recommended values of clean metal surface work functions *J. Vac. Sci. Technol.* A **33** 060801
[143] Lindgren S A, Walldén L, Rundgren J and Westrin P 1984 Low-energy electron diffraction from Cu(111): subthreshold effect and energy-dependent inner potential; surface relaxation and metric distances between spectra *Phys. Rev.* B **29** 576–88

[144] Statiris P, Lu H C and Gustafsson T 1994 Temperature dependent sign reversal of the surface contraction of Ag(111) *Phys. Rev. Lett.* **72** 3574–7
[145] Takeuchi N, Chan C T and Ho K M 1991 Au(111): a theoretical study of the surface reconstruction and the surface electronic structure *Phys. Rev.* B **43** 13899–906
[146] Sandy A R, Mochrie S G J, Zehner D M, Huang K G and Gibbs D 1991 Structure and phases of the Au(111) surface: x-ray-scattering measurements *Phys. Rev.* B **43** 4667–87
[147] Hammer B and Nørskov J K 1995 Why gold is the noblest of all the metals *Nature* **376** 238–40
[148] Henze S K M, Bauer O, Lee T L, Sokolowski M and Tautz F S 2007 Vertical bonding distances of PTCDA on Au(111) and Ag(111): relation to the bonding type *Surf. Sci.* **601** 1566–73
[149] Hauschild A, Temirov R, Soubatch S, Bauer O, Schöll A, Cowie B C C, Lee T L, Tautz F S and Sokolowski M 2010 Normal-incidence x-ray standing-wave determination of the adsorption geometry of PTCDA on Ag(111): comparison of the ordered room-temperature and disordered low-temperature phases *Phys. Rev.* B **81** 125432
[150] Gerlach A, Sellner S, Schreiber F, Koch N and Zegenhagen J 2007 Substrate dependent bonding distances of PTCDA—a comparative x-ray standing wave study on Cu(111) and Ag(111) *Phys. Rev.* B **75** 045401
[151] Bürker C, Ferri N, Tkatchenko A, Gerlach A, Niederhausen J, Hosokai T, Duhm S, Zegenhagen J, Koch N and Schreiber F 2013 Exploring the bonding of large hydrocarbons on noble metals: diindoperylene on Cu(111), Ag(111), and Au(111) *Phys. Rev.* B **87** 165443
[152] Shockley W 1939 On the surface states associated with a periodic potential *Phys. Rev.* **56** 317–23
[153] Reinert F, Nicolay G, Schmidt S, Ehm D and Hüfner S 2001 Direct measurements of the L-gap surface states on the (111) face of noble metals by photoelectron spectroscopy *Phys. Rev.* B **63** 115415
[154] Mercurio G *et al* 2013 Adsorption height determination of nonequivalent C and O species of PTCDA on Ag(110) using x-ray standing waves *Phys. Rev.* B **87** 045421
[155] Weiß S, Krieger I, Heepenstrick T, Soubatch S, Sokolowski M and Tautz F S 2017 Determination of the adsorption geometry of PTCDA on the Cu(100) surface *Phys. Rev.* B **96** 075414
[156] Felter J, Franke M, Wolters J, Henneke C and Kumpf C 2019 Two-dimensional growth of dendritic islands of NTCDA on Cu(001) studied in real time *Nanoscale* **11** 1798–812
[157] Bauer O, Schmitz C H, Ikonomov J, Willenbockel M, Soubatch S, Tautz F S and Sokolowski M 2016 Au enrichment and vertical relaxation of the surface studied by normal-incidence x-ray standing waves *Phys. Rev.* B **93** 235429
[158] Stadtmüller B, Grad L, Seidel J, Haag F, Haag N, Cinchetti M and Aeschlimann M 2019 Modification of Pb quantum well states by the adsorption of organic molecules *J. Phys.: Condens. Matter.* **31** 134005
[159] Woodruff D P 2010 The structure of surfaces: what do we know and what would we like to know? *J. Phys.: Condens. Matter.* **22** 084016–15
[160] Bader R F W 1991 A quantum theory of molecular structure and its applications *Chem. Rev.* **91** 893–928
[161] Liang T, Neumann C N and Ritter R 2013 Introduction of fluorine and fluorine-containing functional groups *Angew. Chem., Int. Ed. Engl.* **52** 8214–64
[162] Li Y 2012 Molecular design of photovoltaic materials for polymer solar cells: toward suitable electronic energy levels and broad absorption *Acc. Chem. Res.* **45** 723–33
[163] Bunz U H F 2015 The larger linear n-heteroacenes *Acc. Chem. Res.* **48** 1676–86
[164] Pecher L and Tonner R 2019 Deriving bonding concepts for molecules, surfaces, and solids with energy decomposition analysis for extended systems *WIREs Comput. Mol. Sci.* **9** e1401
[165] Sakamoto Y, Suzuki T, Kobayashi M, Gao Y, Fukai Y, Inoue Y, Sato F and Tokito S 2004 Perfluoropentacene: high-performance p-n junctions and complementary circuits with pentacene *J. Am. Chem. Soc.* **126** 8138–40
[166] Peisert H, Uihlein J, Petraki F and Chasse T 2015 Charge transfer between transition metal phthalocyanines and metal substrates: the role of the transition metal *J. Electron Spectrosc. Relat. Phenom.* **204** 49–60
[167] Yamane H, Gerlach A, Duhm S, Tanaka Y, Hosokai T, Mi Y Y, Zegenhagen J, Koch N, Seki K and Schreiber F 2010 Site-specific geometric and electronic relaxations at organic-metal interfaces *Phys. Rev. Lett.* **105** 046103
[168] Bröker B *et al* 2010 Density-dependent reorientation and rehybridization of chemisorbed conjugated molecules for controlling interface electronic structure *Phys. Rev. Lett.* **104** 246805–4
[169] Franco-Cañellas A, Wang Q, Broch K, Shen B, Gerlach A, Bettinger H F, Duhm S and Schreiber F 2018 Resolving intramolecular-distortion changes induced by the partial fluorination of pentacene adsorbed on Cu(111) *Phys. Rev. Mater.* **2** 044002
[170] Yang A *et al* 2016 Nitrogen substitution impacts organic-metal interface energetics *Phys. Rev.* B **94** 155426
[171] Salzmann I *et al* 2012 Epitaxial growth of π-stacked perfluoropentacene on graphene-coated quartz *ACS Nano* **6** 10874–83
[172] Hinderhofer A and Schreiber F 2012 Organic-organic heterostructures: concepts and applications *ChemPhysChem* **13** 628–43
[173] Fukagawa H, Yamane H, Kera S, Okudaira K K and Ueno N 2006 Experimental estimation of the electric dipole moment and polarizability of titanyl phthalocyanine using ultraviolet photoelectron spectroscopy *Phys. Rev.* B **73** 041302
[174] Bouju X, Mattioli C, Franc G, Pujol A and Gourdon A 2017 Bicomponent supramolecular architectures at the vacuum-solid interface *Chem. Rev.* **117** 1407–444
[175] El-Sayed A *et al* 2013 Understanding energy-level alignment in donor-acceptor/metal interfaces from core-level shifts *ACS Nano* **7** 6914–20
[176] Kilian L *et al* 2008 Role of intermolecular interactions on the electronic and geometric structure of a large π-conjugated molecule adsorbed on a metal surface *Phys. Rev. Lett.* **100** 136103
[177] Schöll A, Kilian L, Zou Y, Ziroff J, Hame S, Reinert F, Umbach E and Fink R H 2010 Disordering of an organic overlayer on a metal surface upon cooling *Science* **329** 303
[178] Kröger I, Stadtmüller B, Kleimann C, Rajput P and Kumpf C 2011 Normal-incidence x-ray standing-wave study of copper phthalocyanine submonolayers on Cu(111) and Au(111) *Phys. Rev.* B **83** 195414
[179] Duhm S *et al* 2013 Pentacene on Ag(111): correlation of bonding distance with intermolecular interaction and order *ACS Appl. Mater. Interfaces* **5** 9377–81
[180] Wießner M, Kübert J, Feyer V, Puschnig P, Schöll A and Reinert F 2013 Lateral band formation and hybridization in molecular monolayers: NTCDA on Ag(110) and Cu(100) *Phys. Rev.* B **88** 075437

[181] Lu M C, Wang R B, Yang A and Duhm S 2016 Pentacene on Au(111), Ag(111) and Cu(111): from physisorption to chemisorption *J. Phys.: Condens. Matter.* **28** 094005

[182] Mannsfeld S C B and Fritz T 2006 Advanced modelling of epitaxial ordering of organic layers on crystalline surfaces *Mod. Phys. Lett.* B **20** 585–605

[183] Hooks D E, Fritz T and Ward M D 2001 Epitaxy and molecular organization on solid substrates *Adv. Mater.* **13** 227–41

[184] Forker R, Meissner M and Fritz T 2017 Classification of epitaxy in reciprocal and real space: rigid versus flexible lattices *Soft Matter* **13** 1748–58

[185] Batterman B W 1964 Effect of dynamical diffraction in x-ray fluorescence scattering *Phys. Rev.* **133** A759

[186] Batterman B W 1969 Detection of foreign atom sites by their x-ray fluorescence scattering *Phys. Rev. Lett.* **22** 703

[187] Andersen S K, Golovchenko J A and Mair G 1976 New applications of x-ray standing-wave fields to solid state physics *Phys. Rev. Lett.* **37** 1141–5

[188] Zegenhagen J 2019 X-ray standing waves technique: Fourier imaging active sites *Japan. J. Appl. Phys.* **58** 110502

[189] Bedzyk M, Bilderback D, Bommarito G, Caffrey M and Schildkraut J 1988 X-ray standing waves: a molecular yardstick for biological membranes *Science* **241** 1788–91

[190] Lee T L, Qian Y, Lyman P F, Woicik J C, Pellegrino J G and Bedzyk M J 1996 The use of x-ray standing waves and evanescent-wave emission to study buried strained-layer heterostructures *Physica* B **221** 437–44

[191] Schneck E and Demé B 2015 Structural characterization of soft interfaces by standing-wave fluorescence with x-rays and neutrons *Curr. Opin. Colloid Interface Sci.* **20** 244–52

[192] Nakagiri T, Sakai K, Iida A, Ishikawa T and Matsushita T 1985 X-ray standing wave method applied to the structural study of Langmuir–Blodgett-films *Thin Solid Films* **133** 219–25

[193] Bedzyk M J, Bommarito G M and Schildkraut J S 1989 X-ray standing waves at a reflecting mirror surface *Phys. Rev. Lett.* **62** 1376–9

[194] Sugiyama M, Maeyama S, Heun S and Oshima M 1995 Chemical-state-resolved x-ray standing-wave analysis using chemical-shift in photoelectron-spectra *Phys. Rev.* B **51** 14778–81

[195] Fenter P, Schreiber F, Berman L, Scoles G, Eisenberger P and Bedzyk M J 1998 On the structure and evolution of the buried S/Au interface in self-assembled monolayers: x-ray standing wave results *Surf. Sci.* **412** 213–35

[196] Shuttleworth I, Fisher C, Lee J, Jones R G and Woodruff D 2002 A NIXSW structural investigation of the low temperature silyl phase formed by SiH4 reaction with Cu(111) *Chem. Phys. Lett.* **351** 208–12

[197] Mulligan A, Johnston S M, Miller G, Dhanak V and Kadodwala M 2003 A TPD and NIXSW investigation of furan and tetrahydrofuran adsorption on Cu(111) *Surf. Sci.* **541** 3–13

[198] Kilian L, Weigang W, Umbach E, Langner A, Sokolowski M, Meyerheim H L, Maltor H, Cowie B C C, Lee T and Bäuerle P 2002 Adsorption site determination of a large π-conjugated molecule by normal incidence x-ray standing waves: end-capped quaterthiophene on Ag(111) *Phys. Rev.* B **66** 075412

[199] Stanzel J, Weigand W, Kilian L, Meyerheim H L, Kumpf C and Umbach E 2004 Chemisorption of NTCDA on Ag(111): a NIXSW study including non-dipolar and electron-stimulated effects *Surf. Sci.* **571** L311–8

[200] Authier A 2003 *Dynamical Theory of X-ray Diffraction* (Oxford: Oxford University Press)

[201] Woodruff D P 1998 Normal incidence x-ray standing wave determination of adsorbate structures *Prog. Surf. Sci.* **57** 1–60

[202] Vartanyants I A and Kovalchuk M V 2001 Theory and applications of x-ray standing waves in real crystals *Rep. Prog. Phys.* **64** 1009–84

[203] Bürker C 2014 Adsorption geometry of π-conjugated organic molecules on metal surfaces studied with the x-ray standing wave technique *PhD Thesis* Eberhard Karls Universität Tübingen http://hdl.handle.net/10900/56266

[204] Schreiber F, Ritley K A, Vartanyants I A, Dosch H, Zegenhagen J and Cowie B C C 2001 Non-dipolar contributions in XPS detection of x-ray standing waves *Surf. Sci.* **486** L519–23

[205] van Straaten G, Franke M, Bocquet F C, Tautz F S and Kumpf C 2018 Non-dipolar effects in photoelectron-based normal incidence x-ray standing wave experiments *J. Electron Spectrosc. Relat. Phenom.* **222** 106–16

[206] Materlik G and Zegenhagen J 1984 X-ray standing wave analysis with synchrotron radiation applied for surface and bulk systems *Phys. Lett.* A **104** 47–50

[207] Zegenhagen J, Detlefs B, Lee T L, Thiess S, Isern H, Petit L, André L, Roy J, Mi Y and Joumard I 2010 X-ray standing waves and hard x-ray photoelectron spectroscopy at the insertion device beamline ID32 *J. Electron Spectrosc. Relat. Phenom.* **178–179** 258–67

[208] Zegenhagen J and Kazimirov A (ed) 2013 *The X-ray Standing Wave Technique. Principles and Applications* (Singapore: World Scientific)

[209] Lee T L and Duncan D A 2018 A two-color beamline for electron spectroscopies at diamond light source *Synchrotron Radiat. News* **31** 16–22

[210] Woodruff D P, Seymour D L, McConville C F, Riley C E, Crapper M D, Prince N P and Jones R G 1988 A simple x-ray standing wave technique for surface structure determination—theory and an application *Surf. Sci.* **195** 237–54

[211] Blowey P J, Rochford L A, Duncan D A, Warr D, Lee T L, Woodruff D P and Costantini G 2017 Probing the interplay between geometric and electronic structure in a two-dimensional K-TCNQ charge transfer network *Faraday Discuss.* **204** 97–110

[212] Smith M, Scudiero L, Espinal J, McEwen J S and Garcia-Perez M 2016 Improving the deconvolution and interpretation of XPS spectra from chars by ab initio calculations *Carbon* **110** 155–71

[213] Diller K, Maurer R J, Müller M and Reuter K 2017 Interpretation of x-ray absorption spectroscopy in the presence of surface hybridization *J. Chem. Phys.* **146** 214701

[214] Baby A, Lin H, Brivio G P, Floreano L and Fratesi G 2015 Core-level spectra and molecular deformation in adsorption: v-shaped pentacene on Al(001) *Beilstein J. Nanotechnol.* **6** 2242–51

[215] Casa Software Ltd Bay House, 5 Grosvenor Terrace, Teigmnmouth, Devon, TQ14 8NE, UK 2017 http://casaxps.com/

[216] Bocquet F, Mercurio G, Franke M, van Straaten G, Wei S, Soubatch S, Kumpf C and Tautz F 2019 Torricelli: a software to determine atomic spatial distributions from normal incidence x-ray standing wave data *Comput. Phys. Commun.* **235** 502–13

[217] Cheng L, Fenter P, Bedzyk M J and Sturchio N C 2003 Fourier-expansion solution of atom distributions in a crystal using x-ray standing waves *Phys. Rev. Lett.* **90** 255503

[218] Egelhoff W 1987 Core-level binding-energy shifts at surfaces and in solids *Surf. Sci. Rep.* **6** 253–415

[219] M Cardona and L Ley (ed) 1978 *Photoemission in Solids I* (Topics in Applied Physics vol 26) (Berlin: Springer)

[220] Nefedov V and Shartse N 1988 *X-ray Photoelectron Spectroscopy of Solid Surfaces* (London: Taylor and Francis)

[221] Hüfner S 2003 *Photoelectron Spectroscopy* (Berlin: Springer)

[222] W Schattke and M A Van Hove (ed) 2008 *Solid-State Photoemission and Related Methods: Theory and Experiment* (Weinheim: Wiley)

[223] Fadley C 2010 X-ray photoelectron spectroscopy: progress and perspectives *J. Electron Spectrosc. Relat. Phenom.* **178–179** 2–32

[224] Bagus P S, Ilton E S and Nelin C J 2013 The interpretation of XPS spectra: insights into materials properties *Surf. Sci. Rep.* **68** 273–304

[225] Suga S and Sekiyama A 2014 *Photoelectron Spectroscopy* (Berlin: Springer)

[226] Moser S 2017 An experimentalist's guide to the matrix element in angle resolved photoemission *J. Electron Spectrosc. Relat. Phenom.* **214** 29–52

[227] Dil J H 2019 Spin- and angle-resolved photoemission on topological materials *Electron. Struct.* **1** 023001

[228] Cahen D and Kahn A 2003 Electron energetics at surfaces and interfaces: concepts and experiments *Adv. Mater.* **15** 271–7

[229] Rao C N R, Basu P K and Hegde M S 1979 Systematic organic UV photoelectron spectroscopy *Appl. Spectrosc. Rev.* **15** 1–193

[230] Seki K, Ueno N, Karlsson U O, Engelhardt R and Koch E E 1986 Valence bands of oriented finite linear chain molecular solids as model compounds of polyethylene studied by angle-resolved photoemission *Chem. Phys.* **105** 247–65

[231] Netzer F P and Ramsey M G 1992 Structure and orientation of organic molecules on metal surfaces *Crit. Rev. Solid State Mater. Sci.* **17** 397–475

[232] Crispin X, Marciniak S, Osikowicz W, Zotti G, van der Gon A W D, Louwet F, Fahlman M, Groenendaal L, De Schryver F and Salaneck W R 2003 Conductivity, morphology, interfacial chemistry, and stability of poly(3,4-ethylene dioxythiophene)-poly(styrene sulfonate): a photoelectron spectroscopy study *J. Polym. Sci.* B **41** 2561–83

[233] Crispin X *et al* 2004 Electronic delocalization in discotic liquid crystals: a joint experimental and theoretical study *J. Am. Chem. Soc.* **126** 11889–99

[234] Rocco M L M, Haeming M, Batchelor D R, Schöll R F and Umbach E 2008 Electronic relaxation effects in condensed polyacenes: a high-resolution photoemission study *J. Chem. Phys.* **129** 074702

[235] Ueno N and Kera S 2008 Electron spectroscopy of functional organic thin films: deep insights into valence electronic structure in relation to charge transport property *Prog. Surf. Sci.* **83** 490–557

[236] Puschnig P, Berkebile S, Fleming A J, Koller G, Emtsev K, Seyller T, Riley J D, Ambrosch-Draxl C, Netzer F P and Ramsey M G 2009 Reconstruction of molecular orbital densities from photoemission data *Science* **326** 702–6

[237] Bussolotti F 2015 High-sensitivity ultraviolet photoemission spectroscopy technique for direct detection of gap states in organic thin films *J. Electron Spectrosc. Relat. Phenom.* **204** 29–38

[238] Schultz T, Lenz T, Kotadiya N, Heimel G, Glasser G, Berger R, Blom P W M, Amsalem P, de Leeuw D M and Koch N 2017 Reliable work function determination of multicomponent surfaces and interfaces: the role of electrostatic potentials in ultraviolet photoelectron spectroscopy *Adv. Mater. Interfaces* 1700324

[239] Muñoz W A, Crispin X, Fahlman M and Zozoulenko I V 2018 Understanding the impact of film disorder and local surface potential in ultraviolet photoelectron spectroscopy of pedot *Macromol. Rapid Commun.* **39** 1700533

[240] Kirchhuebel T, Monti O L A, Munakata T, Kera S, Forker R and Fritz T 2019 The role of initial and final states in molecular spectroscopies *Phys. Chem. Chem. Phys.* **21** 12730–47

[241] Seah M P and Dench W A 1979 Quantitative electron spectroscopy of surfaces: a standard data base for electron inelastic mean free paths in solids *Surf. Interface Anal.* **1** 2–11

[242] Koller G, Winter B, Oehzelt M, Ivanco J, Netzer F P and Ramsey M G 2007 The electronic band alignment on nanoscopically patterned substrates *Org. Electron.* **8** 63–8

[243] Duhm S, Salzmann I, Johnson R L and Koch N 2009 Electronic non-equilibrium conditions at C60-pentacene heterostructures *J. Electron Spectrosc. Relat. Phenom.* **174** 40–4

[244] Schultz T, Amsalem P, Kotadiya N B, Lenz T, Blom P W M and Koch N 2019 Importance of substrate work function homogeneity for reliable ionization energy determination by photoelectron spectroscopy *Phys. Status Solidi* B **256** 201800299–6

[245] Wang T, Kafle T R, Kattel B, Liu Q, Wu J and Chan W L 2016 Growing ultra-flat organic films on graphene with a face-on stacking via moderate molecule-substrate interaction *Sci. Rep.* **6** 28895–99

[246] Tada A, Geng Y F, Wei Q S, Hashimoto K and Tajima K 2011 Tailoring organic heterojunction interfaces in bilayer polymer photovoltaic devices *Nat. Mater.* **10** 450–5

[247] Siles P F, Devarajulu M, Zhu F and Schmidt O G 2018 Direct imaging of space-charge accumulation and work function characteristics of functional organic interfaces *Small* **14** 1870051

[248] Kahn A 2016 Fermi level, work function and vacuum level *Mater. Horiz.* **3** 7–10

[249] Venables J A, Spiller G D T and Hanbücken M 1984 Nucleation and growth of thin films *Rep. Prog. Phys.* **47** 399–459

[250] Yang J, Yan D and Jones T S 2015 Molecular template growth and its applications in organic electronics and optoelectronics *Chem. Rev.* **115** 5570–603

[251] Winkler A 2016 On the nucleation and initial film growth of rod-like organic molecules *Surf. Sci.* **652** 367–77

[252] Kowarik S 2017 Thin film growth studies using time-resolved x-ray scattering *J. Phys.: Condens. Matter.* **29** 043003

[253] Schreiber F 2004 Organic molecular beam deposition: growth studies beyond the first monolayer *Phys. Status Solidi* A **201** 1037–54

[254] Kuroda H and Flood E A 1961 Effect of ambient oxygen on electrical properties of an evaporated film of pentacene *Can. J. Chem.* **39** 1981–8

[255] Lee K O and Gan T T 1977 Influence of substrate temperature on optical-properties of evaporated-films of pentacene *Chem. Phys. Lett.* **51** 120–4

[256] Sebastian L, Weiser G and Bassler H 1981 Charge-transfer transitions in solid tetracene and pentacene studied by electro-absorption *Chem. Phys.* **61** 125–35

[257] Moerner W E and Orrit M 1999 Illuminating single molecules in condensed matter *Science* **283** 1670–6

[258] Kang J H and Zhu X Y 2003 Pi-stacked pentacene thin films grown on Au(111) *Appl. Phys. Lett.* **82** 3248–50

[259] Eremtchenko M, Temirov R, Bauer D, Schaefer J and Tautz F 2005 Formation of molecular order on a disordered interface layer: pentacene/Ag(111) *Phys. Rev.* B **72** 115430

[260] Fukagawa H, Yamane H, Kataoka T, Kera S, Nakamura M, Kudo K and Ueno N 2006 Origin of the highest occupied

band position in pentacene films from ultraviolet photoelectron spectroscopy: hole stabilization versus band dispersion *Phys. Rev.* B **73** 245310
[261] Käfer D, Ruppel L and Witte G 2007 Growth of pentacene on clean and modified gold surfaces *Phys. Rev.* B **75** 085309–14
[262] Koch N, Vollmer A, Duhm S, Sakamoto Y and Suzuki T 2007 The effect of fluorination on pentacene/gold interface energetics and charge reorganization energy *Adv. Mater.* **19** 112–6
[263] Zheng Y, Qi D, Chandrasekhar N, Gao X, Troadec C and Wee A T S 2007 Effect of molecule-substrate interaction on thin-film structures and molecular orientation of pentacene on silver and gold *Langmuir* **23** 8336–42
[264] Dougherty D B, Jin W, Cullen W G, Reutt-Robey J E and Robey S W 2008 Variable temperature scanning tunneling microscopy of pentacene monolayer and bilayer phases on Ag(111) *J. Phys. Chem.* C **112** 20334–9
[265] Yamane H, Kanai K, Ouchi Y, Ueno N and Seki K 2009 Impact of interface geometric structure on organic-metal interface energetics and subsequent films electronic structure *J. Electron Spectrosc. Relat. Phenom.* **174** 28–34
[266] Han W, Yoshida H, Ueno N and Kera S 2013 Electron affinity of pentacene thin film studied by radiation-damage free inverse photoemission spectroscopy *Appl. Phys. Lett.* **103** 123303–5
[267] Park S H and Kwon S 2016 Dynamics of molecular orientation observed using angle resolved photoemission spectroscopy during deposition of pentacene on graphite *Anal. Chem.* **88** 4565–70
[268] Ji R R, Wang Q, Hu J X and Duhm S 2017 Impact of room temperature on pentacene thin film growth and electronic structure *Can. J. Chem.* **95** 1130–4
[269] Zhang P, Zhao S, Wang H, Zhang J, Shi J, Wang H and Yan D 2017 Relation between interfacial band-bending and electronic properties in organic semiconductor pentacene *Adv. Electron. Mater.* **3** 1700136–6
[270] Choi H H, Cho K, Frisbie C D, Sirringhaus H and Podzorov V 2018 Critical assessment of charge mobility extraction in fets *Nat. Mater.* **17** 2–7
[271] Hoffmann-Vogel R 2018 Imaging prototypical aromatic molecules on insulating surfaces: a review *Rep. Prog. Phys.* **81** 016501
[272] Klues M and Witte G 2018 Crystalline packing in pentacene-like organic semiconductors *CrystEngComm* **20** 63–74
[273] Döring R C, Rosemann N W, Huttner A, Breuer T, Witte G and Chatterjee S 2019 Charge-transfer processes and carrier dynamics at the pentacene-C60 interface *J. Phys.: Condens. Matter.* **31** 134001
[274] Nakayama Y *et al* 2019 Widely dispersed intermolecular valence bands of epitaxially grown perfluoropentacene on pentacene single crystals *J. Phys. Chem. Lett.* **10** 1312–8
[275] Tadano S, Nakayama Y, Kinjo H, Ishii H and Krüger P 2019 Obtaining the highest occupied molecular orbital peak of organic matter from photoelectron yield spectra *Phys. Rev. Appl.* **11** 054081
[276] Bussolotti F, Kera S, Kudo K, Kahn A and Ueno N 2013 Gap states in pentacene thin film induced by inert gas exposure *Phys. Rev. Lett.* **110** 267602–5
[277] Graber T, Forster F, Schöll A and Reinert F 2011 Experimental determination of the attenuation length of electrons in organic molecular solids: the example of PTCDA *Surf. Sci.* **605** 878–82
[278] Ozawa Y, Nakayama Y, Machida S, Kinjo H and Ishii H 2014 Maximum probing depth of low-energy photoelectrons in an amorphous organic semiconductor film *J. Electron Spectrosc. Relat. Phenom.* **197** 17–21
[279] Kera S, Yamane H and Ueno N 2009 First-principles measurements of charge mobility in organic semiconductors: valence hole–vibration coupling in organic ultrathin films *Prog. Surf. Sci.* **84** 135–54
[280] Kera S and Ueno N 2015 Photoelectron spectroscopy on the charge reorganization energy and small polaron binding energy of molecular film *J. Electron Spectrosc. Relat. Phenom.* **204** 2–11
[281] Liu Y, Ikeda D, Nagamatsu S, Nishi T, Ueno N and Kera S 2014 Impact of molecular orbital distribution on photoelectron intensity for picene film *J. Electron Spectrosc. Relat. Phenom.* **195** 287–92
[282] Yagishita A 2015 Photoelectron angular distributions from single oriented molecules: past, present and future *J. Electron Spectrosc. Relat. Phenom.* **200** 247–56
[283] Käfer D and Witte G 2007 Evolution of pentacene films on Ag(111): growth beyond the first monolayer *Chem. Phys. Lett.* **442** 376–83
[284] Yoshida H and Sato N 2008 Crystallographic and electronic structures of three different polymorphs of pentacene *Phys. Rev.* B **77** 235205–11
[285] Yamane H and Kosugi N 2013 Substituent-induced intermolecular interaction in organic crystals revealed by precise band-dispersion measurements *Phys. Rev. Lett.* **111** 086602–5
[286] Ules T, Lüftner D, Reinisch E M, Koller G, Puschnig P and Ramsey M G 2014 Orbital tomography of hybridized and dispersing molecular overlayers *Phys. Rev.* B **90** 155430–8
[287] Salzmann I, Duhm S, Opitz R, Rabe J P and Koch N 2007 Impact of low 6,13-pentacenequinone concentration on pentacene thin film growth *Appl. Phys. Lett.* **91** 051919
[288] Witte G and Wöll C 2008 Molecular beam deposition and characterization of thin organic films on metals for applications in organic electronics *Phys. Status Solidi* A **205** 497–510
[289] Breuer T, Salzmann I, Götzen J, Oehzelt M, Morherr A, Koch N and Witte G 2011 Interrelation between substrate roughness and thin-film structure of functionalized acenes on graphite *Cryst. Growth Des.* **11** 4996–5001
[290] Jones A O F, Chattopadhyay B, Geerts Y H and Resel R 2016 Substrate-induced and thin-film phases: polymorphism of organic materials on surfaces *Adv. Funct. Mater.* **26** 2233–55
[291] Cocchi C, Breuer T, Witte G and Draxl C 2018 Polarized absorbance and davydov splitting in bulk and thin-film pentacene polymorphs *Phys. Chem. Chem. Phys.* **20** 29724–36
[292] Moulder J F, Stickle W F, Sobol P E and Bomben K D 1995 *Handbook of X-ray Photoelectron Spectroscopy* (Eden Prairie: Physical Electronics)
[293] Crist B V 2019 XPS in industry: problems with binding energies in journals and binding energy databases *J. Electron Spectrosc. Relat. Phenom.* **231** 75–87
[294] Chadwick D and Karolewski M 1981 Calibration of XPS core-level binding energies: influence of the surface chemical shift *J. Electron Spectrosc. Relat. Phenom.* **24** 181–7
[295] Travnikova O, Børve K J, Patanen M, Söderström J, Miron C, Sæthre L J, Måtensson N and Svensson S 2012 The ESCA molecule-historical remarks and new results *J. Electron Spectrosc. Relat. Phenom.* **185** 191–7
[296] Freund H J and Roberts M 1996 Surface chemistry of carbon dioxide *Surf. Sci. Rep.* **25** 225–73
[297] Schöll A, Zou Y, Jung M, Schmidt T, Fink R and Umbach E 2004 Line shapes and satellites in high-resolution x-ray photoemission spectra of large π-conjugated molecules *J. Chem. Phys.* **121** 10260

[298] Lanzilotto V *et al* 2018 Spectroscopic fingerprints of intermolecular h-bonding interactions in carbon nitride model compounds *Chem. Eur. J.* **24** 14198–206
[299] Woodruff D P 2007 Adsorbate structure determination using photoelectron diffraction: methods and applications *Surf. Sci. Rep.* **62** 1–38
[300] Kreikemeyer Lorenzo D, Bradley M K, Unterberger W, Duncan D A, Lerotholi T J, Robinson J and Woodruff D P 2011 The structure of methoxy species on Cu(110): a combined photoelectron diffraction and density functional theory determination *Surf. Sci.* **605** 193–205
[301] Duncan D A, Bradley M K, Unterberger W, Kreikemeyer-Lorenzo D, Lerotholi T J, Robinson J and Woodruff D P 2012 Deprotonated glycine on Cu(111): quantitative structure determination by energy-scanned photoelectron diffraction *J. Phys. Chem.* C **116** 9985–95
[302] White T W, Duncan D A, Fortuna S, Wang Y L, Moreton B, Lee T L, Blowey P, Costantini G and Woodruff D P 2018 A structural investigation of the interaction of oxalic acid with Cu(110) *Surf. Sci.* **668** 134–43
[303] Duncan D A, Unterberger W, Hogan K A, Lerotholi T J, Lamont C L A and Woodruff D P 2010 A photoelectron diffraction investigation of vanadyl phthalocyanine on Au(111) *Surf. Sci.* **604** 47–53
[304] Salomon E, Beato-Medina D, Verdini A, Cossaro A, Cvetko D, Kladnik G, Floreano L and Angot T 2015 Correlation between charge transfer and adsorption site in CoPc overlayers adsorbed on Ag(100) *J. Phys. Chem.* C **119** 23422–9
[305] Feidenhansĺ R 1989 Surface structure determination by x-ray diffraction *Surf. Sci. Rep.* **10** 105–88
[306] Robinson I K and Tweet D J 1992 Surface x-ray diffraction *Rep. Prog. Phys.* **55** 599–651
[307] Meyerheim H and Moritz W 1998 Structure and dynamics of clean and adsorbate-covered crystal surfaces studied by surface x-ray diffraction *Appl. Phys.* A **67** 645–56
[308] Stöhr J 1992 *NEXAFS Spectroscopy* (Berlin: Springer)
[309] Diller K, Klappenberger F, Marschall M, Hermann K, Nefedov A, Wöll C and Barth J V 2012 Self-metalation of 2H-tetraphenylporphyrin on Cu(111): an x-ray spectroscopy study *J. Chem. Phys.* **136** 014705
[310] Breuer T, Klues M and Witte G 2015 Characterization of orientational order in π-conjugated molecular thin films by NEXAFS *J. Electron Spectrosc. Relat. Phenom.* **204** 102–15
[311] Schmitz-Hübsch T, Fritz T, Sellam F, Staub R and Leo K 1997 Epitaxial growth of 3,4,9,10-perylene-tetracarboxylic-dianhydride on Au(111): a STM and RHEED study *Phys. Rev.* B **55** 7972–6
[312] Rosei F, Schunack M, Naitoh Y, Jiang P, Gourdon A, Laegsgaard E, Stensgaard I, Joachim C and Besenbacher F 2003 Properties of large organic molecules on metal surfaces *Prog. Surf. Sci.* **71** 95–146
[313] Barth J V 2007 Molecular architectonic on metal surfaces *Annu. Rev. Phys. Chem.* **58** 375–407
[314] Han P and Weiss P S 2012 Electronic substrate-mediated interactions *Surf. Sci. Rep.* **67** 19–81
[315] Wagner C and Temirov R 2015 Tunnelling junctions with additional degrees of freedom: an extended toolbox of scanning probe microscopy *Prog. Surf. Sci.* **90** 194–222
[316] Gottfried J M 2015 Surface chemistry of porphyrins and phthalocyanines *Surf. Sci. Rep.* **70** 259–379
[317] Dong L, Gao Z and Lin N 2016 Self-assembly of metal-organic coordination structures on surfaces *Prog. Surf. Sci.* **91** 101–35
[318] Wakayama Y 2016 On-surface molecular nanoarchitectonics: from self-assembly to directed assembly *Japan. J. Appl. Phys.* **55** 1102AA–13
[319] He Y, Kröger J and Wang Y 2017 Organic multilayer films studied by scanning tunneling microscopy *ChemPhysChem* **18** 429–50
[320] Goronzy D P *et al* 2018 Supramolecular assemblies on surfaces: nanopatterning, functionality, and reactivity *ACS Nano* **12** 7445–81
[321] Woodruff D P 2019 Quantitative determination of molecular adsorption structures: STM and DFT are not enough *Japan. J. Appl. Phys.* **58** 100501
[322] Schuler B, Liu W, Tkatchenko A, Moll N, Meyer G, Mistry A, Fox D and Gross L 2013 Adsorption geometry determination of single molecules by atomic force microscopy *Phys. Rev. Lett.* **111** 106103
[323] Kilian L, Umbach E and Sokolowski M 2004 Molecular beam epitaxy of organic films investigated by high resolution low energy electron diffraction (SPA-LEED): 3,4,9,10-perylenetetracarboxylicacid-dianhydride (PTCDA) on Ag(111) *Surf. Sci.* **573** 359–78
[324] Lévesque P L, Marchetto H, Schmidt T, Maier F C, Freund H J and Umbach E 2016 Correlation between substrate morphology and the initial stages of epitaxial organic growth: PTCDA/Ag(111) *J. Phys. Chem.* C **120** 19271–9
[325] Henneke C, Felter J, Schwarz D, Stefan Tautz F and Kumpf C 2017 Controlling the growth of multiple ordered heteromolecular phases by utilizing intermolecular repulsion *Nat. Mater.* **16** 628–33
[326] Offenbacher H, Lüftner D, Ules T, Reinisch E M, Koller G, Puschnig P and Ramsey M G 2015 Orbital tomography: molecular band maps, momentum maps and the imaging of real space orbitals of adsorbed molecules *J. Electron Spectrosc. Relat. Phenom.* **204** 92–101
[327] Udhardt C *et al* 2017 Influence of film and substrate structure on photoelectron momentum maps of coronene thin films on Ag(111) *J. Phys. Chem.* C **121** 12285–93
[328] Bussolotti F *et al* 2017 Hole-phonon coupling effect on the band dispersion of organic molecular semiconductors *Nat. Commun.* **8** 173
[329] Yamane H and Kosugi N 2017 High hole-mobility molecular layer made from strong electron acceptor molecules with metal adatoms *J. Phys. Chem. Lett.* **8** 5366–71
[330] Koller G, Berkebile S, Oehzelt M, Puschnig P, Ambrosch-Draxl C, Netzer F P and Ramsey M G 2007 Intra- and intermolecular band dispersion in an organic crystal *Science* **317** 351–5
[331] Kakuta H, Hirahara T, Matsuda I, Nagao T, Hasegawa S, Ueno N and Sakamoto K 2007 Electronic structures of the highest occupied molecular orbital bands of a pentacene ultrathin film *Phys. Rev. Lett.* **98** 247601–4
[332] Aghdassi N, Wang Q, Ji R R, Wang B, Fan J and Duhm S 2018 Ultraviolet photoelectron spectroscopy reveals energy-band dispersion for π-stacked 7,8,15,16-tetraazaterrylene thin films in a donor–acceptor bulk heterojunction *Nanotechnology* **29** 194002–8
[333] Coropceanu V, Malagoli M, da Silva Filho D A, Gruhn N E, Bill T G and Brédas J L 2002 Hole- and electron-vibrational couplings in oligoacene crystals: intramolecular contributions *Phys. Rev. Lett.* **89** 275503
[334] Perroni A C, Gargiulo F, Nocera A, Ramaglia M V and Cataudella V 2014 The effects of different electron-phonon couplings on the spectral and transport properties of small molecule single-crystal organic semiconductors *Electronics* **3** 165–89
[335] He Y, Bussolotti F, Xin Q, Yang J, Kera S, Ueno N and Duhm S 2016 Transient monolayer structure of rubrene on graphite: impact on hole-phonon coupling *J. Phys. Chem.* C **120** 14568–74
[336] Graus M, Grimm M, Metzger C, Dauth M, Tusche C, Kirschner J, Kümmel S, Schöll A and Reinert F 2016

Electron-vibration coupling in molecular materials: assignment of vibronic modes from photoelectron momentum mapping *Phys. Rev. Lett.* **116** 147601
[337] Yang X *et al* 2019 Coexisting charge states in a unary organic monolayer film on a metal *J. Phys. Chem. Lett.* **10** 6438–45
[338] Dauth M, Wiessner M, Feyer V, Schöll A, Puschnig P, Reinert F and Kümmel S 2014 Angle resolved photoemission from organic semiconductors: orbital imaging beyond the molecular orbital interpretation *New J. Phys.* **16** 103005
[339] Graus M, Metzger C, Grimm M, Feyer V, Puschnig P, Schöll A and Reinert F 2018 Degeneracy lifting of adsorbate orbitals imaged by high-resolution momentum microscopy *J. Phys. Soc. Japan* **87** 061009–6
[340] Egger L *et al* 2019 Can photoemission tomography be useful for small, strongly-interacting adsorbate systems? *New J. Phys.* **21** 043003
[341] Ueba T, Terawaki R, Morikawa T, Kitagawa Y, Okumura M, Yamada T, Kato H S and Munakata T 2013 Diffuse unoccupied molecular orbital of rubrene causing image-potential state mediated excitation *J. Phys. Chem.* C **117** 20098–103
[342] Marks M, Schöll A and Höfer U 2014 Formation of metal-organic interface states studied with 2PPE *J. Electron Spectrosc. Relat. Phenom.* **195** 263–71
[343] Gerbert D, Maaß F and Tegeder P 2017 Extended space charge region and unoccupied molecular band formation in epitaxial tetrafluorotetracyanoquinodimethane films *J. Phys. Chem.* C **121** 15696–701
[344] Yamada T and Munakata T 2018 Spectroscopic and microscopic investigations of organic ultrathin films: correlation between geometrical structures and unoccupied electronic states *Prog. Surf. Sci.* **93** 108–30
[345] Lerch A, Zimmermann J E, Namgalies A, Stallberg K and Höfer U 2018 Two-photon photoemission spectroscopy of unoccupied electronic states at CuPc/PTCDA/Ag(111) interfaces *J. Phys.: Condens. Matter.* **30** 494001–6
[346] Schwalb C H, Sachs S, Marks M, Schöll A, Reinert F, Umbach E and Höfer U 2008 Electron lifetime in a Shockley-type metal-organic interface state *Phys. Rev. Lett.* **101** 146801
[347] Zaitsev N L, Nechaev I A, Höfer U and Chulkov E V 2016 Adsorption geometry and electronic properties of flat-lying monolayers of tetracene on the Ag(111) surface *Phys. Rev.* B **94** 155452
[348] Lerch A *et al* 2017 Electronic structure of titanylphthalocyanine layers on Ag(111) *J. Phys. Chem.* C **121** 25353–63
[349] Kanai K, Akaike K, Koyasu K, Sakai K, Nishi T, Kamizuru Y, Nishi T, Ouchi Y and Seki K 2009 Determination of electron affinity of electron accepting molecules *Appl. Phys.* A **95** 309–13
[350] Krause S, Schöll A and Umbach E 2013 Interplay of geometric and electronic structure in thin films of diindenoperylene on Ag(111) *Org. Electron.* **14** 584–90
[351] Yoshida H 2015 Principle and application of low energy inverse photoemission spectroscopy: a new method for measuring unoccupied states of organic semiconductors *J. Electron Spectrosc. Relat. Phenom.* **204** 116–24
[352] Song Z *et al* 2017 Electronic properties of a 1D intrinsic/p-doped heterojunction in a 2D transition metal dichalcogenide semiconductor *ACS Nano* **11** 9128–35
[353] Kraft A, Temirov R, Henze S, Soubatch S, Rohlfing M and Tautz F 2006 Lateral adsorption geometry and site-specific electronic structure of a large organic chemisorbate on a metal surface *Phys. Rev.* B **74** 041402(R)
[354] Rohlfing M, Temirov R and Tautz F S 2007 Adsorption structure and scanning tunneling data of a prototype organic-inorganic interface: PTCDA on Ag(111) *Phys. Rev.* B **76** 115421
[355] Gonzalez-Lakunza N, Cañas-Ventura M E, Ruffieux P, Rieger R, Müllen K, Fasel R and Arnau A 2009 Hydrogen-bonding fingerprints in electronic states of two-dimensional supramolecular assemblies *ChemPhysChem* **10** 2943–6
[356] Fernandez Torrente I, Franke K and Pascual J I 2008 Spectroscopy of C60 single molecules: the role of screening on energy level alignment *J. Phys.: Condens. Matter.* **20** 184001
[357] Nazin G V, Qiu X H and Ho W 2003 Visualization and spectroscopy of a metal-molecule-metal bridge *Science* **302** 77–81
[358] Eremtchenko M, Schaefer J and Tautz F S 2003 Understanding and tuning the epitaxy of large aromatic adsorbates by molecular design *Nature* **425** 602–5
[359] Lu J and Loh K P 2009 High resolution electron energy loss spectroscopy study of zinc phthalocyanine and tetrafluoro tetracyanoquinodimethane on Au(111) *Chem. Phys. Lett.* **468** 28–31
[360] Navarro P, Bocquet F C, Deperasinska I, Pirug G, Tautz F S and Orrit M 2015 Electron energy loss of terrylene deposited on Au(111): vibrational and electronic spectroscopy *J. Phys. Chem.* C **119** 277–83
[361] Rückerl F, Waas D, Büchner B, Knupfer M, Zahn D R T, Haidu F, Hahn T and Kortus J 2017 Charge transfer from and to manganese phthalocyanine: bulk materials and interfaces *Beilstein J. Nanotechnol.* **8** 1601–15
[362] Forker R and Fritz T 2009 Optical differential reflectance spectroscopy of ultrathin epitaxial organic films *Phys. Chem. Chem. Phys.* **11** 2142–55
[363] Forker R, Gruenewald M and Fritz T 2012 Optical differential reflectance spectroscopy on thin molecular films *Annu. Rep. Prog. Chem., Sect. C: Phys. Chem.* **108** 34
[364] Navarro-Quezada A, Aiglinger M, Ghanbari E, Wagner T and Zeppenfeld P 2015 Polarization-dependent differential reflectance spectroscopy for real-time monitoring of organic thin film growth *Rev. Sci. Instrum.* **86** 113108
[365] Nickel F, Bernien M, Krüger D, Miguel J, Britton A J, Arruda L M, Kipgen L and Kuch W 2018 Highly efficient and bidirectional photochromism of spirooxazine on Au(111) *J. Phys. Chem.* C **122** 8031–6
[366] Meisel T, Sparenberg M, Gawek M, Sadofev S, Kobin B, Grubert L, Hecht S, List-Kratochvil E and Blumstengel S 2018 Fingerprint of charge redistribution in the optical spectra of hybrid inorganic/organic semiconductor interfaces *J. Phys. Chem.* C **122** 12913–9
[367] Redhead P 1962 Thermal desorption of gases *Vacuum* **12** 203–11
[368] Lord F M and Kittelberger J 1974 On the determination of activation energies in thermal desorption experiments *Surf. Sci.* **43** 173–82
[369] Chan C M, Aris R and Weinberg W 1978 An analysis of thermal desorption mass spectra. I *Appl. Surf. Sci.* **1** 360–76
[370] Chan C M and Weinberg W 1978 An analysis of thermal desorption mass spectra. II *Appl. Surf. Sci.* **1** 377–87
[371] Habenschaden E and Küppers J 1984 Evaluation of flash desorption spectra *Surf. Sci.* **138** L147–50
[372] Fichthorn K A and Miron R A 2002 Thermal desorption of large molecules from solid surfaces *Phys. Rev. Lett.* **89** 196103
[373] Maaß F, Jiang Y, Liu W, Tkatchenko A and Tegeder P 2018 Binding energies of benzene on coinage metal surfaces:

equal stability on different metals *J. Chem. Phys.* **148** 214703
[374] Haq S, Hanke F, Dyer M S, Persson M, Iavicoli P, Amabilino D B and Raval R 2011 Clean coupling of unfunctionalized porphyrins at surfaces to give highly oriented organometallic oligomers *J. Am. Chem. Soc.* **133** 12031–9
[375] Röckert M *et al* 2014 Coverage- and temperature-dependent metalation and dehydrogenation of tetraphenylporphyrin on Cu(111) *Chem. Eur. J.* **20** 8948–53
[376] Chen M, Röckert M, Xiao J, Drescher H J, Steinrück H P, Lytken O and Gottfried J M 2014 Coordination reactions and layer exchange processes at a buried metal-organic interface *J. Phys. Chem.* C **118** 8501–7
[377] Ferrighi L *et al* 2015 Control of the intermolecular coupling of dibromotetracene on Cu(110) by the sequential activation of C–Br and C–H bonds *Chem. Eur. J.* **21** 5826–35
[378] Lukas S, Vollmer S, Witte G and Wöll C 2001 Adsorption of acenes on flat and vicinal Cu(111) surfaces: step induced formation of lateral order *J. Chem. Phys.* **114** 10123–30
[379] Käfer D, Wöll C and Witte G 2009 Thermally activated dewetting of organic thin films: the case of pentacene on SiO_2 and gold *Appl. Phys.* A **95** 273–84
[380] Frank P, Koch N, Koini M, Rieger R, Müllen K, Resel R and Winkler A 2009 Layer growth and desorption kinetics of a discoid molecular acceptor on Au(111) *Chem. Phys. Lett.* **473** 321–5
[381] Götzen J, Schwalb C H, Schmidt C, Mette G, Marks M, Höfer U and Witte G 2011 Structural evolution of perfluoro-pentacene films on Ag(111): transition from 2D to 3D growth *Langmuir* **27** 993–9
[382] Breuer T and Witte G 2013 Thermally activated intermixture in pentacene-perfluoropentacene heterostructures *J. Chem. Phys.* **138** 114901
[383] Thussing S and Jakob P 2017 Thermal stability and interlayer exchange processes in heterolayers of CuPc and PTCDA on Ag(111) *J. Phys. Chem.* C **121** 13680–91
[384] Matena M, Björk J, Wahl M, Lee T L, Zegenhagen J, Gade L H, Jung T A, Persson M and Stöhr M 2014 On-surface synthesis of a two-dimensional porous coordination network: unraveling adsorbate interactions *Phys. Rev.* B **90** 125408–8
[385] de Oteyza D G *et al* 2010 Copper-phthalocyanine based metal–organic interfaces: the effect of fluorination, the substrate, and its symmetry *J. Chem. Phys.* **133** 214703
[386] Gerlach A, Hosokai T, Duhm S, Kera S, Hofmann O T, Zojer E, Zegenhagen J and Schreiber F 2011 Orientational ordering of nonplanar phthalocyanines on Cu(111): strength and orientation of the electric dipole moment *Phys. Rev. Lett.* **106** 156102
[387] Blowey P *et al* 2019 The structure of VOPc on Cu(111): does V=O point up, or down, or both? *J. Phys. Chem.* C **123** 8101–11
[388] Bürker C, Franco-Cañellas A, Broch K, Lee T L, Gerlach A and Schreiber F 2014 Self-metalation of 2H-tetraphenylporphyrin on Cu(111) studied with XSW: influence of the central metal atom on the adsorption distance *J. Phys. Chem.* C **118** 13659–66
[389] Schwarz M *et al* 2018 Adsorption conformation and lateral registry of cobalt porphine on Cu(111) *J. Phys. Chem.* C **122** 5452–61
[390] Willenbockel M, Maurer R J, Bronner C, Schulze M, Stadtmüller B, Soubatch S, Tegeder P, Reuter K and Stefan Tautz F 2015 Coverage-driven dissociation of azobenzene on Cu(111): a route towards defined surface functionalization *Chem. Commun.* **51** 15324–7
[391] Klein B P *et al* 2019 Molecular topology and the surface chemical bond: alternant versus nonalternant aromatic systems as functional structural elements *Phys. Rev.* X **9** 011030
[392] Duhm S *et al* 2010 Influence of intramolecular polar bonds on interface energetics in perfluoro-pentacene on Ag(111) *Phys. Rev.* B **81** 045418
[393] Stadler C, Hansen S, Schöll A, Lee T L, Zegenhagen J, Kumpf C and Umbach E 2007 Molecular distortion of NTCDA upon adsorption on Ag(111): a normal incidence x-ray standing wave study *New J. Phys.* **9** 50
[394] Stadtmüller B, Haag N, Seidel J, van Straaten G, Franke M, Kumpf C, Cinchetti M and Aeschlimann M 2016 Adsorption heights and bonding strength of organic molecules on a Pb–Ag surface alloy *Phys. Rev.* B **94** 235436
[395] Kleimann C, Stadtmüller B, Schröder S and Kumpf C 2014 Electrostatic interaction and commensurate registry at the heteromolecular F16CuPc-CuPc interface *J. Phys. Chem.* C **118** 1652–60
[396] Deimel P S *et al* 2016 Direct quantitative identification of the 'surface trans-effect'? *Chem. Sci.* **7** 5647–56
[397] Kröger I, Bayersdorfer P, Stadtmüller B, Kleimann C, Mercurio G, Reinert F and Kumpf C 2012 Submonolayer growth of H2-phthalocyanine on Ag(111) *Phys. Rev.* B **86** 195412
[398] Stadler C, Hansen S, Pollinger F, Kumpf C, Umbach E, Lee T L and Zegenhagen J 2006 Structural investigation of the adsorption of SnPc on Ag(111) using normal-incidence x-ray standing waves *Phys. Rev.* B **74** 035404
[399] Kröger I, Stadtmüller B and Kumpf C 2016 Submonolayer and multilayer growth of titaniumoxide-phthalocyanine on Ag(111) *New J. Phys.* **18** 113022
[400] Mercurio G *et al* 2010 Structure and energetics of azobenzene on Ag(111): benchmarking semiempirical dispersion correction approaches *Phys. Rev. Lett.* **104** 036102
[401] Mercurio G *et al* 2013 Quantification of finite-temperature effects on adsorption geometries of π-conjugated molecules: azobenzene/Ag(111) *Phys. Rev.* B **88** 035421
[402] Mercurio G, Maurer R J, Hagen S, Leyssner F, Meyer J, Tegeder P, Soubatch S, Reuter K and Tautz F S 2014 X-ray standing wave simulations based on Fourier vector analysis as a method to retrieve complex molecular adsorption geometries *Front. Phys.* **2** 1–13
[403] Hofmann O T *et al* 2017 Orientation-dependent work-function modification using substituted pyrene-based acceptors *J. Phys. Chem.* C **121** 24657–68
[404] McNellis E R, Mercurio G, Hagen S, Leyssner F, Meyer J, Soubatch S, Wolf M, Reuter K, Tegeder P and Tautz F S 2010 Bulky spacer groups—a valid strategy to control the coupling of functional molecules to surfaces? *Chem. Phys. Lett.* **499** 247–9
[405] Javaid S *et al* 2013 Chemisorption of manganese phthalocyanine on Cu(001) surface promoted by van der Waals interactions *Phys. Rev.* B **87** 155418
[406] Wechsler D *et al* 2017 Adsorption structure of cobalt tetraphenylporphyrin on Ag(100) *J. Phys. Chem.* C **121** 5667–74
[407] Bauer O, Mercurio G, Willenbockel M, Reckien W, Heinrich Schmitz C, Fiedler B, Soubatch S, Bredow T, Tautz F S and Sokolowski M 2012 Role of functional groups in surface bonding of planar π-conjugated molecules *Phys. Rev.* B **86** 235431
[408] Mercurio G, Bauer O, Willenbockel M, Fiedler B, Sueyoshi T, Weiss C, Temirov R, Soubatch S, Sokolowski M and Tautz F S 2013 Tuning and probing interfacial bonding channels for a functionalized organic molecule by surface modification *Phys. Rev.* B **87** 121409(R)
[409] Runte S, Lazić P, Vo-Van C, Coraux J, Zegenhagen J and Busse C 2014 Graphene buckles under stress: an x-ray

standing wave and scanning tunneling microscopy study *Phys. Rev.* B **89** 155427
[410] Emery J D, Detlefs B, Karmel H J, Nyakiti L O, Gaskill D K, Hersam M C, Zegenhagen J and Bedzyk M J 2013 Chemically resolved interface structure of epitaxial graphene on SiC(0001) *Phys. Rev. Lett.* **111** 215501
[411] Sforzini J *et al* 2015 Approaching truly freestanding graphene: the structure of hydrogen-intercalated graphene on 6H–SiC(0001) *Phys. Rev. Lett.* **114** 106804
[412] Sforzini J *et al* 2016 Structural and electronic properties of nitrogen-doped graphene *Phys. Rev. Lett.* **116** 126805
[413] Farwick zum Hagen F H *et al* 2016 Structure and growth of hexagonal boron nitride on Ir(111) *ACS Nano* **10** 11012–26
[414] Dürr A C, Schreiber F, Ritley K A, Kruppa V, Krug J, Dosch H and Struth B 2003 Rapid roughening in thin film growth of an organic semiconductor (diindenoperylene) *Phys. Rev. Lett.* **90** 016104
[415] Kowarik S, Gerlach A, Sellner S, Schreiber F, Cavalcanti L and Konovalov O 2006 Real-time observation of structural and orientational transitions during growth of organic thin films *Phys. Rev. Lett.* **96** 125504
[416] Heinemeyer U, Broch K, Hinderhofer A, Kytka M, Scholz R, Gerlach A and Schreiber F 2010 Real-time changes in the optical spectrum of organic semiconducting films and their thickness regimes during growth *Phys. Rev. Lett.* **104** 257401
[417] Banerjee R, Novák J, Frank C, Lorch C, Hinderhofer A, Gerlach A and Schreiber F 2013 Evidence for kinetically limited thickness dependent phase separation in organic thin film blends *Phys. Rev. Lett.* **110** 185506
[418] Kurrle D and Pflaum J 2008 Exciton diffusion length in the organic semiconductor diindenoperylene *Appl. Phys. Lett.* **92** 133306
[419] Wagner J *et al* 2012 Identification of different origins for s-shaped current voltage characteristics in planar heterojunction organic solar cells *J. Appl. Phys.* **111** 054509
[420] Simbrunner J, Hofer S, Schrode B, Garmshausen Y, Hecht S, Resel R and Salzmann I 2019 Indexing grazing-incidence x-ray diffraction patterns of thin films: lattices of higher symmetry *J. Appl. Crystallogr.* **52** 428–39
[421] Huang H, Sun J T, Feng Y P, Chen W and Wee A T S 2011 Epitaxial growth of diindenoperylene ultrathin films on Ag(111) investigated by LT-STM and LEED *Phys. Chem. Chem. Phys.* **13** 20933–8
[422] Yonezawa K, Suda Y, Yanagisawa S, Hosokai T, Kato K, Yamaguchi T, Yoshida H, Ueno N and Kera S 2016 Charge transfer states appear in the π-conjugated pure hydrocarbon molecule on Cu(111) *Appl. Phys. Express* **9** 045201
[423] Hosokai T, Yonezawa K, Yang J, Koswattage K and Kera S 2017 Significant reduction in the hole-injection barrier by the charge-transfer state formation: diindenoperylene contacted with silver and copper electrodes *Org. Electron.* **49** 39–44
[424] de Oteyza D, Barrena E, Ruiz-Osés M, Silanes I, Doyle B, Ortega J, Arnau A, Dosch H and Wakayama Y 2008 Crystallographic and electronic structure of self-assembled DIP monolayers on Au(111) substrates *J. Phys. Chem.* C **112** 7168–72
[425] de Oteyza D G, Barrena E, Dosch H and Wakayama Y 2009 Nanoconfinement effects in the self-assembly of diindenoperylene (DIP) on Cu(111) surfaces *Phys. Chem. Chem. Phys.* **11** 8741–4
[426] Aldahhak H, Matencio S, Barrena E, Ocal C, Schmidt W G and Rauls E 2015 Structure formation in diindenoperylene thin films on copper(111) *Phys. Chem. Chem. Phys.* **17** 8776–83
[427] Weiß S *et al* 2015 Exploring three-dimensional orbital imaging with energy-dependent photoemission tomography *Nat. Commun.* **6** 8287–8
[428] Puschnig P *et al* 2017 Energy ordering of molecular orbitals *J. Phys. Chem. Lett.* **8** 208–13
[429] Weinhardt L *et al* 2016 Site- and symmetry-resolved resonant x-ray emission study of a highly ordered PTCDA thin film *J. Phys. Chem.* C **120** 8607–15
[430] Ziroff J, Forster F, Schöll A, Puschnig P and Reinert F 2010 Hybridization of organic molecular orbitals with substrate states at interfaces: PTCDA on silver *Phys. Rev. Lett.* **104** 233004–4
[431] Romaner L, Nabok D, Puschnig P, Zojer E and Ambrosch-Draxl C 2009 Theoretical study of PTCDA adsorbed on the coinage metal surfaces, Ag(111), Au(111) and Cu(111) *New J. Phys.* **11** 053010–21
[432] Tautz F S 2007 Structure and bonding of large aromatic molecules on noble metal surfaces: the example of PTCDA *Prog. Surf. Sci.* **82** 479
[433] Zou Y, Kilian L, Schöll A, Schmidt T, Fink R and Umbach E 2006 Chemical bonding of on Ag surfaces and the formation of interface states *Surf. Sci.* **600** 1240–51
[434] Stallberg K, Namgalies A and Höfer U 2019 Photoluminescence study of the exciton dynamics at PTCDA/noble-metal interfaces *Phys. Rev.* B **99** 125410
[435] Nicoara N, Gómez-Rodríguez J M and Méndez J 2019 Growth of PTCDA films on various substrates studied by scanning tunneling microscopy and spectroscopy *Phys. Status Solidi* B **256** 1800333
[436] Liu W, Tkatchenko A and Scheffler M 2014 Modeling adsorption and reactions of organic molecules at metal surfaces *Acc. Chem. Res.* **47** 3369–77
[437] Yanagisawa S, Okuma K, Inaoka T and Hamada I 2015 Recent progress in predicting structural and electronic properties of organic solids with the van der Waals density functional *J. Electron Spectrosc. Relat. Phenom.* **204** 159–67
[438] Morbec J M and Kratzer P 2017 The role of the van der Waals interactions in the adsorption of anthracene and pentacene on the Ag(111) surface *J. Chem. Phys.* **146** 034702
[439] Braun K F and Hla S W 2008 Charge transfer in the TCNQ-sexithiophene complex *J. Chem. Phys.* **129** 064707–7
[440] Rangger G M, Hofmann O T, Romaner L, Heimel G, Bröker B, Blum R P, Johnson R L, Koch N and Zojer E 2009 F4TCNQ on Cu, Ag, and Au as prototypical example for a strong organic acceptor on coinage metals *Phys. Rev.* B **79** 165306
[441] Duhm S, Salzmann I, Bröker B, Glowatzki H, Johnson R L and Koch N 2009 Interdiffusion of molecular acceptors through organic layers to metal substrates mimics doping-related energy level shifts *Appl. Phys. Lett.* **95** 093305
[442] Borghetti P, Sarasola A, Merino-Díez N, Vasseur G, Floreano L, Lobo-Checa J, Arnau A, de Oteyza D G and Ortega J E 2017 Symmetry, shape, and energy variations in frontier molecular orbitals at organic/metal interfaces: the case of F4TCNQ *J. Phys. Chem.* C **121** 28412–9
[443] Duhm S, Xin Q, Koch N, Ueno N and Kera S 2011 Impact of alkyl side chains at self-assembly, electronic structure and charge arrangement in sexithiophene thin films *Org. Electron.* **12** 903–10
[444] Faraggi M N, Jiang N, Gonzalez-Lakunza N, Langner A, Stepanow S, Kern K and Arnau A 2012 Bonding and charge transfer in metal-organic coordination networks on Au(111) with strong acceptor molecules *J. Phys. Chem.* C **116** 24558–65

[445] Gerbert D, Hofmann O T and Tegeder P 2018 Formation of occupied and unoccupied hybrid bands at interfaces between metals and organic donors/acceptors *J. Phys. Chem.* C **122** 27554–60
[446] Koshino M, Kurata H and Isoda S 2004 DV-Xα calculation of electron energy-loss near edge-structures of 2,3,5,6-tetrafluoro-7,7,8,8-tetracyanoquinodimethane (F4TCNQ) *J. Electron Spectrosc. Relat. Phenom.* **135** 191–200
[447] Blowey P J, Velari S, Rochford L A, Duncan D A, Warr D A, Lee T L, De Vita A, Costantini G and Woodruff D P 2018 Re-evaluating how charge transfer modifies the conformation of adsorbed molecules *Nanoscale* **10** 14984–92
[448] Hofmann O T, Rangger G M and Zojer E 2008 Reducing the metal work function beyond pauli pushback: a computational investigation of tetrathiafulvalene and viologen on coinage metal surfaces *J. Phys. Chem.* C **112** 20357–65
[449] Fukagawa H, Hosoumi S, Yamane H, Kera S and Ueno N 2011 Dielectric properties of polar-phthalocyanine monolayer systems with repulsive dipole interaction *Phys. Rev.* B **83** 085304–8
[450] Natan A, Kronik L, Haick H and Tung R T 2007 Electrostatic properties of ideal and non-ideal polar organic monolayers: implications for electronic devices *Adv. Mater.* **19** 4103–17
[451] Hofmann O T, Egger D A and Zojer E 2010 Work-function modification beyond pinning: when do molecular dipoles count? *Nano Lett.* **10** 4369–74
[452] Koch N, Duhm S, Rabe J P, Rentenberger S, Johnson R L, Klankermayer J and Schreiber F 2005 Tuning the hole injection barrier height at organic/metal interfaces with (sub-) monolayers of electron acceptor molecules *Appl. Phys. Lett.* **87** 101905
[453] Amsalem P, Wilke A, Frisch J, Niederhausen J, Vollmer A, Rieger R, Müllen K, Rabe J P and Koch N 2011 Interlayer molecular diffusion and thermodynamic equilibrium in organic heterostructures on a metal electrode *J. Appl. Phys.* **110** 113709–16
[454] Maughan B, Zahl P, Sutter P and Monti O L A 2017 Configuration-specific electronic structure of strongly interacting interfaces: TiOPc on Cu(110) *Phys. Rev.* B **96** 235133–10
[455] Stadtmüller B, Kröger I, Reinert F and Kumpf C 2011 Submonolayer growth of CuPc on noble metal surfaces *Phys. Rev.* B **83** 085416–10
[456] Ruocco A, Evangelista F, Gotter R, Attili A and Stefani G 2008 Evidence of charge transfer at the Cu-phthalocyanine/Al(100) interface *J. Phys. Chem.* C **112** 2016–25
[457] Thussing S and Jakob P 2016 Structural and vibrational properties of CuPc/Ag(111) ultrathin films *J. Phys. Chem.* C **120** 9904–13
[458] Della Pia A, Riello M, Stassen D, Jones T S, Bonifazi D, De Vita A and Costantini G 2016 Two-dimensional core-shell donor-acceptor assemblies at metal-organic interfaces promoted by surface-mediated charge transfer *Nanoscale* **8** 19004–13
[459] Stradi D, Borca B, Barja S, Garnica M, Diaz C, Rodriguez-Garcia J M, Alcami M, Vazquez de Parga A L, Miranda R and Martin F 2016 Understanding the self-assembly of TCNQ on Cu(111): a combined study based on scanning tunnelling microscopy experiments and density functional theory simulations *RSC Adv.* **6** 15071–9
[460] Lindquist J M and Hemminger J C 1988 High-resolution core level photoelectron spectra of solid TCNQ: determination of molecular orbital spatial distribution from localized shake-up features *J. Phys. Chem.* **92** 1394–6
[461] Tang C W 1986 Two-layer organic photovoltaic cell *Appl. Phys. Lett.* **48** 183–5
[462] Liao L S, Slusarek W K, Hatwar T K, Ricks M L and Comfort D L 2008 Tandem organic light-emitting diode using hexaazatriphenylene hexacarbonitrile in the intermediate connector *Adv. Mater.* **20** 324–9
[463] Zhang L, Zu F S, Deng Y L, Igbari F, Wang Z K and Liao L S 2015 Origin of enhanced hole injection in organic light-emitting diodes with an electron-acceptor doping layer: p-type doping or interfacial diffusion? *ACS Appl. Mater. Interfaces* **7** 11965–71
[464] Jung M C, Kojima H, Matsumura I, Benten H and Nakamura M 2018 Diffusion and influence on photovoltaic characteristics of p-type dopants in organic photovoltaics for energy harvesting from blue-light *Org. Electron.* **52** 17–21
[465] Méndez H *et al* 2013 Doping of organic semiconductors: impact of dopant strength and electronic coupling *Angew. Chem., Int. Ed. Engl.* **52** 7751–5
[466] Jacobs I E and Moulé A J 2017 Controlling molecular doping in organic semiconductors *Adv. Mater.* **29** 1703063–39
[467] Méndez H *et al* 2015 Charge-transfer crystallites as molecular electrical dopants *Nat. Commun.* **6** 8560
[468] Salzmann I and Heimel G 2015 Toward a comprehensive understanding of molecular doping organic semiconductors (review) *J. Electron Spectrosc. Relat. Phenom.* **204** 208–22
[469] Salzmann I, Heimel G, Oehzelt M, Winkler S and Koch N 2016 Molecular electrical doping of organic semiconductors: fundamental mechanisms and emerging dopant design rules *Acc. Chem. Res.* **49** 370–8
[470] Wang Q K, Wang R B, Shen P F, Li C, Li Y Q, Liu L J, Duhm S and Tang J X 2015 Energy level offsets at lead halide perovskite/organic hybrid interfaces and their impacts on charge separation *Adv. Mater. Interfaces* **2** 1400528–7
[471] Zhang X, Shao Z, Zhang X, He Y and Jie J 2016 Surface charge transfer doping of low-dimensional nanostructures toward high-performance nanodevices *Adv. Mater.* **28** 10409–42
[472] Schultz T *et al* 2016 Tuning the work function of GaN with organic molecular acceptors *Phys. Rev.* B **93** 125309–5
[473] Zu F, Amsalem P, Ralaiarisoa M, Schultz T, Schlesinger R and Koch N 2017 Surface state density determines the energy level alignment at hybrid perovskite/electron acceptors interfaces *ACS Appl. Mater. Interfaces* **9** 41546–52
[474] Abellán G, Lloret V, Mundloch U, Marcia M, Neiss C, Görling A, Varela M, Hauke F and Hirsch A 2016 Noncovalent functionalization of black phosphorus *Angew. Chem., Int. Ed. Engl.* **55** 14557–62
[475] Winkler S, Xin Q, Li C, Kera S, Müllen K, Ueno N, Koch N and Duhm S 2019 Modification of TiO_2(110)/organic hole transport layer interface energy levels by a dipolar perylene derivative *Electron. Struct.* **1** 015007
[476] Schamoni H, Hetzl M, Hoffmann T, Stoiber K, Matich S and Stutzmann M 2019 Growth mechanisms of F4-TCNQ on inorganic substrates and nanostructures *Mater. Res. Express* **6** 025903
[477] Wang H, Levchenko S V, Schultz T, Koch N, Scheffler M and Rossi M 2019 Modulation of the work function by the atomic structure of strong organic electron acceptors on H-Si(111) *Adv. Electron. Mater.* **5** 1800891
[478] Lindell L, Unge M, Osikowicz W, Stafstrom S, Salaneck W R, Crispin X and de Jong M P 2008 Integer charge transfer at the tetrakis(dimethylamino)ethylene/Au interface *Appl. Phys. Lett.* **92** 163302–3

[479] Akaike K *et al* 2016 Effective work function reduction of practical electrodes using an organometallic dimer *Adv. Funct. Mater.* **26** 2493–502
[480] Shi X Q, Li Y, Van Hove M A and Zhang R Q 2012 Interactions between organics and metal surfaces in the intermediate regime between physisorption and chemisorption *J. Phys. Chem.* C **116** 23603–7
[481] Babudri F, Farinola G M, Naso F and Ragni R 2007 Fluorinated organic materials for electronic and optoelectronic applications: the role of the fluorine atom *Chem. Commun.* **10** 1003–22
[482] Milián-Medina B and Gierschner J 2017 'Though it be but little, it is fierce': excited state engineering of conjugated organic materials by fluorination *J. Phys. Chem. Lett.* **8** 91–101
[483] Lukas S, Sohnchen S, Witte G and Woll C 2004 Epitaxial growth of pentacene films on metal surfaces *ChemPhysChem* **5** 266–70
[484] Ferretti A, Baldacchini C, Calzolari A, Felice R D, Ruini A, Molinari E and Betti M G 2007 Mixing of electronic states in pentacene adsorption on copper *Phys. Rev. Lett.* **99** 046802
[485] Gross L, Mohn F, Moll N, Liljeroth P and Meyer G 2009 The chemical structure of a molecule resolved by atomic force microscopy *Science* **325** 1110–4
[486] de Oteyza D G, Wakayama Y, Liu X, Yang W, Cook P L, Himpsel F J and Ortega J E 2010 Effect of fluorination on the molecule–substrate interactions of pentacene/Cu(100) interfaces *Chem. Phys. Lett.* **490** 54–7
[487] Glowatzki H, Heimel G, Vollmer A, Wong S L, Huang H, Chen W, Wee A T S, Rabe J P and Koch N 2012 Impact of fluorination on initial growth and stability of pentacene on Cu(111) *J. Phys. Chem.* C **116** 7726–34
[488] Schmidt C, Breuer T, Wippermann S, Schmidt W G and Witte G 2012 Substrate induced thermal decomposition of perfluoro-pentacene thin films on the coinage metals *J. Phys. Chem.* C **116** 24098–106
[489] Marks M, Schmidt C, Schwalb C H, Breuer T, Witte G and Höfer U 2012 Temperature dependent structural phase transition at the perfluoropentacene/Ag(111) interface *J. Phys. Chem.* C **116** 1904–11
[490] Goiri E, García-Lastra J M, Corso M, Adb El-Fattah Z M, Ortega J E and de Oteyza D G 2012 Understanding periodic dislocations in 2D supramolecular crystals: the PFP/Ag(111) interface *J. Phys. Chem. Lett.* **3** 848–52
[491] Lo Y Y, Chang J H, Hoffmann G, Su W B, Wu C I and Chang C S 2013 A comparative study on the adsorption behavior of pentacene and perfluoropentacene molecules on Au(111) surfaces *Japan. J. Appl. Phys.* **52** 101601
[492] Wang Q, Franco-Cañellas A, Gerlach A and Schreiber F 2020 in preparation
[493] Peisert H, Knupfer M, Schwieger T, Fuentes G G, Olligs D, Fink J and Schmidt T 2003 Fluorination of copper phthalocyanines: electronic structure and interface properties *J. Appl. Phys.* **93** 9683–92
[494] Peisert H, Knupfer M and Fink J 2002 Electronic structure of partially fluorinated copper phthalocyanine (CuPCF4) and its interface to Au(100) *Surf. Sci.* **515** 491–8
[495] Schwieger T, Peisert H and Knupfer M 2004 Direct observation of interfacial charge transfer from silver to organic semiconductors *Chem. Phys. Lett.* **384** 197–202
[496] Schwarze M *et al* 2016 Band structure engineering in organic semiconductors *Science* **352** 1446–9
[497] Anger F, Glowatzki H, Franco-Cañellas A, Bürker C, Gerlach A, Scholz R, Sakamoto Y, Suzuki T, Koch N and Schreiber F 2015 Interface dipole and growth mode of partially and fully fluorinated rubrene on Au(111) and Ag(111) *J. Phys. Chem.* C **119** 6769–76
[498] Reisz B *et al* 2017 Structural, optical, and electronic characterization of perfluorinated sexithiophene films and mixed films with sexithiophene *J. Mater. Res.* **32** 1908–20
[499] Navarro-Quezada A, Ghanbari E, Wagner T and Zeppenfeld P 2018 Molecular reorientation during the initial growth of perfluoropentacene on Ag(110) *J. Phys. Chem.* C **122** 12704–11
[500] Savu S A, Sonström A, Bula R, Bettinger H F, Chassé T and Casu M B 2015 Intercorrelation of electronic, structural, and morphological properties in nanorods of 2,3,9,10-tetrafluoropentacene *ACS Appl. Mater. Interfaces* **7** 19774–80
[501] Savu S A, Biddau G, Pardini L, Bula R, Bettinger H F, Draxl C, Chassé T and Casu M B 2015 Fingerprint of fractional charge transfer at the metal/organic interface *J. Phys. Chem.* C **119** 12538–44
[502] Salzmann I, Duhm S, Heimel G, Oehzelt M, Kniprath R, Johnson R L, Rabe J P and Koch N 2008 Tuning the ionization energy of organic semiconductor films: the role of intramolecular polar bonds *J. Am. Chem. Soc.* **130** 12870–1
[503] Li F, Yuan J, Ling X, Huang L, Rujisamphan N, Li Y, Chi L and Ma W 2018 Metallophthalocyanine-based molecular dipole layer as a universal and versatile approach to realize efficient and stable perovskite solar cells *ACS Appl. Mater. Interfaces* **10** 42397–405
[504] Taucher T C, Hehn I, Hofmann O T, Zharnikov M and Zojer E 2016 Understanding chemical versus electrostatic shifts in x-ray photoelectron spectra of organic self-assembled monolayers *J. Phys. Chem.* C **120** 3428–37
[505] Huang Y L, Chen W, Bussolotti F, Niu T C, Wee A T S, Ueno N and Kera S 2013 Impact of molecule-dipole orientation on energy level alignment at the submolecular scale *Phys. Rev.* B **87** 085205–6
[506] Lin M K *et al* 2017 Control of the dipole layer of polar organic molecules adsorbed on metal surfaces via different charge-transfer channels *Phys. Rev.* B **95** 085425–9
[507] Peisert H, Knupfer M, Schwieger T, Auerhammer J M, Golden M S and Fink J 2002 Full characterization of the interface between the organic semiconductor copper phthalocyanine and gold *J. Appl. Phys.* **91** 4872–8
[508] Schwieger T, Peisert H, Golden M S, Knupfer M and Fink J 2002 Electronic structure of the organic semiconductor copper phthalocyanine and K-CuPc studied using photoemission spectroscopy *Phys. Rev.* B **66** 155207
[509] Petraki F, Peisert H, Biswas I and Chasse T 2010 Electronic structure of co-phthalocyanine on gold investigated by photoexcited electron spectroscopies: indication of Co ion-metal interaction *J. Phys. Chem.* C **114** 17638–43
[510] Woolley R A J, Martin C P, Miller G, Dhanak V R and Moriarty P J 2007 Adsorbed molecular shuttlecocks: an NIXSW study of Sn phthalocyanine on Ag(111) using Auger electron detection *Surf. Sci.* **601** 1231
[511] Petraki F, Peisert H, Uihlein J, Aygul U and Chasse T 2014 CoPc and CoPcF16 on gold: site-specific charge-transfer processes *Beilstein J. Nanotechnol.* **5** 524–31
[512] Auwärter W, Ecija D, Klappenberger F and Barth J V 2015 Porphyrins at interfaces *Nat. Chem.* **7** 105
[513] Hipps K W and Mazur U 2018 Kinetic and thermodynamic control in porphyrin and phthalocyanine self-assembled monolayers *Langmuir* **34** 3–17
[514] Zhao W, Zhu H, Song H, Liu J, Chen Q, Wang Y and Wu K 2018 Adsorption and assembly of photoelectronic TiOPc molecules on coinage metal surfaces *J. Phys. Chem.* C **122** 7695–701
[515] Singh J, Sharma R K, Goutam U K, Sule U S, Gupta J, Gadkari S C and Rao P N 2019 Orientation study of iron

phthalocyanine (FePc) thin films deposited on silicon and gold surfaces *Mater. Res. Express* **6** 016411
[516] Wang Y, Kröger J, Berndt R and Hofer W A 2009 Pushing and pulling a Sn ion through an adsorbed phthalocyanine molecule *J. Am. Chem. Soc.* **131** 3639–43
[517] Baran J D and Larsson J A 2012 Structure and energetics of shuttlecock-shaped tin-phthalocyanine on Ag(111): a density functional study employing dispersion correction *J. Phys. Chem.* C **116** 9487–97
[518] Greif M, Castiglioni L, Seitsonen A P, Roth S, Osterwalder J and Hengsberger M 2013 Photoelectron diffraction in the x-ray and ultraviolet regime: Sn-phthalocyanine on Ag(111) *Phys. Rev.* B **87** 085429–10
[519] Schwarz F, Wang Y F, Hofer W A, Berndt R, Runge E and Kröger J 2015 Electronic and vibrational states of single tin-phthalocyanine molecules in double layers on Ag(111) *J. Phys. Chem.* C **119** 15716–22
[520] Kashimoto Y, Yonezawa K, Meissner M, Gruenewald M, Ueba T, Kera S, Forker R, Fritz T and Yoshida H 2018 The evolution of intermolecular energy bands of occupied and unoccupied molecular states in organic thin films *J. Phys. Chem.* C **122** 12090–7
[521] Kera S, Yamane H, Honda H, Fukagawa H, Okudaira K and Ueno N 2004 Photoelectron fine structures of uppermost valence band for well-characterized ClAl-phthalocyanine ultrathin film: UPS and MAES study *Surf. Sci.* **566–568** 571–8
[522] Ilyas N, Harivyasi S S, Zahl P, Cortes R, Hofmann O T, Sutter P, Zojer E and Monti O L A 2016 Sticking with the pointy end? Molecular configuration of chloro boron-subphthalocyanine on Cu(111) *J. Phys. Chem.* C **120** 7113–21
[523] Niu T, Zhou M, Zhang J, Feng Y and Chen W 2013 Dipole orientation dependent symmetry reduction of chloroaluminum phthalocyanine on Cu(111) *J. Phys. Chem.* C **117** 1013–9
[524] Wruss E, Hofmann O T, Egger D A, Verwüster E, Gerlach A, Schreiber F and Zojer E 2016 Adsorption behavior of nonplanar phthalocyanines: competition of different adsorption conformations *J. Phys. Chem.* C **120** 6869–75
[525] Harivyasi S, Hofmann O T, Ilyas N, Monti O L A and Zojer E 2018 van der Waals interaction activated strong electronic coupling at the interface between chloro boron-subphthalocyanine and Cu(111) *J. Phys. Chem.* C **122** 14621–30
[526] Karacuban H, Lange M, Schaffert J, Weingart O, Wagner T and Möller R 2009 Substrate-induced symmetry reduction of CuPc on Cu(111): an LT-STM study *Surf. Sci.* **603** L39–43
[527] Mugarza A, Lorente N, Ordejón P, Krull C, Stepanow S, Bocquet M L, Fraxedas J, Ceballos G and Gambardella P 2010 Orbital specific chirality and homochiral self-assembly of achiral molecules induced by charge transfer and spontaneous symmetry breaking *Phys. Rev. Lett.* **105** 115702
[528] Snezhkova O *et al* 2016 Iron phthalocyanine on Cu(111): coverage-dependent assembly and symmetry breaking, temperature-induced homocoupling, and modification of the adsorbate-surface interaction by annealing *J. Chem. Phys.* **144** 094702
[529] Sforzini J, Bocquet F C and Tautz F S 2017 Adsorption-induced symmetry reduction of metal-phthalocyanines studied by vibrational spectroscopy *Phys. Rev.* B **96** 165410
[530] Matencio S, Palacios-Rivera R, Martinez J I, Ocal C and Barrena E 2018 Chiral organization and charge redistribution in chloroaluminum phthalocyanine on Au(111) beyond the monolayer *J. Phys. Chem.* C **122** 16033–41
[531] Huang Y L, Lu Y, Niu T C, Huang H, Kera S, Ueno N, Wee A T S and Chen W 2012 Reversible single-molecule switching in an ordered monolayer molecular dipole array *Small* **8** 1423–8
[532] Song H *et al* 2017 On the shuttling mechanism of a chlorine atom in a chloroaluminum phthalocyanine based molecular switch *Phys. Chem. Chem. Phys.* **19** 22401–5
[533] Fan J, Zhang L, Briseno A L and Wudl F 2012 Synthesis and characterization of 7,8,15,16-tetraazaterrylene *Org. Lett.* **14** 1024–6
[534] Wise A J, Zhang Y, Fan J, Wudl F, Briseno A L and Barnes M D 2014 Spectroscopy of discrete vertically oriented single-crystals of n-type tetraazaterrylene: understanding the role of defects in molecular semiconductor photovoltaics *Phys. Chem. Chem. Phys.* **16** 15825–30
[535] Hirose Y, Kahn A, Aristov V, Soukiassian P, Bulovic V and Forrest S R 1996 Chemistry and electronic properties of metal–organic semiconductor interfaces: Al, Ti, In, Sn, Ag, and Au on PTCDA *Phys. Rev.* B **54** 13748–58
[536] Glöckler K, Seidel C, Soukopp A, Sokolowski M, Umbach E, Böhringer M, Berndt R and Schneider W D 1998 Highly ordered structures and submolecular scanning tunnelling microscopy contrast of PTCDA and DM-PBDCI monolayers on Ag(111) and Ag(110) *Surf. Sci.* **405** 1
[537] Guillermet O, Glachant A, Hoarau J, Mossoyan J and Mossoyan M 2004 Perylene tetracarboxylic diimide ultrathin film deposition on Pt(100): a LEED, AES, REELS and STM study *Surf. Sci.* **548** 129–37
[538] Temirov R, Soubatch S, Luican A and Tautz F S 2006 Free-electron-like dispersion in an organic monolayer film on a metal substrate *Nature* **444** 350–3
[539] Mura M, Silly F, Briggs G A D, Castell M R and Kantorovich L N 2009 H-bonding supramolecular assemblies of PTCDI molecules on the Au(111) surface *J. Phys. Chem.* C **113** 21840–8
[540] Weiss C, Wagner C, Kleimann C, Rohlfing M, Tautz F S and Temirov R 2010 Imaging Pauli repulsion in scanning tunneling microscopy *Phys. Rev. Lett.* **105** 086103
[541] Yu M *et al* 2012 From zero to two dimensions: supramolecular nanostructures formed from perylene-3,4,9,10-tetracarboxylic diimide (PTCDI) and Ni on the Au(111) surface through the interplay between hydrogen-bonding and electrostatic metal-organic interactions *Nano Res.* **5** 903–16
[542] Zaitsev N L, Jakob P and Tonner R 2018 Structure and vibrational properties of the PTCDA/Ag(111) interface: bilayer versus monolayer *J. Phys.: Condens. Matter.* **30** 354001–8
[543] Yang X *et al* 2018 On the decoupling of molecules at metal surfaces *Chem. Commun.* **54** 9039–42
[544] Yamada K, Yanagisawa S, Koganezawa T, Mase K, Sato N and Yoshida H 2018 Impact of the molecular quadrupole moment on ionization energy and electron affinity of organic thin films: experimental determination of electrostatic potential and electronic polarization energies *Phys. Rev.* B **97** 245206
[545] Braatz C, Esat T, Wagner C, Temirov R, Tautz F and Jakob P 2016 Switching orientation of adsorbed molecules: reverse domino on a metal surface *Surf. Sci.* **643** 98–107
[546] Müllegger S, Salzmann I, Resel R and Winkler A 2003 Epitaxial growth of quaterphenyl thin films on gold(111) *Appl. Phys. Lett.* **83** 4536–8
[547] Huempfner T, Hafermann M, Udhardt C, Otto F, Forker R and Fritz T 2016 Insight into the unit cell: structure of picene thin films on Ag(100) revealed with complementary methods *J. Chem. Phys.* **145** 174706–7

[548] Wang Q, Xin Q, Wang R B, Oehzelt M, Ueno N, Kera S and Duhm S 2017 Picene thin films on metal surfaces: impact of molecular shape on interfacial coupling *Phys. Status Solidi* **11** 1700012–5

[549] Pang C L, Lindsay R and Thornton G 2013 Structure of clean and adsorbate-covered single-crystal rutile TiO_2 surfaces *Chem. Rev.* **113** 3887–948

[550] Diebold U 2003 The surface science of titanium dioxide *Surf. Sci. Rep.* **48** 53–229

[551] Kaindl G, Chiang T C, Eastman D E and Himpsel F J 1980 Distance-dependent relaxation shifts of photoemission and Auger energies for Xe on Pd(001) *Phys. Rev. Lett.* **45** 1808–11

[552] Repp J, Meyer G, Paavilainen S, Olsson F E and Persson M 2006 Imaging bond formation between a gold atom and pentacene on an insulating surface *Science* **312** 1196–9

[553] Wang H, Amsalem P, Heimel G, Salzmann I, Koch N and Oehzelt M 2014 Band-bending in organic semiconductors: the role of alkali-halide interlayers *Adv. Mater.* **26** 925–30

[554] Imai-Imada M, Imada H, Miwa K, Jung J, Shimizu T K, Kawai M and Kim Y 2018 Energy-level alignment of a single molecule on ultrathin insulating film *Phys. Rev.* B **98** 201403

[555] Zwick C, Baby A, Gruenewald M, Verwüster E, Hofmann O T, Forker R, Fratesi G, Brivio G P, Zojer E and Fritz T 2016 Complex stoichiometry-dependent reordering of 3,4,9,10-perylenetetracarboxylic dianhydride on Ag(111) upon K intercalation *ACS Nano* **10** 2365–74

[556] Jung T A, Schlittler R R and Gimzewski J K 1997 Conformational identification of individual adsorbed molecules with the STM *Nature* **386** 696–8

[557] Lindner R and Kühnle A 2015 On-surface reactions *ChemPhysChem* **16** 1582–92

[558] de Oteyza D G *et al* 2013 Direct imaging of covalent bond structure in single-molecule chemical reactions *Science* **340** 1434

[559] Zhang J L, Zhong J Q, Lin J D, Hu W P, Wu K, Xu G Q, Wee A T S and Chen W 2015 Towards single molecule switches *Chem. Soc. Rev.* **44** 2998–3022

[560] Li Q *et al* 2016 Surface-controlled mono/diselective ortho C–H bond activation *J. Am. Chem. Soc.* **138** 2809–14

[561] Björk J 2016 Reaction mechanisms for on-surface synthesis of covalent nanostructures *J. Phys.: Condens. Matter.* **28** 083002–15

[562] Shen Q, Gao H Y and Fuchs H 2017 Frontiers of on-surface synthesis: from principles to applications *Nano Today* **13** 77–96

[563] Lackinger M 2017 Surface-assisted Ullmann coupling *Chem. Commun.* **53** 7872–85

[564] Shchyrba A *et al* 2014 Controlling the dimensionality of on-surface coordination polymers via endo- or exoligation *J. Am. Chem. Soc.* **136** 9355–63

[565] Marbach H 2015 Surface-mediated in situ metalation of porphyrins at the solid-vacuum interface *Acc. Chem. Res.* **48** 2649–58

[566] Diller K, Papageorgiou A C, Klappenberger F, Allegretti F, Barth J V and Auwärter W 2016 In vacuo interfacial tetrapyrrole metallation *Chem. Soc. Rev.* **45** 1629–56

[567] González-Moreno R *et al* 2011 Following the metalation process of protoporphyrin IX with metal substrate atoms at room temperature *J. Phys. Chem.* C **115** 6849–54

[568] Xiao J, Ditze S, Chen M, Buchner F, Stark M, Drost M, Steinrück H P, Gottfried J M and Marbach H 2012 Temperature-dependent chemical and structural transformations from 2H-tetraphenylporphyrin to copper(ii)-tetraphenylporphyrin on Cu(111) *J. Phys. Chem.* C **116** 12275–82

[569] Röckert M, Ditze S, Stark M, Xiao J, Steinrück H P, Marbach H and Lytken O 2014 Abrupt coverage-induced enhancement of the self-metalation of tetraphenylporphyrin with Cu(111) *J. Phys. Chem.* C **118** 1661–7

[570] Lepper M, Köbl J, Schmitt T, Gurrath M, de Siervo A, Schneider M A, Steinrück H P, Meyer B, Marbach H and Hieringer W 2017 'Inverted' porphyrins: a distorted adsorption geometry of free-base porphyrins on Cu(111) *Chem. Commun.* **53** 8207–10

[571] Morgenstern K 2011 Switching individual molecules by light and electrons: from isomerisation to chirality flip *Prog. Surf. Sci.* **86** 115–61

[572] Comstock M J *et al* 2007 Reversible photomechanical switching of individual engineered molecules at a metallic surface *Phys. Rev. Lett.* **99** 038301

[573] Maurer R J and Reuter K 2012 Bistability loss as a key feature in azobenzene (non-)switching on metal surfaces *Angew. Chem., Int. Ed. Engl.* **51** 12009–11

[574] Hieringer W, Flechtner K, Kretschmann A, Seufert K, Auwärter W, Barth J V, Görling A, Steinrück H P and Gottfried J M 2011 The surface trans effect: influence of axial ligands on the surface chemical bonds of adsorbed metalloporphyrins *J. Am. Chem. Soc.* **133** 6206–22

[575] Huang H, Wong S L, Chen W and Wee A T S 2011 LT-STM studies on substrate-dependent self-assembly of small organic molecules *J. Phys. D: Appl. Phys.* **44** 464005–13

[576] Zhong J Q, Qin X, Zhang J L, Kera S, Ueno N, Wee A T S, Yang J and Chen W 2014 Energy level realignment in weakly interacting donor-acceptor binary molecular networks *ACS Nano* **8** 1699–707

[577] Borghetti P, de Oteyza D G, Rogero C, Goiri E, Verdini A, Cossaro A, Floreano L and Ortega J E 2016 Molecular-level realignment in donor-acceptor bilayer blends on metals *J. Phys. Chem.* C **120** 5997–6005

[578] Stadtmüller B, Gruenewald M, Peuker J, Forker R, Fritz T and Kumpf C 2014 Molecular exchange in a heteromolecular PTCDA/CuPc bilayer film on Ag(111) *J. Phys. Chem.* C **118** 28592–602

[579] Egger D A, Ruiz V G, Saidi W A, Bučko T, Tkatchenko A and Zojer E 2013 Understanding structure and bonding of multilayered metal-organic nanostructures *J. Phys. Chem.* C **117** 3055–61

[580] Stadtmüller B, Henneke C, Soubatch S, Tautz F S and Kumpf C 2015 Tailoring metal-organic hybrid interfaces: heteromolecular structures with varying stoichiometry on Ag(111) *New J. Phys.* **17** 023046

[581] Gruenewald M, Sauer C, Peuker J, Meissner M, Sojka F, Schöll A, Reinert F, Forker R and Fritz T 2015 Commensurism at electronically weakly interacting phthalocyanine/PTCDA heterointerfaces *Phys. Rev.* B **91** 155432

[582] van Straaten G, Franke M, Soubatch S, Stadtmüller B, Duncan D A, Lee T L, Tautz F S and Kumpf C 2018 Role of the central metal atom in substrate-mediated molecular interactions in phthalocyanine-based heteromolecular monolayers *J. Phys. Chem.* C **122** 8491–504

[583] Häming M, Greif M, Sauer C, Schöll A and Reinert F 2010 Electronic structure of ultrathin heteromolecular organic–metal interfaces: SnPc/PTCDA/Ag(111) and SnPc/Ag(111) *Phys. Rev.* B **82** 235432

[584] McEwan J A, Clulow A J, Nelson A, Wang R, Burn P L and Gentle I R 2018 Influence of dopant concentration and steric bulk on interlayer diffusion in OLEDs *Adv. Mater. Interfaces* **5** 1700872–10

[585] Armbrust N, Schiller F, Güdde J and Höfer U 2017 Model potential for the description of metal/organic interface states *Sci. Rep.* **7** 46561

[586] Niederhausen J, Franco-Cañellas A, Erker S, Schultz T, Broch K, Hinderhofer A, Duhm S, Thakur P D, Duncan D A, Gerlach A, Lee T L, Hofmann O T, Schreiber F and Koch N 2020 X-ray standing waves reveal lack of OH termination at hydroxylated ZnO(0001) surfaces *Phys. Rev. Materials* **4** 020602(R)

[587] Wang Q, Franco-Cañellas A, Yang J, Hausch J, Struzek S, Chen M, Thakur P K, Gerlach A, Duhm S and Schreiber F 2020 Heteromolecular bilayers on a weakly interacting substrate: Physisorptive bonding and molecular distortions of copper-hexadecafluorophthalocyanine *ACS Appl. Mater. Interfaces* **12** 14542–51